5-1-2015

Bandwidth Based Methodology for Designing a Hybrid Energy Storage System for a Series Hybrid Electric Vehicle with Limited All Electric Mode

Masood Shahverdi

Bandwidth based methodology for designing a hybrid energy storage system for a series hybrid electric vehicle with limited all electric mode

By

Masood Shahverdi

A Dissertation
Submitted to the Faculty of
Mississippi State University
in Partial Fulfillment of the Requirements
for the Degree of Doctor of Philosophy
in Electrical Engineering
in the Department of Electrical and Computer Engineering

Mississippi State, Mississippi

May 2015

Bandwidth based methodology for designing a hybrid energy storage system for a series hybrid electric vehicle with limited all electric mode

By

Masood Shahverdi

Approved:

_____

Michael Mazzola
(Major Professor)

_____

G. Marshall Molen
(Minor Professor)

_____

Sherif Abdelwahed
(Committee Member)

_____

Masoud Karimi Ghatremani
(Committee Member)

_____

James E. Fowler
(Graduate Coordinator)

_____

Jason M. Keith
Interim Dean
Bagley College of Engineering

Name: Masood Shahverdi

Date of Degree: May 8, 2015

Institution: Mississippi State University

Major Field: Electrical Engineering

Major Professor: Dr. Michael S. Mazzola

Title of Study: Bandwidth based methodology for designing a hybrid energy storage system for a series hybrid electric vehicle with limited all electric mode

Pages in Study: 123

Candidate for Degree of Doctor of Philosophy

The cost and fuel economy of hybrid electrical vehicles (HEVs) are significantly dependent on the power-train energy storage system (ESS). A series HEV with a minimal all-electric mode (AEM) permits minimizing the size and cost of the ESS. This manuscript, pursuing the minimal size tactic, introduces a bandwidth based methodology for designing an efficient ESS. First, for a mid-size reference vehicle, a parametric study is carried out over various minimal-size ESSs, both hybrid (HESS) and non-hybrid (ESS), for finding the highest fuel economy. The results show that a specific type of high power battery with 4.5 kWh capacity can be selected as the winning candidate to study for further minimization.

In a second study, following the twin goals of maximizing Fuel Economy (FE) and improving consumer acceptance, a sports car class Series-HEV (SHEV) was considered as a potential application which requires even more ESS minimization. The challenge with this vehicle is to reduce the ESS size compared to 4.5 kWh, because the available space allocation is only one fourth of the allowed battery size in the mid-size study by volume. Therefore, an advanced bandwidth-based controller is developed that

allows a hybridized Subaru BRZ model to be realized with a light ESS. The result allows a SHEV to be realized with 1.13 kWh ESS capacity.

In a third study, the objective is to find optimum SHEV designs with minimal AEM assumption which cover the design space between the fuel economies in the mid-size car study and the sports car study. Maximizing FE while minimizing ESS cost is more aligned with customer acceptance in the current state of market. The techniques applied to manage the power flow between energy sources of the power-train significantly affect the results of this optimization. A Pareto Frontier, including ESS cost and FE, for a SHEV with limited AEM, is introduced using an advanced bandwidth-based control strategy teamed up with duty ratio control. This controller allows the series hybrid's advantage of tightly managing engine efficiency to be extended to lighter ESS, as compared to the size of the ESS in available products in the market.

DEDICATION

The author would like to dedicate this dissertation to his devoted mother, supportive father, and his loving wife for their unconditional love and continued support. The author also wants to dedicate this dissertation to his son Ryan for the joy he brought by coming to our life just before defending this dissertation.

ACKNOWLEDGEMENTS

The author would like to express his deepest appreciation to Dr. Michael S. Mazzola, his major professor, for his excellent guidance, patience, and support. Without his persistent help and unending enthusiasm this dissertation would not have been possible.

I extend my gratitude to Mr. James W. Bagley for his interest in this research, for his financial support, and for his invaluable idea for a "battery light series hybrid electric vehicle" that inspired this research.

The author also thanks Dr. Marshall Molen, Dr. Masoud Karimi, and Dr. Sherif Abdelwahed for their suggestions and discussions while serving on his committee. In addition, the author would like to extend the gratitude to the Car of The Future research group, Mr. Zach Rowland, Matthew Doude, Quintin Grice, Blake Brown, and Jeremiah Hayes for their advice and experiment support.

TABLE OF CONTENTS

LIST OF TABLES

LIST OF FIGURES

CHAPTER I

INTRODUCTION

1.1 Background and motivation

Environmental and energy concerns in recent years [1] [2] [3] persuaded policy makers to encourage the automotive industry to change their direction to produce vehicles with higher fuel economy, lower emission and superior performance [4] [5] [6] [7] [8]. In 2010, light-duty vehicles were responsible for 45% of US oil consumption which shows the dependency of the transportation system on petroleum. On the other hand, oil-fired power plants are only responsible for 1% of US electricity consumption which shows the lower dependency on petroleum in producing electricity [9] [10]. Therefore there is a great interest in using electrical energy sources in the power-trains of the vehicles [11]. Different types of Electrified Vehicles have been manufactured such as the Hybrid Electric Vehicle (HEV), the Plug-in Hybrid Electric Vehicle (PHEV), the Battery Electric Vehicle (BEV), and the Fuel Cell Vehicle (FCV) [4] [5] [7] [12].

Among all EV products, the HEV owns the largest share of the US vehicle market with 3.6 % while the contribution from other options are much smaller [13]. HEVs are classified into micro, mild, medium, and full HEV based on the degree of hybridization [14]. The full HEV class, from this point on in this manuscript denoted simply HEV, has the potential to have engine duty-cycling, regenerative braking, motor assistance, and All-Electric Mode (AEM). In each case, the power-train is hybridized to some extent

with an energy storage system (ESS) to improve the performance of the ICE [4] [5]. Despite the superior performance, the HEV is still not as competitive as conventional vehicles with consumers; one main reason is the ESS cost and durability limitations. Therefore, one of the major challenges is to minimize the ESS cost while not compromising the overall power-train efficiency; this is a multi-objective optimization problem which is influenced by different parameters [15] [16]. The power flow management technique that is used to distribute the load between ICE and ESS is one of the major contributors which significantly affects the result of the optimization study [17].

1.2 Literature Review

Electrified vehicle literature and other literatures contain many references related to the topic of the energy storage system (ESS). Several subjects have been studied in this literature which affect the size and performance of the ESS. One subject is hybridization. A hybrid ESS (HESS) is one in which various energy storage devices (ESDs) with different characteristics are combined to achieve lower overall loss and better power and energy density. Another subject that affects ESS size is the methodology of design which can be classified into time domain and frequency domain techniques. The third influential subject, which in the electrified vehicle domain is known as control strategy, is the methodology of distributing the power between the energy sources in the power-train. The last but not least is the applied optimization technique for both optimizing the size of the ESS and/or optimizing the performance of the vehicle. Reviewing and finally appropriately using the listed subjects allows optimized design to be achieved. Therefore,

in order to organize the discussion, the literature reviewed will be broken down into several categories, which are enumerated below.

1. Time-domain analysis on the topic of HESS in electrified vehicles or in general applications
2. Frequency domain analysis for designing or analyzing ESS
3. Impacts of power management on the design of ESS in electrified vehicles
4. Optimization studies on the cost of ESS and efficiency of the power-train in electrified vehicles

In order to maintain consistency and increase clarity throughout the literature review and the entire document, the term "bandwidth" will be used to identify the band of frequency over which a specific energy source operates with respectively high efficiency. However, when the term "bandwidth" is used for a study or analysis, the range of frequencies considered in the study is intended.

1.2.1 Time-domain study on HESS topic in electrified vehicle or in general applications

The first category of papers directly studies the HESS design either in electrified vehicles or in general applications. Many papers have studied the direct parallel combination of battery and Ultra-Capacitor (UC), the so called passive connection [18] [19] [20] [21] [22] [23] [24]. Active connection via a dc-dc converter is another method of hybridization which has been shown to be a more efficient solution. The HESS literature can be classified based on main concentration. By doing so, they can be categorized into sizing, topology, and converter control study although they are usually a mixture of these three. In sizing studies, battery weight can be simply computed based on

the energy requirement of the system and the battery specific energy while UC weight can be calculated based on the power requirement of the system and UC specific power [25] [26]. In some cases, the sizing optimization problem is solved through maximizing the fuel economy. Battery weight, UC weight, and the power distribution ratio between UC and battery, or Degree of Hybridization, can be taken as optimization variables [27]. In topology studies, various configurations of battery-UC HESS, from simple passive to different types of active, in HEV, PHEV, and BEV application have been classified and well-reviewed; moreover, pros and cons of each in addition to their operating details have been discussed [28]. More topologies have also been proposed, tested, evaluated, and added to the list of topologies [29] [30] [31]. Different control methods could also be considered for the dc-dc converter in the HESS, each of which impacts size, cost, and/or lifetime [27] [32] [33].

These ESS are usually large, because the size and performance reflect the assumption of having significant AEM. Therefore the results of these studies are not the indicator of their performance in a situation where HEV with minimal AEM is assumed. They usually are time domain analyses where independently dedicating energy sources based on their frequency response characteristics for managing the load is not an option.

1.2.2 Frequency domain analysis for designing or analyzing HESS

The study of the frequency domain analysis of hybrid energy storage systems is of interest because the methodology is capable of decoupling various transient phenomena. This allows studying the impacts of different phenomena on HESS independently.

1.2.2.1 Kuperman, Alon, Ilan Aharon, Avi Kara, and Shalev Malki. "A frequency domain approach to analyzing passive battery–ultracapacitor hybrids supplying periodic pulsed current loads." Energy Conversion and Management 52, no. 12 (2011): 3433-3438.

In [34], the authors study the hybrid energy storage topic not for a specific application, but for general application. The passive configuration rather than an active topology is chosen for hybridizing a high energy battery and a UC because of simplicity, reduced cost and volume, and better reliability. The authors mention that the frequency domain method is selected for analysis because it offers a better understanding of the steady state operation in terms of design trade-offs as compared to a time domain study which gives good understanding of transient performance.

Ultra-capacitors act as a low pass filter for the battery. The transfer function below, which is the ratio of battery current to load current, becomes constant at $\frac{r_C}{r_C+r_B}$when the frequency tends to infinity. This constant approaches zero at higher frequency if capacitor resistance is considerably smaller than battery internal resistance (1.1). Sizing the UC is done using the frequency domain technique.

$$|H_C(j\omega)| = \frac{1 + j\omega C r_C}{1 + j\omega C(r_B + r_C)} = \sqrt{\frac{1 + (\omega C r_C)^2}{1 + \left(\omega C(r_B + r_C)\right)^2}} \qquad (1-1)$$

$$|H_C(\infty)| = \frac{r_C}{r_C + r_B} \xrightarrow{r_C \ll r_B} 0. \qquad (1.1)$$

The degree of hybridization, K, is found in the frequency domain by $|H_C(j\omega)| \leq K \; \forall\omega \geq \frac{2\pi}{T}$ inequality constraint to set the UC as a low pass filter where T is the frequency of the pulse load which was used for this analysis.

Frequency domain techniques allow better dedication of available energy sources because the time-domain transient phenomena can be decoupled and treated independently based on the bandwidth of the energy source. However, the authors do this analysis for a general application, so obviously the result cannot be directly applied for applications like the HEV where sources such as ICE, battery, and UC are combined to manage a random load. Pulse loading is not generally representative of the load in electrified vehicles, so the results should be seen as informative but incomplete if extended to vehicle application.

1.2.2.2 Brubaker, M. A., D. El Hage, T. A. Hosking, H. C. Kirbie, and E. D. Sawyer. "Increasing the life of electrolytic capacitor banks using integrated high performance film capacitors." PCIM 2013 Europe (2013).

In solar and wind applications [35], electrolytic capacitor banks are used at the dc link of voltage source inverters to provide a local reservoir of charge during switching and to store energy for ride-through events associated with grids. Film capacitors with higher bandwidth are an advanced technology used in parallel with electrolytic capacitors to supply high frequency current and increase the lifetime of the electrolytic capacitors. This prevents the electrolytic capacitor from being de-rated to increase service life. In other words, the best combination of capacitor density is obtained and there is no need to increase the number of electrolytic capacitors to meet the current-ripple requirement because the film capacitor takes care of a significant portion of the ripple current. In other words, a hybrid dc link capacitor bank reduces overall energy storage power loss.

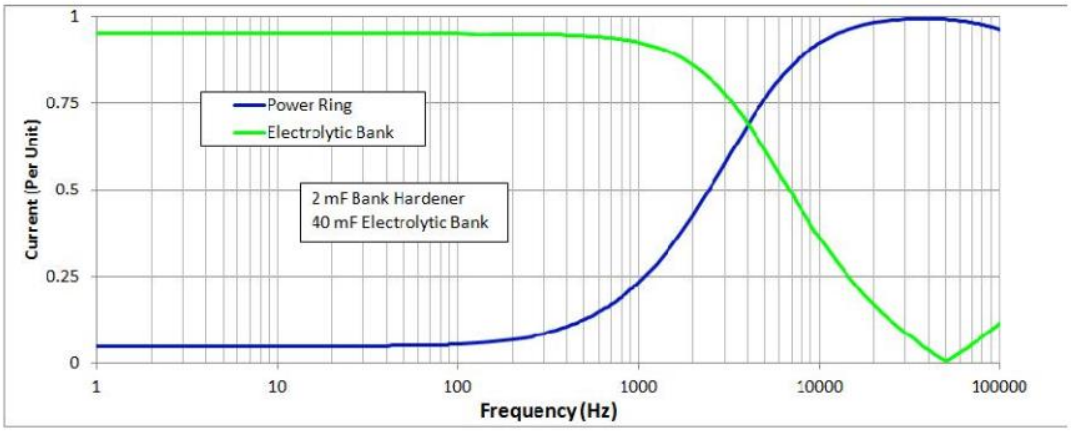

Figure 1.1 Covering wide range of frequency bands by different energy storage devices. "After Ref. [35]"

In addition, the thermal resistance of the film capacitor at 2.3ºC/W improves thermal management of the overall bank. The idea of covering a wide range of frequency bands with different energy source devices (Figure 1.1) can be extended and applied to designing the ESS and ICE in general, for example the combining the ESS and ICE in a way that uses each one over its efficient bandwidth. In addition, power loss reduction and lifetime increases from use of hybridized sources of energy is a valuable advantage. However, this design is proposed for solar and wind applications which have different requirements compared to that of an electrified vehicle.

1.2.3 Impacts of power management on the design of electrified vehicles ESS

The applied method for distributing the load between energy sources is called power management or control strategy. The method used significantly affects the problem of sizing energy sources as well as the overall efficiency of the system. Usually in an electrified vehicle these controls rely on time domain techniques; however, the

frequency domain technique has been also used. In the following, a time domain control strategy is discussed first. Then a frequency-domain technique is reviewed.

1.2.3.1 Lei Wang, Emmanuel G. Collins, Jr., and Hui Li, "Optimal Design and Real-Time Control for Energy Management in Electric Vehicles", Vehicular Technology, IEEE Transactions on 60, no. 4 (2011): 1419-1429.

In [27], the active HESS, including high energy battery and UC, is studied for applications such as BEV and PHEV. The problem of sizing the battery and UC and finding a degree of hybridization (DH) is solved for maximizing FE. A control strategy is developed in real time which consists of battery power reference generation, UC SOC regulation, and forecast control based on the driver commands. This method is based on estimating the future power requirement by past power information and current efficiency. It has been exclusively developed for the All Electric Range (AER) mode.

This article has two sections: off-line ESS size optimization and real time control strategy for power distribution. In an off-line optimization, to determine the size of the ESS the simplified ECE40 drive schedule is used which does not have sufficient accelerations/decelerations to model urban driving behavior. For energy calculation, the single overall efficiency is considered for the whole system over the entire drive cycle. To derive the optimization objective function, it has been considered that FE decreases proportionally to the added ESS mass; however, in reality this relationship is not necessarily linear. The mass of UC or battery are considered continuous variables; however, in reality they are discrete variables. Many other assumptions, for example arbitrary duty ratio for UC operation time, also have been considered in order that the authors can use the simplified energy equation derived for minimizing the ESS loss. Therefore, the found solution is may not be an optima. They use fmincon optimization of

MATLAB to solve the optimization equation for sizing the component. Three variables are optimized: *DH*, degree of hybridization, n_{mass}, ratio of UC mass to ESS mass and M_{ESS}, ESS mass.

$$DH = \frac{P_{UC}}{P_{BU} + P_{UC}} \tag{1.2}$$

Where PUC, is Ultra Capacitor power during duty ratio of D2, and PBU, is battery power in the same duty ratio. D1 is proportional to stop time.

$$T = D_1 + D_2 = 1 \tag{1.3}$$

$$n_{mass} = \frac{\mathrm{M}_{UC}}{\mathrm{M}_{ESS}} \tag{1.4}$$

MUC, and MESS, are UC mass and ESS mass, so n_mass determines UC mass.

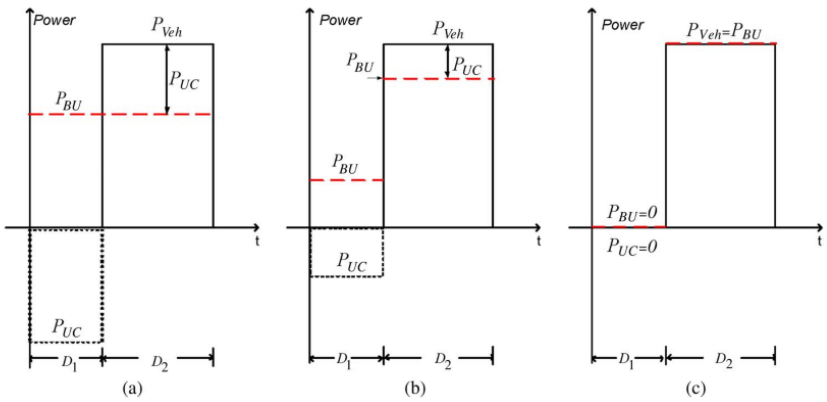

Figure 1.2 Battery power, UC power, and vehicle power for different scenarios for DH: (a) DH =1- D_2 (b) 0 < DH < 1 - D_2 (c) DH=0. "After Ref. [27]"

Fig. 1.2 Shows DH in different situations. DH only determines the ratio between PBU and PUC in D2. Therefore, the frequency characteristics of each energy source not considered for distributing the transient efficiently.

In real time power management, which is the second section of this study, using past information which is updated every 1 second, the stop interval D1 is estimated and based on D1, DH is found to minimize the ESS loss and to maximize FE. A downscaled experiment is also proposed at the end.

The idea of defining and optimizing the degree of hybridizing for maximizing FE is interesting, but the power distribution is carried out based on a duty ratio. The more interesting idea would be to define a variable bandwidth which sets the boundary of operation for each energy source and then solve for the optimized bandwidth value to maximize the FE. In addition, the PHEV and BEV application is very interesting, but their share of the US vehicle market is very small. Applying a similar idea to find the optimal power flow in the HEV will probably have a greater impact on electrifying the automobile market over the next several decades. Specifically, setting an appropriate bandwidth for the efficient operation for the engine which, among available energy sources, has the lowest efficiency in the power-train will have greater impact on FE.

1.2.3.2 Tani, Abdallah, Mamadou Baïlo Camara, and Brayima Dakyo. "Energy management based on frequency approach for hybrid electric vehicle applications: Fuel-cell/lithium-battery and ultracapacitors." Vehicular Technology, IEEE Transactions on 61, no. 8 (2012): 3375-3386:

In [34], two topologies of HEVs are used as references: one is the Fuel Cell (FC) and UC combination, and the other is the Li-Ion battery and UC combination. In the first topology, the FC and UC are connected to the bus with a boost converter and a buck-

boost converter, respectively. In the second topology, the battery is directly connected to the bus while the UC is again connected with a buck-boost converter. For the first topology, the reason for not using an FC alone is described as follows. The Fuel Cell is used [35], [36] in the HEV with a Li-Ion battery or an UC [37], [38] because the FC has low efficiency during low demand. The UC suffers higher cost per watt and slower dynamics during transients.

In the first section of the paper, the energy sources modeled are the FC, battery, and UC. A DC-DC buck-boost converter and a DC/AC traction motor inverter are modeled as well. The main contribution of the work is the distribution of the load between energy sources in the frequency domain using a low pass filter in the controller. In the first topology, the block diagram in Fig. 1.3 is proposed for power flow management between the FC and the UC. The reference current for the UC is created by subtracting the low frequency portion of load current from the overall load current. Therefore, the high frequency segment of the load current is assigned to the UC. Then, polynomial coefficients are found to minimize the static error. A DC link voltage control is also developed because both the FC and the UC are connected to the bus with converters. In the second topology because the battery is directly connected to the bus, the bus voltage is adequately regulated so no voltage control is required. In Fig. 1.4 the power flow management between the battery and the UC is carried out using a low pass filter very similar to the method in first topology shown in Fig. 1.3.

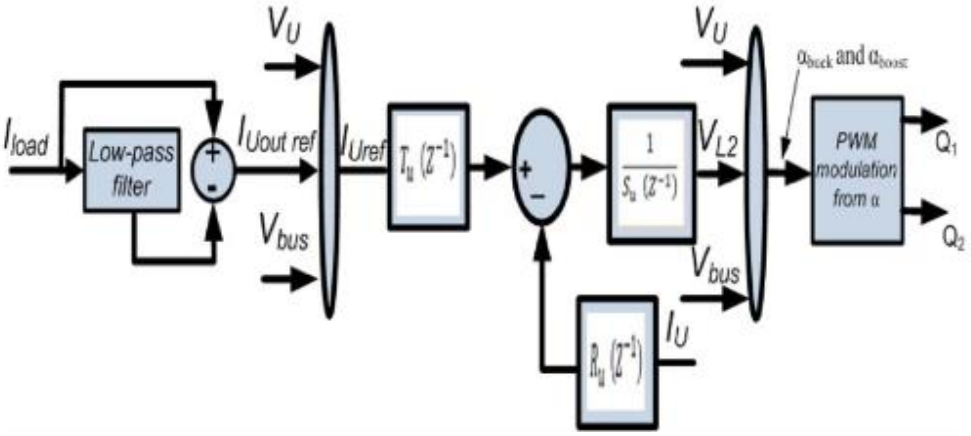

Figure 1.3 Block diagram of UC current control using a low pass filter and polynomial correctors. "After Ref. [36]"

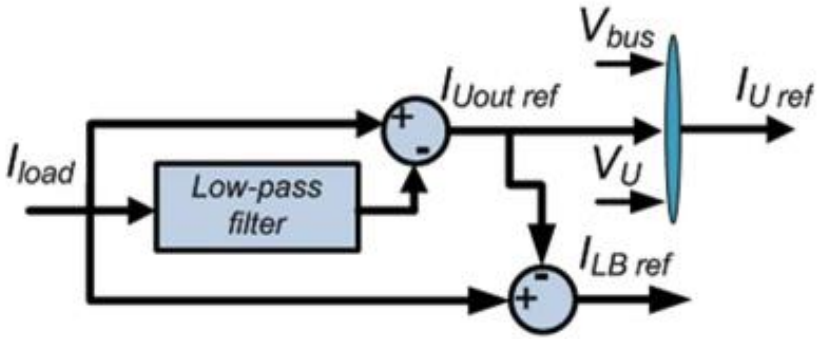

Figure 1.4 Block diagram of UC and battery current control using a low pass filter. "After Ref. [36]"

Both topologies have a series-hybrid architecture. The first topology is a good example of the need to have ESS optimization in a series configuration. Both the Fuel Cell and the ICE share a common feature in that they exhibit poor performance when the bandwidth of the load varies.

For the first topology the Fuel Cell is emulated by a DC source; however the DC source has almost zero internal resistance and so there is a question about whether it can emulate the behavior of a FC. In the second topology although the authors classify the topology as HEV, no engine is applied. Therefore, it can be guessed that they mean PHEV. In this paper, the main problem is that the cut-off frequency of the filter is selected arbitrarily to be 0.025 Hz, equivalent to a time constant of 40 s. There is no analysis to show that this bandwidth is optimal.

1.2.4 Optimization studies on the cost of ESS and efficiency of the power-train in electrified vehicles

1.2.4.1 Wu, Xiaolan, Binggang Cao, Xueyan Li, Jun Xu, and Xiaolong Ren. "Component sizing optimization of plug-in hybrid electric vehicles." *Applied Energy* 88, no. 3 (2011): 799-804:

The platform in [39] is a PHEV. First the authors describe that because the power-train of an electrified vehicle is a complex system relying on many components working together, there is a need to optimize the power-train as a single package. They emphasize that because the system has nonlinear and non-smooth characteristics relying on mechanical and electrical systems operating together, the objective function and constraints are also nonlinear. Therefore, local optima may exist which makes gradient based methods inefficient. They propose a non-gradient-based optimization method called Parallel Chaos Optimization Algorithm (PCOA) which works based on the ergodicity, the stochastic properties, and the regularity of the chaos phenomenon. Like the genetic algorithm, the PCOA is good at finding optima. The cost of the power-train is set as the objective function because of the marketability issues associated with PHEVs. The performance of the power-train is set as the constraints of the optimization problem.

This is a simulation-based optimization where an advanced vehicle simulator (ADVISOR) is used as the simulation tool.

For varying the size of the ICE and the motor, a torque scaling factor is used and for the battery the number of modules and their capacity are used as scaling factors. The cost function is developed for summation of the costs of the engine, motor, battery, and battery replacement. Acceleration, gradeability, maximum speed, and AER are also set as constraints. The standard control strategy of ADVISOR is used; for AER mode the BEV strategy is used, while for the hybrid mode the charge-sustaining strategy is used. In Fig. 1.5, the impact of properly sizing the components are shown for different AERs.

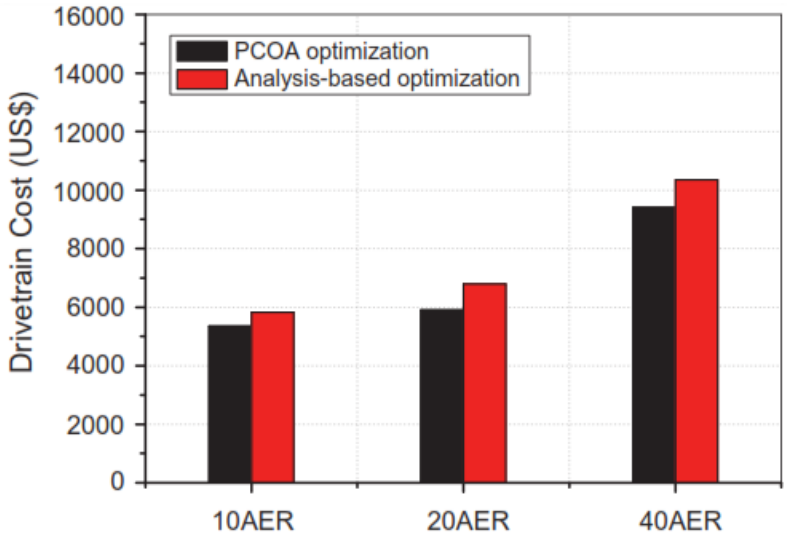

Figure 1.5 Costs of the major part of power-train are compared for PHEV with different AER. "After Ref. [39]"

In this paper, first the marketability issue of PHEV has been presented and based on that it is shown that optimizing the sizes of the major components of the power-train

minimizes the overall cost. Resolving marketability issues of the HEV is also of interest because its market share is still very low compared to conventional vehicles.

However, the effect of customized control strategies were not considered in this study. Therefore, it is not known how sensitive the results are to varying the power flow management between sources. The model does not seem sufficiently detailed to take the effect of the efficiency map of each design (and associated components) into consideration when they change during the optimization process.

The conclusion after reviewing the related prior research reported in the literature is that in the design of electrified vehicles, the use of an active HESS and the application of the frequency domain technique for load distribution during the development of an advanced control strategy may lead to a combination of properly sized hybrid energy sources with superior vehicle overall performance. Of course after these considerations, optimization techniques can help find the optimum design for both the performance and size.

1.3 Research Contribution

The research documented in this dissertation tests the hypothesis that a series hybrid electric power-train can be realized with high fuel economy but far lighter Energy Storage System (ESS) than is conventionally found in such vehicles. It is assumed that an AEM feature is a major contributor to the large ESS and if it is not a requirement for the reference vehicle, then optimal design of the ESS will result in a different far smaller and less costly solution. However, the elimination of the additional capacity margin can expose the engine to drive cycle power variations that reduce the overall fuel economy. Balancing the design trade between a smaller energy storage system and more efficient

engine operation requires a sophisticated optimization methodology that is first reported here.

It is asserted in this dissertation that if there is no AEM, then the role of the ESS is that of a power filter for the engine, rather than a major source of propulsion energy for the vehicle. Based on this concept, frequency domain analysis is proposed and used because it is the classic approach for designing a filter. In this research, a bandwidth-based methodology for designing the energy storage system has been developed.

An investigation of correct Energy Storage Device (ESD) composition and ESS sizing using the low-frequency load spectrum was conducted. In the first step of the methodology, off-the-shelf battery modules and ultra-capacitor modules and combinations of the two were the subject of a parametric study which found the energy storage option with both light weight and high fuel economy. The series HEV Simulink model created by Autonomie was customized for this study to include component models of the ESS and engine and a duty ratio control strategy for the engine. In this low-frequency analysis, the power-train was excited with a 1-Hz sampled standard drive cycle. Therefore, the bandwidth of the analysis is limited to the Nyquist frequency of 0.5 Hz. The analysis compares different ESD technologies (battery cells and ultra-capacitors) and even hybridized options (i.e., combinations of the two) in terms of fuel economy and weight. It showed that there are high power battery technologies which can be candidates for further minimization analysis.

However, two constraints on the first study were recognized which prevent further minimization. The custom control strategy used in the first study had three engine operating points with pulse-width modulation (PWM) used between them to balance

power. Although this strategy successfully prevented deviation of engine operation into inefficient portions of the brake-specific fuel economy map and allowed the ESS to do its filtering job, there is a cost in that a residual energy storage capacity (which can be thought of as an unintended AEM) is required when the engine idles or is turned off to balance power. This is equivalent to the ESS supplying the low-frequency harmonics required to balance the PWM of the engine, which inflates the size of the ESS due to the significant power density in the low end of the bandwidth. To resolve this constraint, additional research is carried out that will further reduce the size of the ESS by employing a hybrid engine control algorithm that blends PWM with proportional control with the goal of zeroing the spectral energy supplied by the battery at the very low end of the power-train load bandwidth. Thus, engine power will replace battery power at very low frequency which will be used in an optimization study to shrink the size of the battery while quantifying the impact on the overall vehicle fuel economy.

To make it possible to shrink the battery by small increments of cells, it is necessary to resolve another constraint. In the parametric study done for this report, a passive ESS was considered which forced using a minimum number of cells or modules to meet the DC bus voltage requirement. This constraint adds unwanted capacity and mass to the ESS. The voltage constraint will be removed for the optimization study by replacing the passive ESS with an active ESS. An abstract bidirectional DC/DC converter model has been added to the ESS model which allows the high voltage DC bus to be mated to an independent number of series cells in the ESS. As a result, fewer cells than the minimum allowed with the passive ESS can be selected during optimization which leads to a lighter ESS.

Making the bandwidth of the engine controller (BW) a variable for use as an optimization parameter requires a hybrid engine-generator controller blending PWM with proportional control. This model has been developed which includes two levels of control. In the higher level, a state-machine with four states of engine operation is proposed in accordance with four possible driving conditions: idle, city, highway, and rated speed. The nominal power associated with each state was estimated based on standard drive cycle and vehicle specifications. The controller uses statistical tests to recognize the general behavior of the driving cycle (e.g., urban, highway, rated speed), and makes state changes as necessary. At the lower level of control, a proportional controller is developed which allows the engine-generator to follow the load with bandwidth below BW in order to zero that component of the battery current which is below BW. This strategy reduces the low frequency power variations in the ESS which allows additional size reductions as compared to the parametric study. The value of BW and the size of the battery are design variables which will be optimized with an algorithm maximizing fuel economy. A software tool to do this has been developed using the Simulink-based vehicle model and a novel optimization algorithm that calls Simulink models. Next, the design space for sizing the ESS has been bracketed between the minimum size required for acceleration and the maximum size found with a passive ESS. A Pareto Frontier, including optimized costs and fuel economy, is computed that covers the entire defined design space by using both bandwidth-based and engine duty ratio control strategies.

1.4 Organization of the dissertation

This dissertation is organized as follows: Chapter 2 introduces the concept of bandwidth based methodology. Chapter 3 presents the parametric study over different sizes of ESS either hybrid or non-hybrid which results in a hybrid electric vehicle with minimal energy storage system given the assumptions. Chapter 4 proposes an advanced bandwidth-based control strategy to actively control the bandwidth of ICE operation and this chapter also validates the performance of the controller in a SHEV sports car example. Chapter 5 achieves the Pareto Frontier, including both maximized FE and minimized EES cost, for a SHEV with limited AEM. Chapter 6 presents the conclusions of the dissertation.

CHAPTER II

BANDWIDTH CONCEPT FOR DESIGNING HYBRID ENERGY STORAGE SYSTEM OF A HEV

2.1 Introduction

The concept of bandwidth-based methodology is presented in this chapter. First, the characteristics of power-train energy sources such as Internal Combustion Engines (ICE), Fuel Cells (FC), batteries, and capacitors are compared from the aspect of frequency response. Next, the definition of bandwidth for each energy source is clarified. Then, by doing an experiment on a concept HEV, the load characteristics of a power-train is specified and transformed into the frequency domain. Analyzing this data shows the potentialfor a bandwidth based method of designing the energy sources in the power-train. At the end, the configuration of the hybrid combination of energy sources is presented in general form.

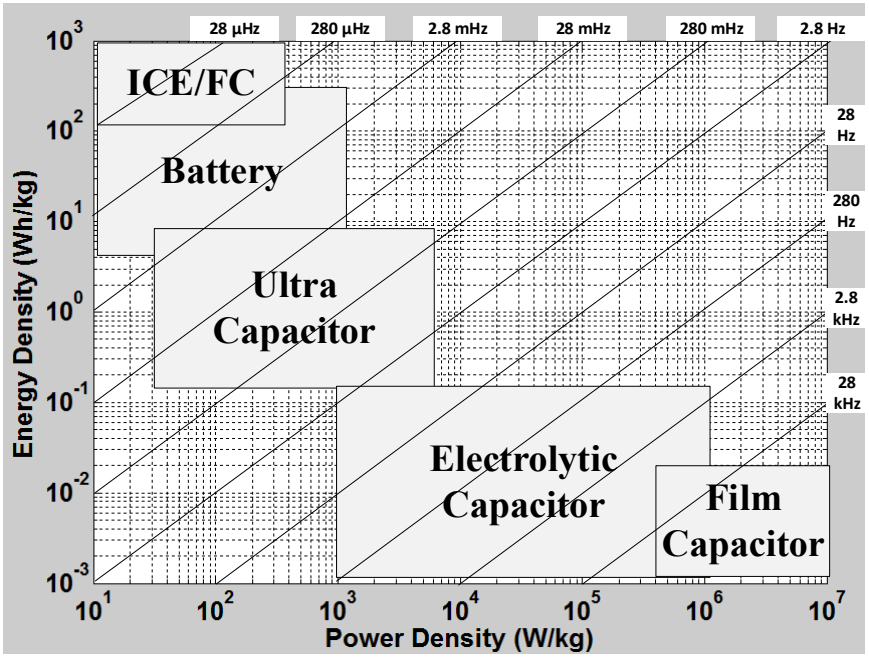

Figure 2.1 Ragone plots: energy-power specification of various energy sources. "After Ref. [40]"

2.2 Bandwidth of energy sources

"Series" is a type of architecture for an HEV power-train in which the engine, generator, and motor are placed on a direct energy line. The generator transfers the ICE mechanical power to the DC power bus and the motor transfers the electrical power available on the DC bus to the final drive axle and wheels. The ESS is on the DC power bus and delivers/absorbs the energy to/from the motor. In order to design the power train for a series HEV (SHEV), different components are available. In a Ragone plot (see Figure 2.1), energy sources are characterized by the energy and the power they can make available to a load. As shown on the plot, Internal Combustion Engines, batteries, and possibly capacitors are available energy sources. The ICE can also be replaced with a Fuel Cell. The power to energy ratios are shown by cross lines in units of Hertz which,

while not exactly representing the efficient bandwidth, to some extent indicates the available frequency range of operation for each energy source. In the following sections, the definition of bandwidth is reviewed for each potential energy source in the power train.

2.2.1. Bandwidth of ICE

In a conventional vehicle, to meet the entire bandwidth of power-train load, the operating point of the ICE may vary over the displayed map in Figure 2.2. Therefore, the overall efficiency corresponding to the efficiency of the average load is expected.

The white spot on the ICE efficiency map represents the efficiency at average load when a driver drives in an urban area. In contrast, in a SHEV with some available ESS, the fixed operating point like the one displayed as a dark spot on the ICE efficiency map can be accomplished. The dark spot with P_{GBE} power and η_{BE} efficiency is the ideal operating point for the ICE because the largest efficiency of 35% is achieved. In other words the bandwidth of ICE operation–meaning the variation of the ICE power in the time domain–is controllable from DC to the full bandwidth of the power-train load.

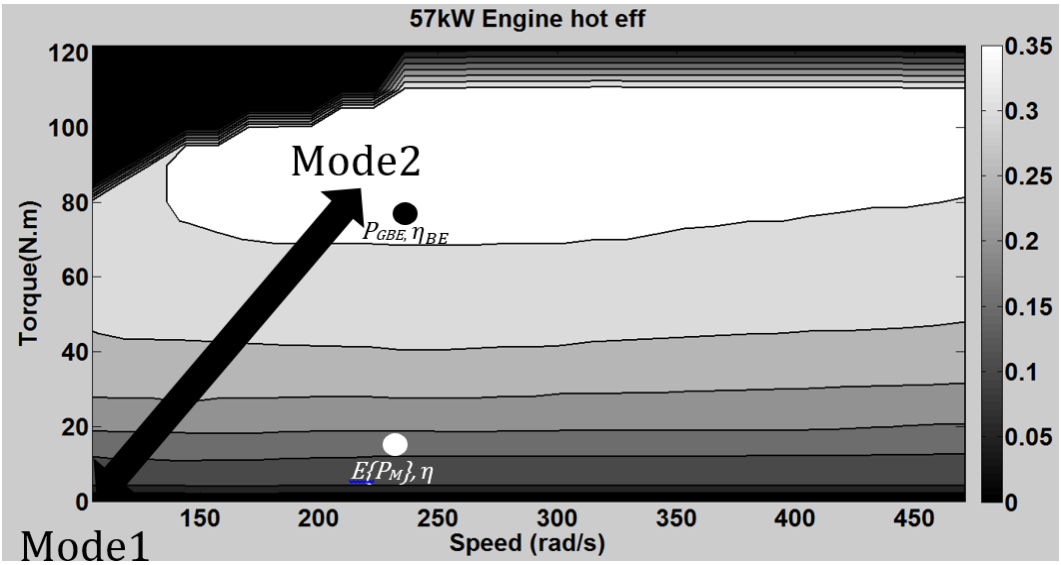

Figure 2.2 Engine operating point on engine efficiency map

2.2.2 Bandwidths of battery/capacitors

The battery can be modeled simply with a nonlinear capacitor, C_X, and an internal resistance, R_{DC}, like shown in Figure 2.3. The capacity of the nonlinear capacitor is proportional to the capacity of the battery in Ampere hour. Depending on the bandwidth of application, series RC networks can also be added in order to model the transient behavior of the battery, which is not shown in the figure. A linear capacitor can be estimated as a surrogate for the nonlinear one, by linearizing around a specific operating point. Therefore, the battery model can with the assumptions given be represented as a simple linear RC network. Figure 2.4 also shows the first order model of a typical capacitor such as an ultracapacitor which is a simple RC network.

Because batteries and UC have similar models, the following analysis is carried out on Figure 2.4 to explain the concept of bandwidth for both. In the Laplace domain, the transfer function of the ratio of voltage drop across the resistor to output voltage and

the transfer function of the ratio of capacitor voltage to the output voltage can be expressed by:

$$\frac{V_R(s)}{V_{out}(s)} = \frac{RCs}{1 + RCs} \quad (2.1)$$
$$-1)$$

$$\frac{V_C(s)}{V_{out}(s)} = \frac{1}{1 + RCs} \quad (2.2)$$
$$-2)$$

When AC power is requested at the output of the RC branch, the ratio of voltage across the capacitor to the output voltage varies depending on the frequency of the applied power signal. For lower frequency this ratio is almost unity and no drop in magnitude is observed; however, at $f = \frac{1}{2\pi RC}$, the so called -3 dB cutoff frequency, the magnitude across the capacitor is reduced by $1/\sqrt{2}$. It is natural that for the same magnitude of power (the same AC current and AC voltage), when the frequency increases, the capacitor voltage decreases; consequently, the resistor voltage increases to meet Kirchhoff's Voltage Law. Therefore, when the RC branch represents an energy storage device such as a battery or an UC, operating beyond the -3 dB cutoff frequency incurs considerable energy dissipation and as a result the efficiency of energy storage drops significantly. The three different lines in Figure 2.5 show this relationship using Bode plots of different RC branches. These RC branches are Bode plots of the $\frac{V_C(s)}{V_{out}(s)}$ transfer function for a typical high power battery, a high energy battery, and an UC.

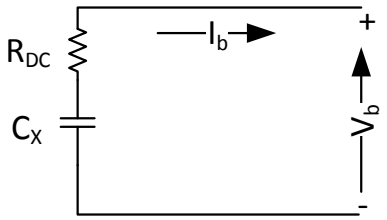

Figure 2.3 Battery first order model

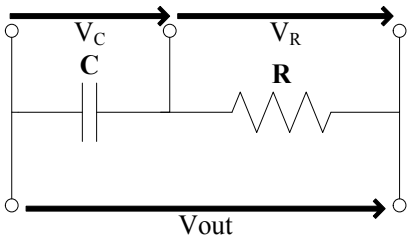

Figure 2.4 Capacitor first order model

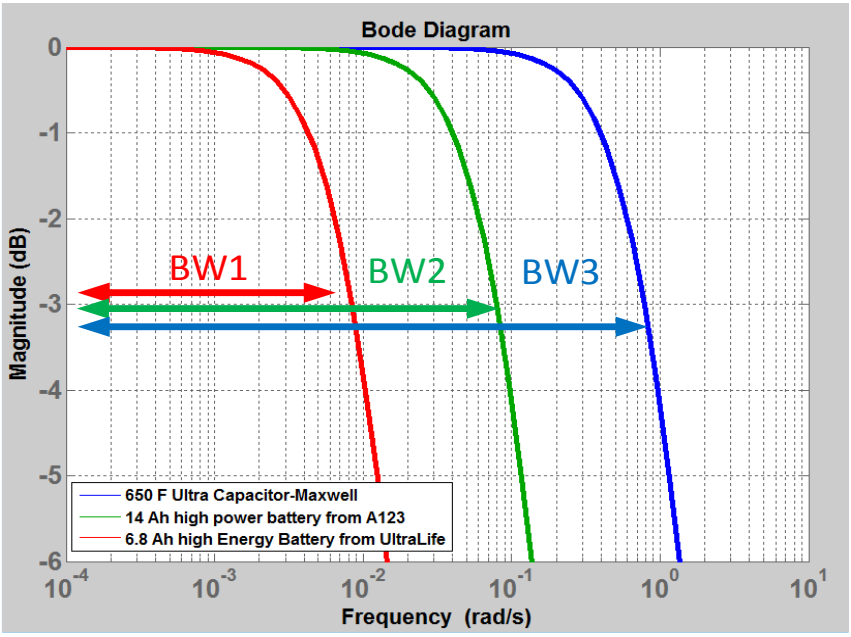

Figure 2.5 Bandwidths of a high power battery, a high energy battery and an UC

2.3 Bandwidth of the power-train load

The United States Environmental Protection Agency (EPA) designs standard drive cycles which simulate city (UDDS), highway (HWFET), and high acceleration aggressive (US06) driving conditions. They are usually vehicle speed profiles sampled at 1 Hz over a certain period of time. Since a real drive schedule is random, the published drive cycles are only examples useful to show the hypothetical performance of a vehicle.

They also do not specify the full bandwidth of the load because of limited sampling rate. In reality, the full bandwidth of instantaneous power on the DC bus can be determined via measurement with sufficient sampling rate. The data illustrated in Figure 2.6 through Figure 2.8 were collected empirically on a chassis dynamometer using a series-hybrid-electric Chevrolet concept car built by the Center for Advanced Vehicular Systems at Mississippi State University for the Department of Energy (DoE) EcoCar competition. The MATLAB Fast Fourier Transform (FFT) function is used to transform the time-domain data into the frequency domain.

The displayed instantaneous power is represented in Fourier series form by summation of a DC value and sinusoidal waveforms. The amplitudes and frequencies of sinusoidal waveforms are estimated by Fourier transform. Lengths of arrows in Figure 2.6 represent magnitudes and the locations of arrows show the frequencies in the following Fourier series equation.

$$P_{DC-bus}(t) \approx P_0 + \sum_{n=1}^{\infty} P_n \sin(\omega_n t + \varphi_n) \quad (2.3)$$

Where $\omega_n = 2n\pi\Delta f$; $\Delta f = \frac{f_s}{k}$; f_s is the sampling frequency; and k is the number of sampled points. In this case, $f_s = 40\ kHz$ is used for measurement.

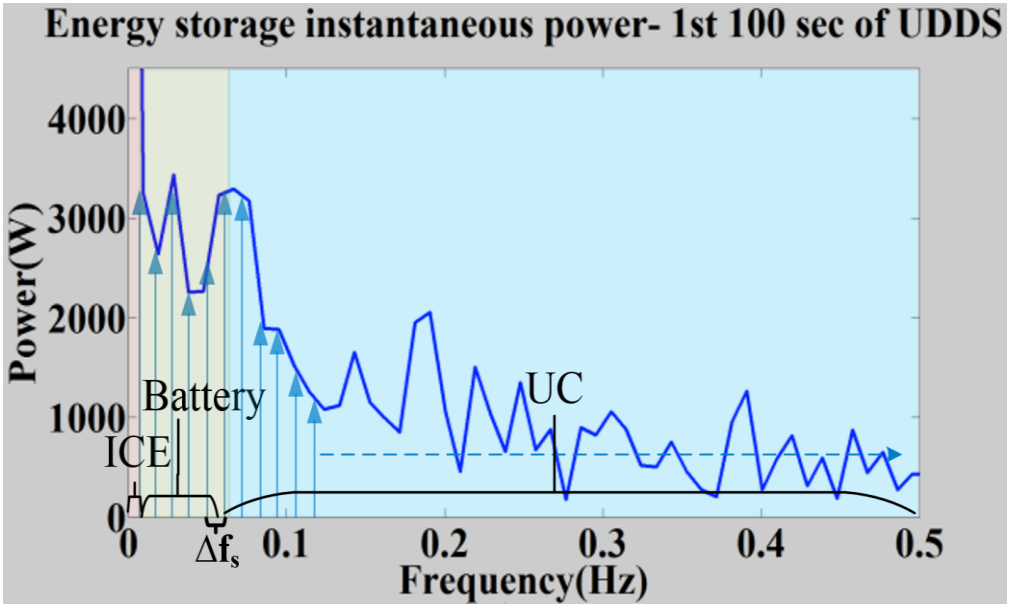

Figure 2.6 Instantaneous power for UDDS drive cycle (result of test on EcoCar1 vehicle); frequency: 0 to 0.5 Hz.

Note: Lengths of arrows represent magnitudes and the locations of arrows show the frequencies in the Fourier series equation (2.3).

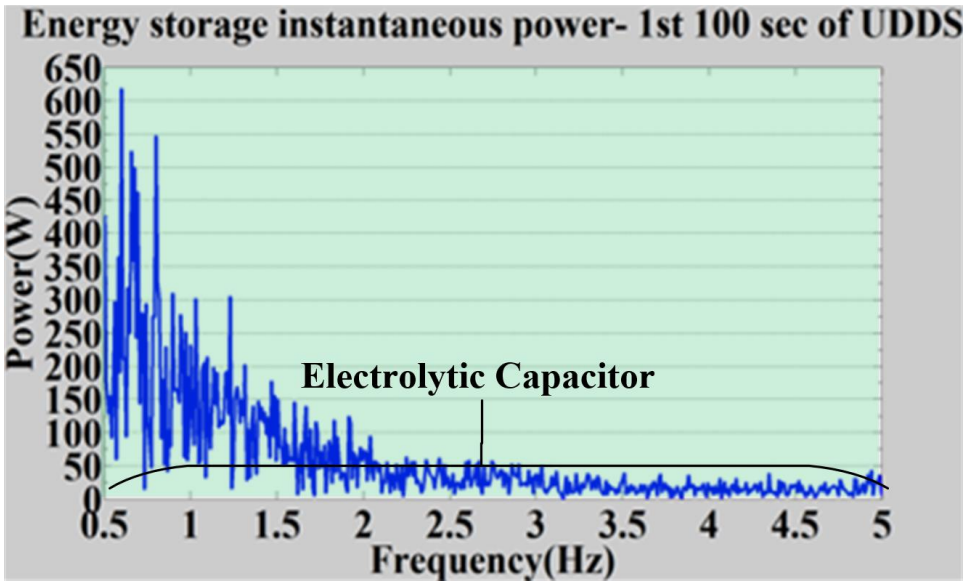

Figure 2.7 Instantaneous power for UDDS drive cycle (result of test on EcoCar1 vehicle); frequency: 0.5 to 5 Hz

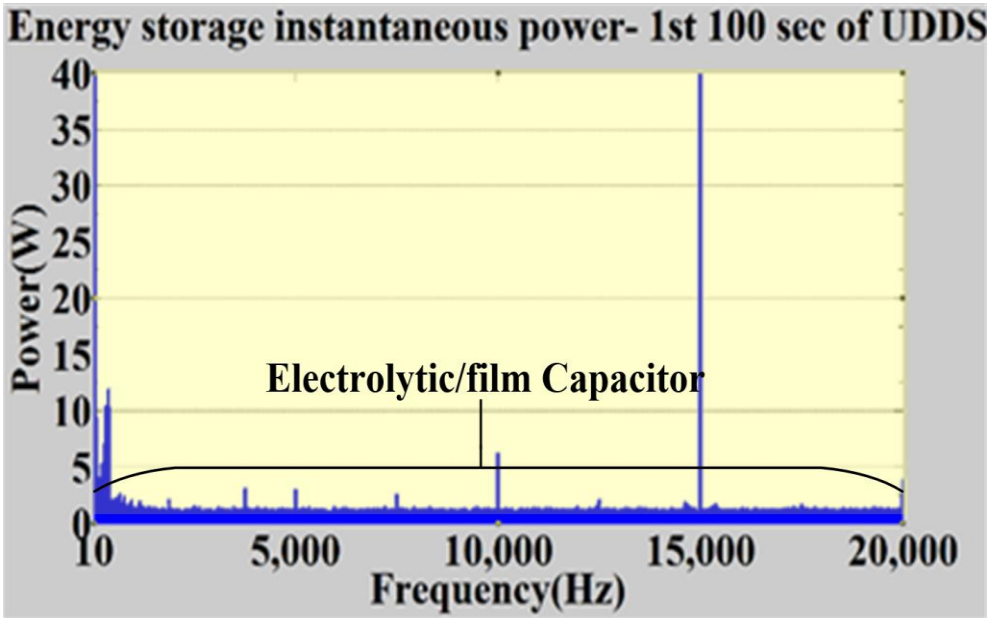

Figure 2.8 Instantaneous power for UDDS drive cycle (result of test on EcoCar1 vehicle); frequency: 10 to 20000 Hz

Therefore, instantaneous power at the output of the energy sources is a complex time-domain waveform represented in the frequency domain with a wide bandwidth. Hence, in order to design an efficient HESS for HEV's, suitable energy sources should be selected by linking the bandwidth characteristics on a Ragone plot/Bode plot to the load bandwidth formulated in (2.3) and displayed in Figures 2.6 to 2.8. Therefore, referring to Figure 2.1 and 2.5, an ICE is efficient for DC, a high energy battery is good up to a few mHz, high power batteries are typically useful for less than tens of mHz; UC are suitable for a frequency band of tens of mHz to hundreds of mHz; Electrolytic capacitors are efficient for a frequency band of hundreds of mHz to a few kHz; and film capacitors are good for a few kHz to tens of MHz.

In a generalized form, the HESS schematic of Figure 2.9 is proposed where three capacitor branches are for modeling the film, electrolytic and UC; and two branches represent two different battery chemistries (one power dense and the other energy dense). Full bandwidth traction power loadings are represented by a current source at the output. A dc current source also is shown on the left to model the engine operating point; a small number of discrete operating points are considered for the engine to improve fuel economy (refer to section 2.2.1). In Figure 2.9, UC and battery values are shown referred to the high-voltage bus taking into consideration the possibility of using dc/dc converters to interface to the bus.

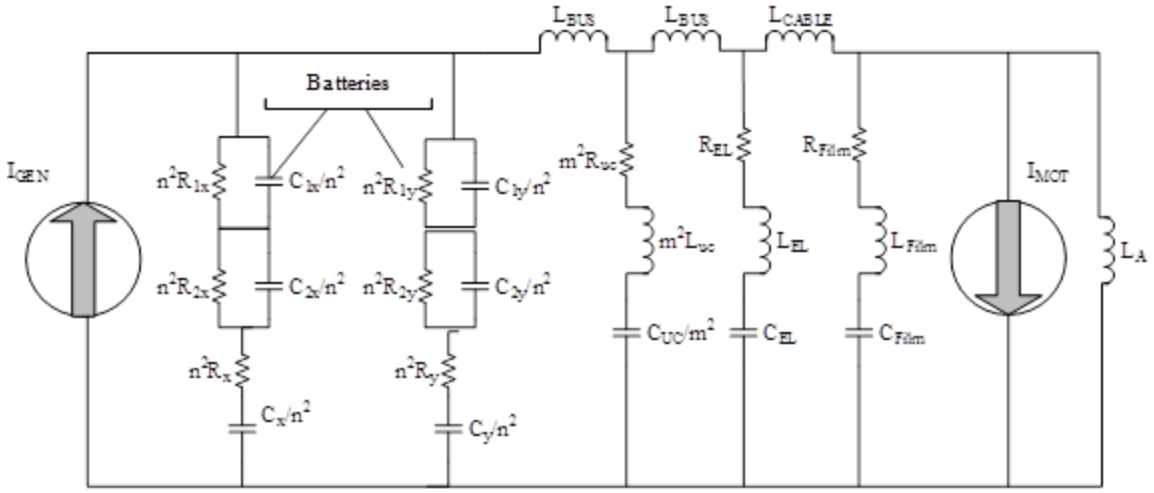

Figure 2.9 Overall diagram of HESS

The methodology of bandwidth-based HESS design is based on two distinct methods, one for the frequency band in Figure 2.6 and one for the frequency band shown in Figure 2.7 and 2.8. However, in this document, the concentration will be on the former which includes sizing and operation problems of energy sources such as ICE, battery, and UC. For the latter, the results are reported in [41] and are not discussed in this document. In the reported work [42], the impacts of designing appropriately sized high bandwidth energy sources–such as electrolytic and film capacitors–on the power loss of the ESS including high energy battery and UC are described. In Chapter 3, using a duty ratio control strategy, the proportional control of the ICE output is avoided. Through a parametric study to size a passive HESS to achieve the highest fuel economy, the best chemistry and size of passive ESS are found. In Chapter 4, an advanced bandwidth-based control strategy will be developed that extends the bandwidth of the ICE in favor of battery minimization.

CHAPTER III

HESS DESIGN ANALYSIS: PARAMETRIC STUDY

3.1 Introduction

Since 1900 when Dr. Porsche built his HEV [13] until now many different HEV designs have been proposed. During these years, depending on petroleum price and policies [43] [44] [45], strategies for building commercially successful HEV's have changed. In recent years, various levels of hybridization in the form of micro, mild, medium and full HEV have been produced [46]. Only the full HEV in the list of possible choices (hereafter called HEV in this text) has full power assist from the ESS and can have a variable all-electric-mode (AEM). The Plug-in HEV (PHEV) and the pure battery electric vehicle (BEV) are capable of absorbing energy from the electric grid, and are in production. Although electrified vehicles in general with high fuel economy look very attractive, they represent only around 4% of the US vehicle market in 2013 [47]. One reason is electrified vehicles typically have large and costly ESS that also represent the biggest future durability issue not found on a conventional vehicle with attendant cost of ownership impacts. The parallel HEV, with a smaller ESS, is not surprisingly the major contributor to electrified vehicle sales with an almost 90% share. The conclusion is that a smaller ESS leads to potentially greater consumer acceptance. Yet higher consumer acceptance might be expected by delivering larger vehicles with fuel economy significantly better than the alternatives.

Available manufactured HEV's mainly rely on the parallel HEV power-train which couples road load variations into the engine which results in a less optimal utilization of the engine efficiency map by the engine control strategy. However, in a series power-train, the engine is mechanically decoupled which enables greater independence between the road-load variations and the engine control strategy. With an appropriately designed ESS there is the opportunity to maintain the engine performance within a narrower and efficient region of the engine map regardless of road load variation.

In this chapter, first, using existing validated power-train simulation software (Autonomie), a reference series-power-train architecture HEV is modeled. Then, the first analysis of a bandwidth based methodology is developed which leads to a straightforward method for the power-train model to be used to conduct a selection study of the two low frequency components (battery and UC). In the study reported in this chapter, proportional control of the ICE is avoided.

3.2 Reference vehicle specifications

Figure 3.1 illustrates the architecture of the reference vehicle in which the Subaru EE20 diesel engine [48] is the main source of energy coupled with one axial flux permanent magnet (AFPM) generator, the YASA-400 [49]. The HESS is charged by the generator and operates as an intermediate energy buffer for a traction motor, which is another YASA-400. The power rating and other specifications of the main components of the power train are shown. In Autonomie, each component is defined by a behavioral model in the Simulink environment and Autonomie couples these models together to run an overall model of the vehicle over selected drive cycles (Figure 3.2). An existing series-

hybrid mid-size vehicle model is modified for this study. For engine modeling, a validated Prius model available in Autonomie is scaled up to 110 kW to reflect the ratings of the Subaru engine. For the generator and motor, the YASA-400 efficiency map data and other specifications of the machine are extracted and used for modifying an available machine model in Autonomie. Next, a modified control strategy is applied in state flow environment (Figure 3.3). Three fixed engine operating points are used for the engine control strategy. They are (1) an idle mode (no load); (2) a high efficiency operating point, and (3) a wide open throttle (WOT) operating point. One of the three operating points is selected by the controller depending on battery state of charge (SOC). The idle operating point is selected when the battery SOC is high enough to provide energy to the propulsion motor for a while. If the SOC falls below the first low threshold, mode two is selected to recharge the battery to the first high threshold; in this way the engine operates at an efficient or high Brake Specific Fuel Consumption (BSFC) operating point. If the SOC goes below a second low threshold, operating point three is activated to supply the load with maximum power from the engine which simultaneously charges the battery back to a second high threshold.

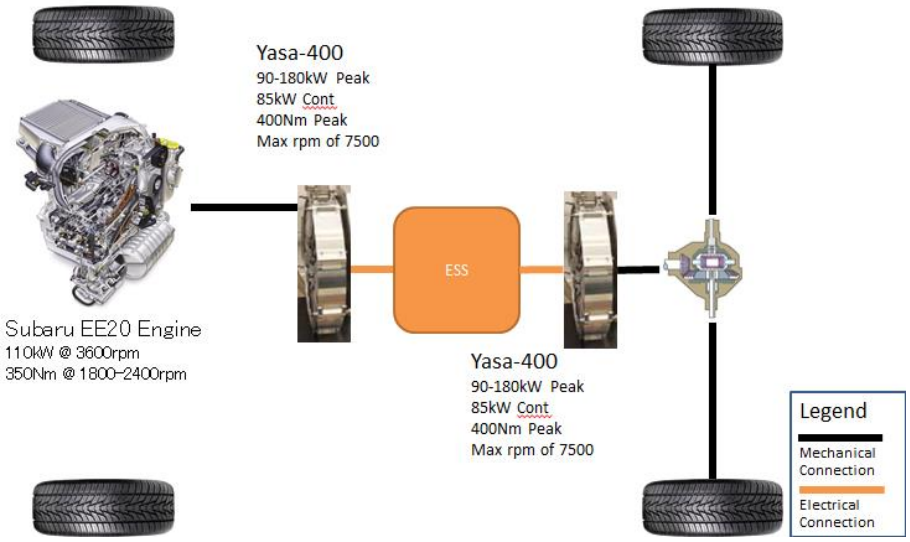

Figure 3.1 The series-hybrid architecture of the reference vehicle

Figure 3.2 Series architecture of the reference vehicle in Autonomie

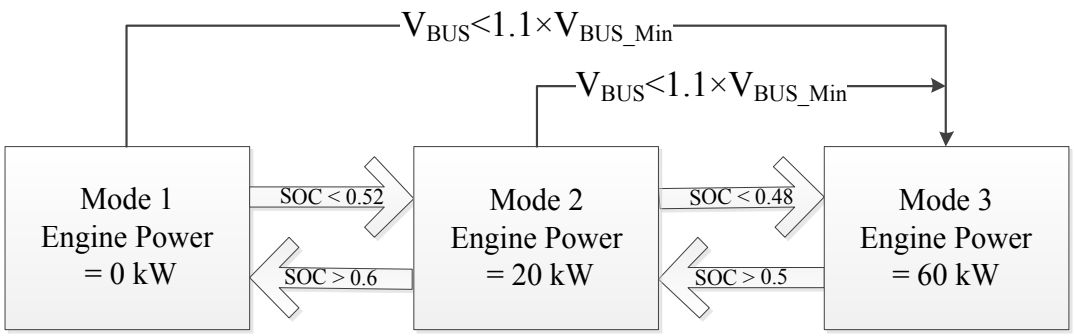

Figure 3.3 Control strategy state flow diagram

3.3 Parametric study for selecting light and efficient ESS

The cost of the battery in an HEV is still high, so any solution for selecting a smaller capacity, lighter battery reduces the total cost of the vehicle. A HESS which ends up with a minimum battery size is called a "battery light" solution. For minimizing the size, one method is to use optimization algorithms. However, because of power-bus voltage constraints in the passive configuration, the size of the battery or the UC string is not a continuously variable parameter which can be set as an optimization variable, but a discrete variable instead. One efficient method for testing for alternatives is to carry out a parametric study over available options which meet the voltage constraints. In this study, a parametric study has been carried out for finding the best available ESS solution. The basic idea is to vary the number of parallel strings and compare fuel economies of the vehicle. Using every possible practical combination of strings from Table 3.1, three possible configurations of battery only, UC only, and combined battery and UC are compared. The upper range of dc voltage of the motor controller recommended for the YASA-400 is 400 V. This is the limiting factor which determines the maximum high line voltage of the ESS. Two Gen4 motor/generator controllers from Sevcon [50] are used to

control both the YASA motor and generator. Battery or UC behavioral Simulink models in the Autonomie library were updated with information from Table 3.1. In the next two sections, a commercially available string of UC and the commercially available strings of batteries are examined, respectively.

3.3.1 One string of UC

Referring to the bus voltage constraint, one string of UC can be sized. From the Ragone plot and also from data available in the UC manufacturers' data sheets, 1 Hz is the assumed bandwidth limitation of UC's. Therefore, the largest demand at 1 Hz is considered as a reference for sizing one string of 400 VDC UC. Among standard drive cycles, US06 is the most aggressive with harsh accelerations and decelerations. Therefore, the power draw from the motor associated with the US06 drive cycle, which contains a peak power of almost 100 kW, is used to size the UC bank.

Maxwell UC cells are used in this study, so the manufacturer's instruction for finding the number of cells and the capacitance of cells is used. In (3-1), WUC is the energy requirement which in this case is 30 Wh. Ur is the high line voltage set to 384 VDC because the 384 VDC is the maximum voltage that can be built with both available battery modules (100% charged) and available UC modules (100% charge). This maximum voltage is the largest that the passive connection of available components can achieve while remaining below the maximum voltage of 400 VDC imposed by the motor drive. K is the factor which determines the ratio of low line to high line voltage. K = 0.5 is the value recommended by the manufacturer [51]. From (3.1)

$$W_{UC} = \frac{C_0 U_r^2 (1 - K^2)}{2(3600)} \quad (3.1)$$
$$-1)$$

1.95 F is computed for C_0; however, considering the manufacturer's recommended margin and also based on available cells (650F, 2.67V), the overall capacitance of 4.51 F is the closest minimized option. 144 650-F cells are used in series to create one string of 384 VDC UC. In Table 3.1, additional specifications for the string of UC are listed.

3.3.2 One string of batteries

Lithium-ion chemistry is recognized as one of the best solutions for current and future EVs and HEVs because of its characteristic high energy and power density. Also, nickel metal hydride (NiMH) batteries are widely used by manufacturers [42]. There are several manufacturers which make Li-ion and NiMH cells; however, the number of options available in the form of modules or packages which have built-in cell balancing function are limited. Selected for consideration here are NiMH prismatic cells from Panasonic used in the Prius, ANR cylindrical cells from A123, and AMP14 prismatic cells from A123 because they come in packaging with balancing specifications. For each of these three options the specifications of the lightest 384 VDC string are shown in Table 3.1. The lightest strings have the lowest costs, and obviously the lowest capacity, so if more power or energy is required one or more strings with the same specifications must be added in parallel. Therefore, battery strings listed in Table 3-1 are the smallest units which fulfill the voltage requirement. When evaluating the battery options, 384 VDC is the targeted maximum voltage of each string when it is fully charged because the Gen4 controller can be used to charge to 100% SOC. Having identical voltage ratings for

the battery and the UC strings allow them to work in parallel using the full SOC range of both.

Table 3.1 UC and batteries strings

Specifications	UC#1	ANR#1	AMP#1	NiMH#1
Cell maximum voltage (V)	2.83	3.6	3.6	1.55
Cell nominal voltage (V)	2.67	3.3	3.2	1.2
Number of cells in modules	6.0	26/27	26/27	6.0
Number of modules in series	24.0	4	4	41.0
Total number of cells	144.0	106	106	246
Nominal Voltage (V)	384.0	349.8	339.2	295.2
Maximum Voltage (V)	407.7	381.6	381.6	381.3
Estimated Cells Mass (kg)	-	8.1	54.06	41.82
Estimated Package Mass (kg)	30.2	16.1	108.12	83.64
Energy capacity (kWh)	-	0.87	4.75	1.9
Continuous power (kW)	14.6	17.5	51.2	26.53
Power in 1 sec (kW)	< 130	>42	>112.15	-

3.3.3 HESS parametric study results

Figure 3.4 shows the result of the parametric study performed by comparing the combined fuel economies of the vehicle with different ESS's. Combined fuel economy is defined as a weighted average of 55% city driving (modeled with the UDDS drive cycle) and 45% highway driving (modeled with the HWFET drive cycle). Fuel Economy (FE) is the ratio of traveled distance in miles and consumed fuel in gallons. On the horizontal axis the type and number of strings is shown; as an example "ANR#2UC#1" represents two parallel strings of ANR cylindrical cells from A123 in parallel with one string of UC from Maxwell. In the ANR case, it is shown that when the number of parallel strings goes up, the fuel economy goes up as well until a peak happens at five strings.

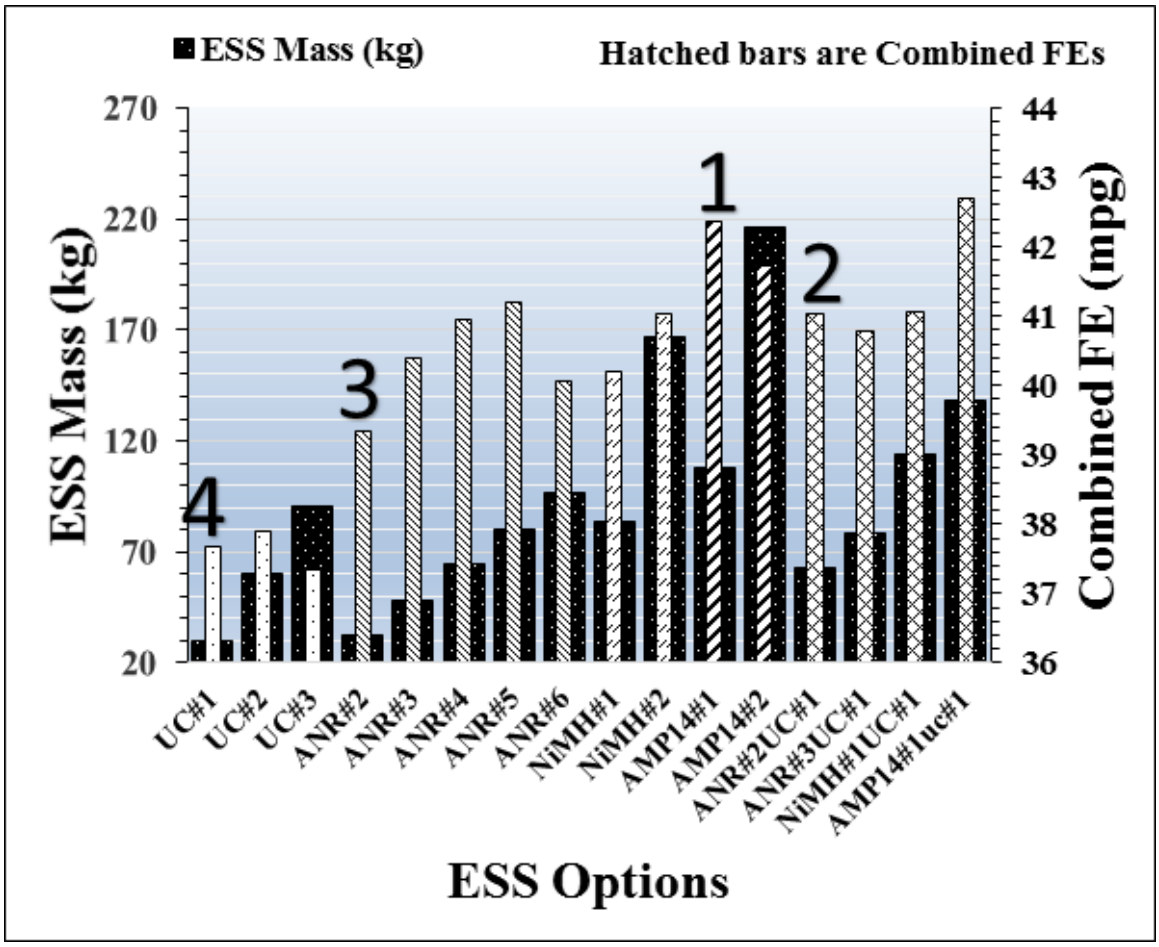

Figure 3.4 Combined fuel economy for possible ESS options for the reference vehicle 110-kW power-train

After this point, the negative impact of added weight on fuel economy outweighs the benefits of extra power and as a result a reduction in combined fuel economy is observed. This trend is clearly seen with the first three UC options.

However, the option with the highest fuel economy is not necessarily the best solution because the additional cost of adding a string must be considered. Therefore, there is always a tradeoff between increasing fuel economy and minimizing the cost and weight of the HESS. From Figure 3.4 it can be argued that it is not worth investing

money for additional strings to achieve only one MPG of additional fuel economy. Also given the minimal AEM strategy pursued in this research, a lighter, less costly battery option is desired if fuel economy is not affected too much. Pursuant to this argument, four options are selected for further study; these options are numbered one through four in Figure 3.4.

In a series HEV where the role defined for the battery is filtering, increasing the battery bandwidth also increases the fuel economy. The battery options in Table 3.1 are in the class of high power density where higher bandwidth is available. Among these options ANR and AMP respectively cover the lowest and highest bandwidth. The following analysis will assist understanding the results in Figure 3.4 achieved for the hybrid cases. In [34], the ratio of magnitude of battery current to the magnitude of load current for a passive HESS is derived as (3.2) below:

$$|H_C(j\omega)| = \sqrt{\frac{1 + (\omega C r_C)^2}{1 + \left(\omega C (r_B + r_C)\right)^2}} \tag{3.2}$$

Where C is the UC capacity, r_B is the battery resistance, and r_C is the UC resistance. In the ANR#2UC#1 case, by drawing the bode plot of (3.2), the cut-off frequency of UC filter is found to be 0.019 Hz. Therefore, referring to Figure 2.6, the more significant portion of the power spectrum is filtered by the UC, which has lower internal resistance. This explains why the hybridized ANR#2UC#1 case is more successful than other hybridized options. Similar analysis of the AMP#1UC#1 case shows the UC filters the portion above 0.15 Hz, which, again referring to Figure 2.6, is

not a significant portion of the power spectrum. This explains why the pure AMP ESS inherently has the better performance per weight as compared to its hybridized version.

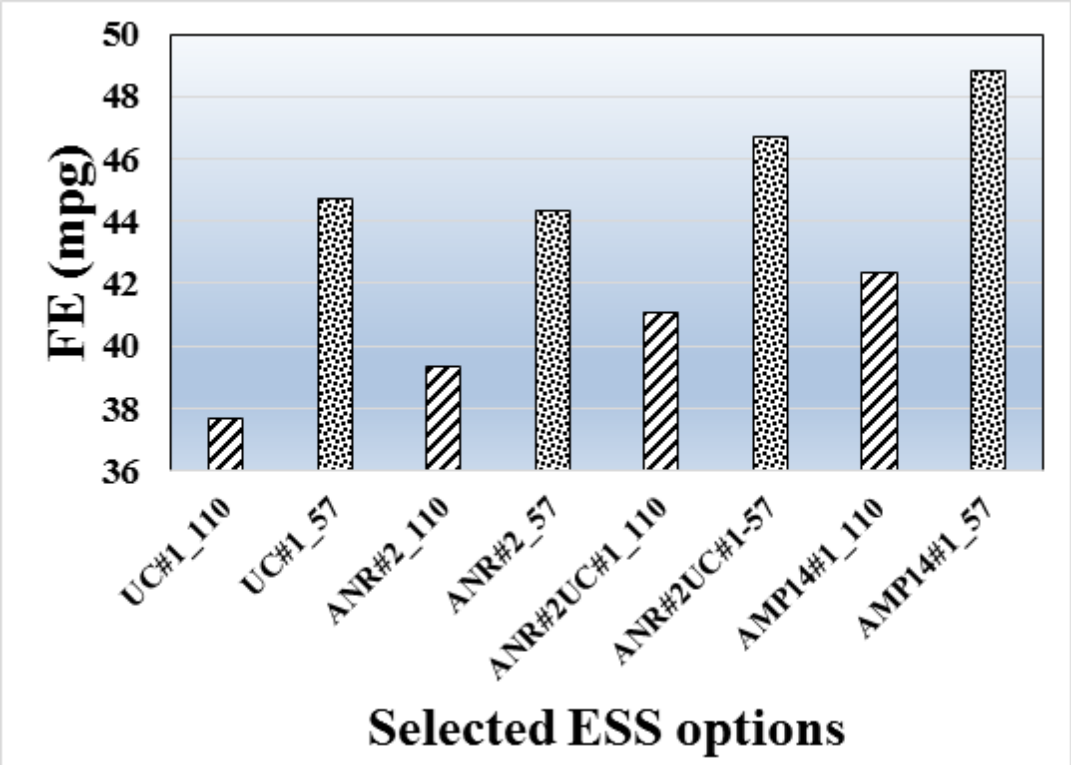

Figure 3.5 Combined fuel economy for best ESS options – 110 kW reference vehicle and 57 kW reference vehicle

For the reference vehicle specification, the average power of the UDDS and HWFET drive cycles are around 4 kW and 10 kW respectively. A gradebility requirement of 30 kW is also considered for this vehicle. Therefore, a 110-kW engine with continuous power of 55 kW is over-sized. Although the control strategy in this car is based on duty cycling the engine with a fixed high efficiency operating point (20 kW),

the corresponding BSFC for the same fixed power is higher when a smaller engine is used.

Figure 3.5 compares combined fuel economies for the assumed Subaru 110-kW engine with the Prius 57-kW engine. For every option the fuel economy increases significantly with the smaller engine, so the results will clearly improve by reducing the engine size to better match the average-power required by the reference drive cycles with the reference vehicle. This is considered a major objective of the battery light option, namely to match average power required by the drive cycle with the most economical production of that average power from the engine. In this strategy, the role of the HESS is to minimize power cycling the engine, not to supply all electric mode.

An issue arose with the pre-defined definition of a combined battery and UC HESS in Autonomie. In the standard Autonomie library a power converter is used to integrate the UC to the common bus. The scope of the study in this chapter covers only passive integration of all energy storage components to the common bus and so it was decided to forego the pre-defined Automomie HESS model in favor of a custom model created in Simulink and manually integrated into the Simulink model that Autonomie otherwise creates automatically. The HESS model reflecting only passive interconnections (i.e., without power converters) is shown in Figure 3.6 [43]. The results shown for the hybrid ESS (UC plus battery) in both Figure 3.4 and Figure 3.5 are achieved using the custom Simulink model.

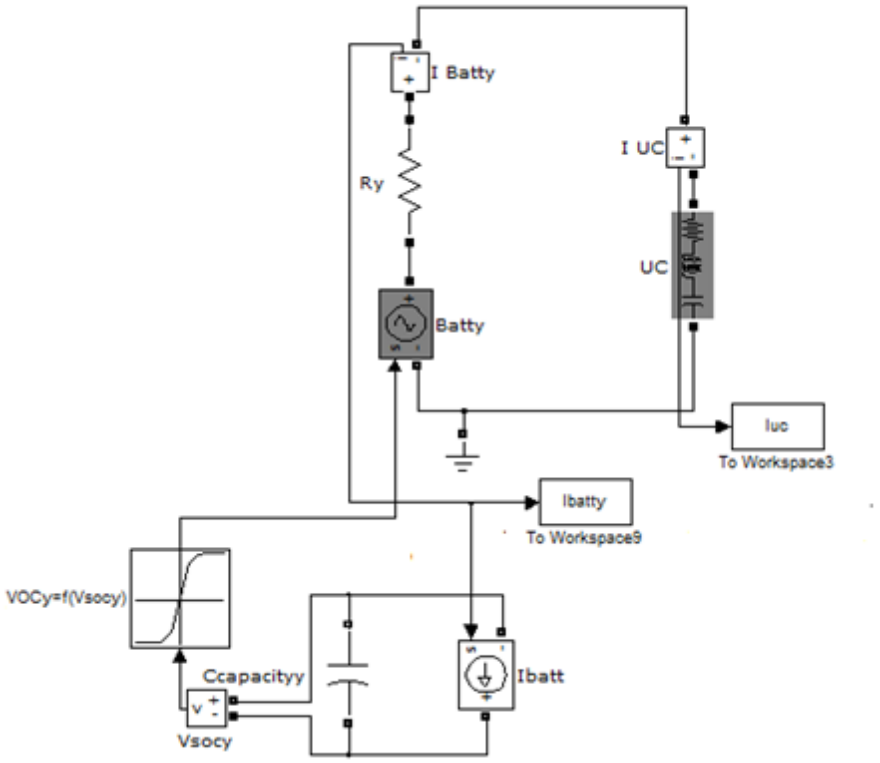

Figure 3.6 ESS power Simulink model

3.4 Experimental work

A test apparatus or "emulator" representing the reference vehicle in Fig. 3.1 (the reference vehicle in this chapter) has been built for design validation as shown in Fig. 3.7. The emulator has been driven on the full chassis dynamometer at the Center for Advanced Vehicular Systems (CAVS) at Mississippi State University with results shown in Fig. 3.8 to Fig. 3.10.

The ESS prototype is the battery pack built with AMP14 cells which provides energy to the YASA-400 drive. The 320-V battery pack includes four 80-VDC AMP14 modules from A123. The overall capacity of the pack is 4.5 kWh. The charging capacity

of the battery pack prototype determines the engine operating point, which in this case is identical to a duty ratio control strategy. For this battery pack, 20 kW is a safe charging operating point; therefore, the engine controller operates using pulse width modulation between 20 kW and almost zero power while in the idle mode. An EE20 110-kW Subaru diesel engine is used for this experiment. In simulation this engine is modeled by a scaled up version of a 66-kW Volkswagen diesel engine.

Figure 3.7 Emulator set up for testing SHEV design on Dynamometer.

A stock microprocessor based controller from Woodward with instruction speedup to 80 MHz is used. “Speedup” is a metric for relative performance improvement when executing a task. The programming environment is Matlab Simulink and all

debugging is done with Woodward MotoTune software. The control of the emulator is implemented using three operator inputs, a system state machine, and several outputs. The operator commands the start of the engine via a digital signal using an external switch and commands a positive and negative acceleration via accelerator and brake analog inputs, respectively. The system state machine tracks the state-of-charge (SOC) of the battery and whenever the SOC falls below a minimum threshold it commands a constant power by commanding the generator using a controller area network bus (CANbus) to apply an opposing torque on the engine and regulating the engine speed via a (0V-5V) analog throttle signal. The state machine returns the engine to idle and the generator to no load when the SOC rises above a maximum threshold.

The emulator has been driven on the dynamometer for 282 s over a UDDS drive cycle. Vehicle power losses, rolling resistance, and aerodynamic drag significantly affect the traction power at the output of the YASA-400 motor.

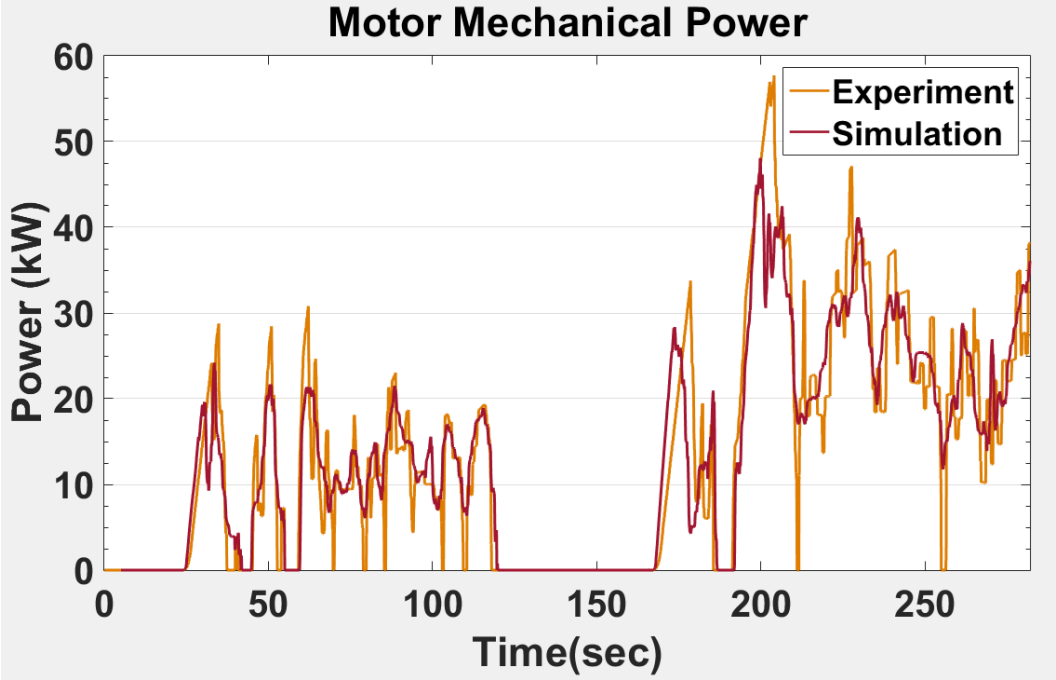

Figure 3.8 Traction power at the output of electric motor.

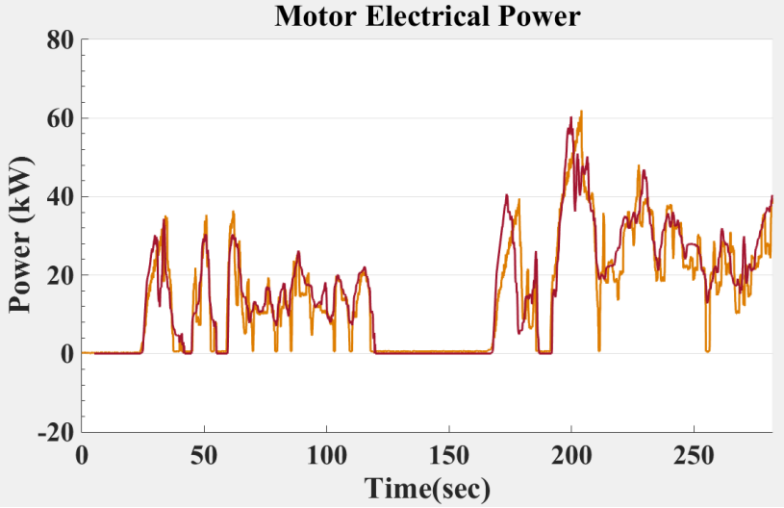

Figure 3.9 Traction power at the input of electric motor.

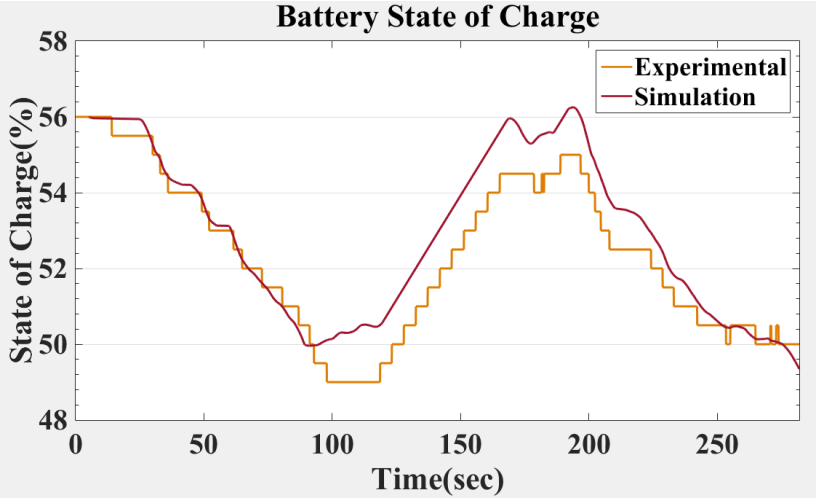

Figure 3.10 Battery state of charge in percent.

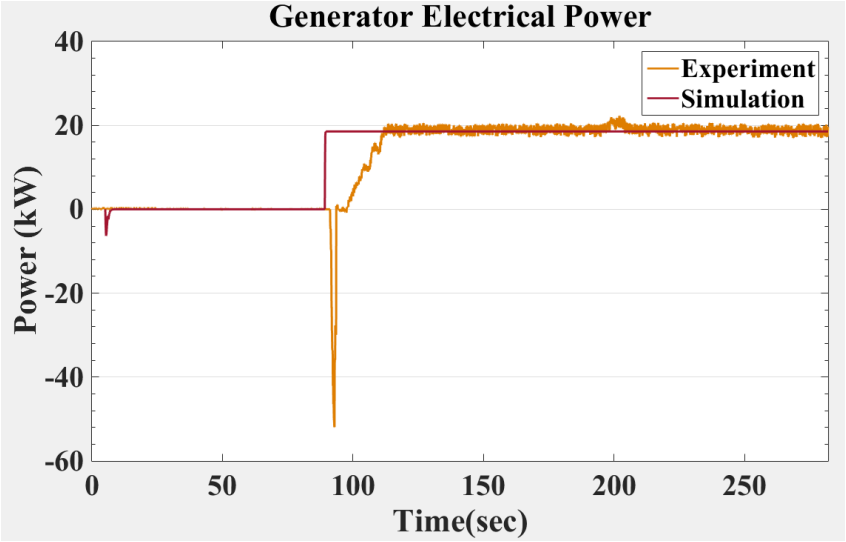

Figure 3.11 Generator Electrical power.

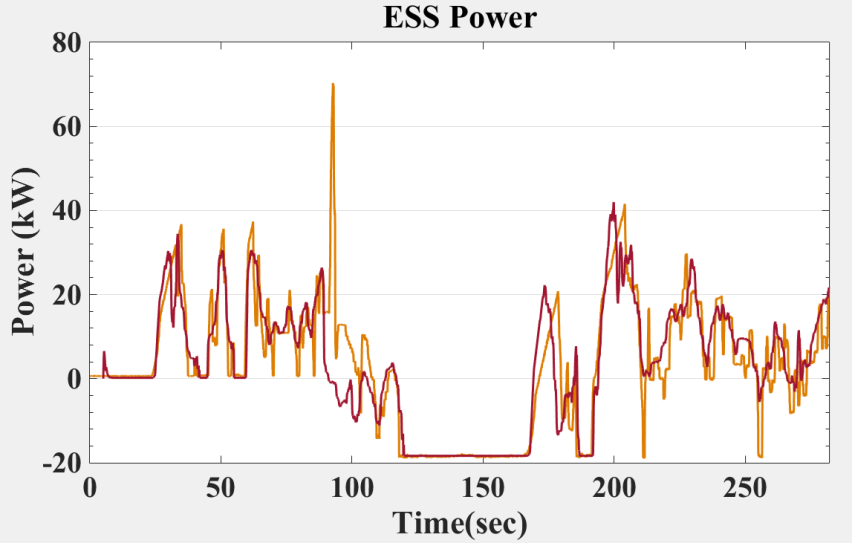

Figure 3.12 Energy storage power.

In this test, rolling resistance and drag coefficient are tuned in the simulation environment to match the traction output energy for both cases (see Appendix I). The two waveforms in Fig. 3.8 have the same energy, but because the simulation model benefits

from having an ideal algorithm for tracking the drive cycle, the power waveform is smoother. The driver's human error and accelerator/brake pedal sensitivity are responsible for the harsher acceleration and deceleration in the experimental case. The low and high SOC thresholds are 50% and 60% respectively. Electrical representation of the requested power in the urban drive cycle is observed in Fig. 3.9 at the DC input of the motor. By comparing SOC (Fig. 3.10) with SOC low and high thresholds, the controller distributes the load between the generator and ESS. For almost 100 s, the ESS solely provides the load in all electric mode (see Fig. 3.12). After the SOC reaches the minimum threshold of 50%, the controller opens the engine throttle and the generator starts transferring energy to the DC bus (see Fig. 3.11). Until 200 s, the engine is charging the battery to its maximum threshold. However, before the SOC maximum is reached, a heavy load is requested, so the ESS joins the engine to provide the load. In the worst case in Fig. 3.10, the SOC of the simulated model follows that of the experiment with less than 3% error. Battery power is also compared which is in reasonable agreement (Fig. 3.12). The power profile from the battery clearly shows that the battery acts like a filter allowing the engine to operate at an efficient operating point.

Fig 3.13 compares the overall efficiency of each component in experiment and simulation. The differences in engine efficiencies can be explained by the use of a different model in simulation compared to the EE20 diesel model. However, because in this chapter and the rest of the document a validated model of a 57-kW gasoline engine is used, this difference will become minimal. The fuel consumptions in both cases also have been measured and computed. In the experiment 0.34 kg of diesel fuel is consumed. In the simulation 0.33 kg diesel fuel is consumed.

The conclusion drawn from the experimental testing is that the component models and the resulting vehicle simulation can be trusted to produce correct results. This validation is helpful in building confidence in the results calculated and the conclusions drawn in the next two chapters.

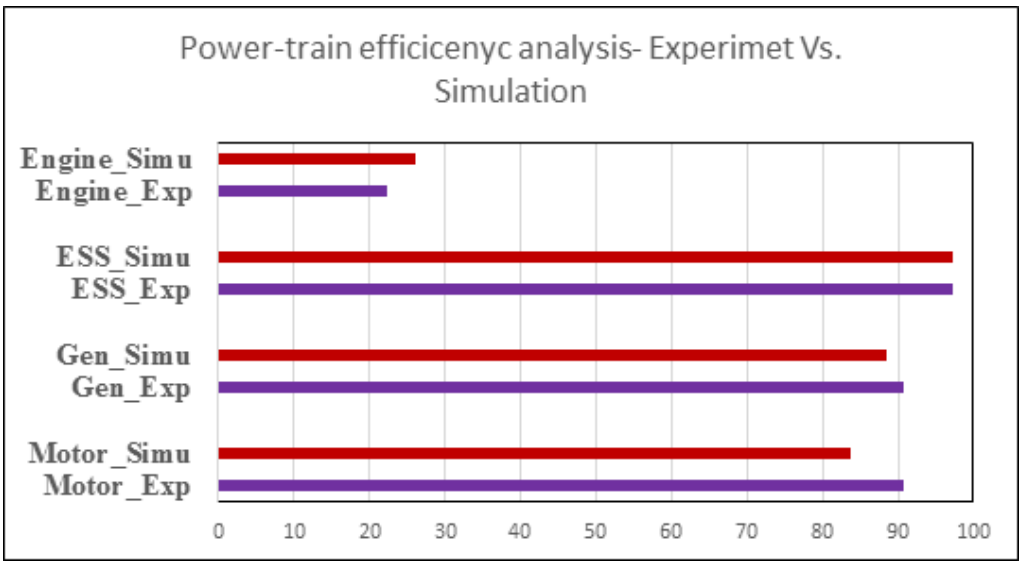

Figure 3.13 The chart compares the average efficiencies of power-train components for experimental and simulation results over the test time.

CHAPTER IV

BANDWIDTH-BASED CONTROL STRATEGY FOR A SERIES SPORT HEV WITH LIGHT ENERGY STORAGE SYSTEM

4.1 Introduction

A parametric study on the size of the ESS for a mid-size SHEV was carried out in Chapter 3 which resulted in a 4.5 kWh ESS. A customized duty-ratio controller was developed to handle the "HEV light" power-train energy management. In this chapter, the goal is to electrify a Subaru BRZ concept sports car in the series hybrid configuration. The reason this example is performed is that such a sports car has a physically limited space allocation for the ESS, which causes a severe challenge to applying the previously developed duty ratio control strategy. A new control strategy is required because, as it will be explained later, duty ratio control imposes limitations on managing the much smaller ESS. The literature classifies power management of electrified vehicles based on either the type of EV or type of applied method. For the former, the power management problem is reviewed for series, parallel, series parallel, and power split HEV's [54] and PHEV's [55], [56], [57]. For the latter, applied methods include control strategies classified either as rule-based or optimization-based methods. Rule-based methods are usually implemented with a state machine operating with variables such as SOC and engine on/off. In this case, controller parameters are set in advance [58], [59], [60] and may be adjusted in real-time with a fuzzy logic algorithm [61], [62]. In contrast with rule-

based methods, which are optimized at the component level, optimization-based methods all the controller to achieve optimal overall vehicle performance. To develop optimal control, they may use regular dynamic programming [63], stochastic dynamic programming or equivalent consumption minimization [64], genetic-fuzzy [65], particle swarm [66], and [67], or Pontryagin's minimum principle [68], or neural network [69] algorithms.

In the cited references above, power flow distribution between sources of energy in the power train are based on either sharing the period of operating time or sharing the requested power instantaneously, for example with a hybridizing factor [70]. However, it is more efficient that the load be shared between energy sources based on the frequency characteristics of each energy source. In [71], two different series configurations are considered: Fuel cell+Capacitor and Battery+Capacitor. Load sharing between energy sources is carried out in the frequency domain with a polynomial correction method. The frequency of the low pass filter which has been used to assign spectral power to the capacitor branch is set by a fixed time constant. Inspired from this literature on power management, in this chapter a controller is developed that allows a hybridized Subaru BRZ to be realized with a light ESS. The controller includes a duty cycling feature that manages the engine performance in multiple efficient regions and a bandwidth-limited proportional controller that limits low bandwidth battery current around each engine operating point.

The performance of the controller has been validated for a SHEV power-train model with an 80-VDC, 1.125-kWh battery, plus an 80-VDC, 46.4-F ultracapacitor module using a customized Autonomie vehicle model. The results show that the

combined FE of the new design is increased by 13 percent comparing to the corresponding FE in the equivalent conventional vehicle.

4.2 Engine duty ratio control

Engine duty ratio control was used in Chapter 3 for the reference vehicle in the parametric study. In this section, first the efficiency benefits of this control are described conceptually which is helpful to review before developing a new controller. Then the limitations of this control as a light battery solution are explained.

4.2.1 Engine duty ratio control and efficiency

Here the concept behind the duty ratio control is described. If sufficient ESS is available on the power train, engine duty ratio control is a method for increasing the overall efficiency. The following analysis shows the comparison between engine duty ratio control in Fig.3.3 and full proportional engine control. Engine power P_c consumed with proportional control in a conventional vehicle is estimated by (4.1).

$$P_c = \frac{E\{P_M\}}{\eta} \tag{4.1}$$

Where $E\{P_M\}$, is the average output power of the generator, and η is the engine-generator overall efficiency at average power. For the reference vehicle, the city drive cycle average power is shown in Fig. 4.1.

On the other hand, power consumed by the engine with the duty ratio control strategy, P_h, is estimated by (4.2).

$$P_h = D \times \frac{P_{GBE}}{\eta_{BE}} + (1 - D) \times \frac{P_{IDLE}}{\eta_{IDLE}} \tag{4.2}$$

where η_{BE} is the engine-generator overall efficiency in mode 2, P_{GBE} is the engine power in mode 2, and D is the duty cycling ratio where $D = \frac{E\{P_M\}}{P_{GBE}}$. For the reference vehicle, mode 2 power is shown with a white circle on Fig. 4.1. η_{IDLE} is the engine efficiency during idling. P_{IDLE}, is negligible, so (4.2) can be written like (4.3).

$$P_h = D \times \frac{P_{GBE}}{\eta_{BE}} \tag{4.3}$$

Fig. 4.1. shows that $\eta_{BE} \gg \eta$; therefore, for the same drive schedule such that $E\{P_M\} = DP_{GBE}$, comparing (4.1) with (4.3) shows that $P_c \gg P_h$. When duty ratio control strategy is utilized, significantly less energy is consumed by the engine for meeting the same drive cycle, so engine efficiency is considerably higher and higher fuel economy is achieved. This effect can be approximated in conventional vehicles using a method of driving popularly known as "pulse and glide" [http://en.wikipedia.org/wiki/Energy-efficient_driving].

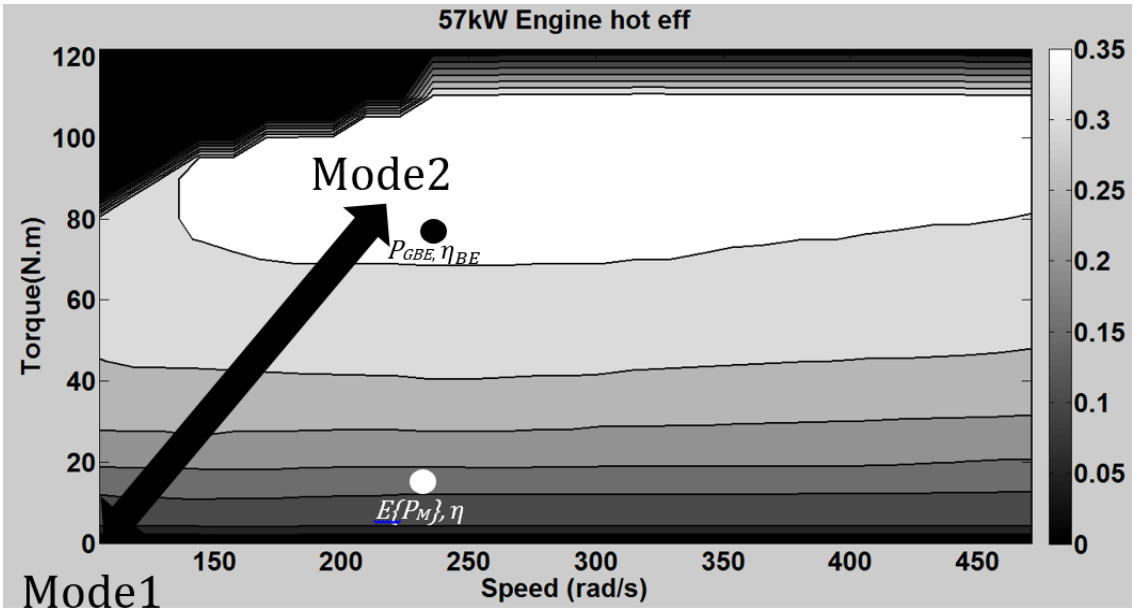

Figure 4.1 Engine operating point on engine efficiency map using engine duty ratio control

4.2.2 Limitations of duty ratio control strategy

Based on the results in Chapter 3, a 4.5 kWh 360 VDC battery is nominated as one of the best candidates. The battery pack includes 100 AMP14 Li-Ion prismatic cells from A123 with total cell weight of 50 kg. In this chapter, a conventional Subaru BRZ sport car is being hybridized. The space allocation is one fourth of the original battery size, $\frac{4.5\ kWh}{4} = 1.125\ kWh$, which already was found for the mid-size vehicle through a parametric study. Therefore, the target here is to hybridize a BRZ power train with a 1.125 kWh ESS. The challenge is to design a viable series hybrid power train with extremely light ESS. If the strategy in Fig. 3.3 is used, in engine-off mode the ESS is responsible for providing for the load independently. Typical load request at the ESS can be fairly estimated by exciting the power train of the reference model in Fig. 3.1 with a

published drive cycle such as the city drive cycle (UDDS) or the highway drive schedule (HWFET). A case study has been carried out for a reference vehicle in city driving conditions. The time domain power signal of the ESS is transformed to the frequency domain using the Fast Fourier Transform (FFT). By using the magnitudes at each frequency, computed via the FFT algorithm in MATLAB, the approximate Fourier series of the ESS power can be written as (4.4).

$$P_{ESS}(t) \approx P_0 + \sum_{n=1}^{\infty} P_n \sin(\omega_n t + \varphi_n) \tag{4.4}$$

where

$\omega_n = 2n\pi\Delta f$

$\Delta f = \frac{f_s}{k}$

f_s and k are the sampling frequency and the number of sampled points in the FFT computation, respectively.

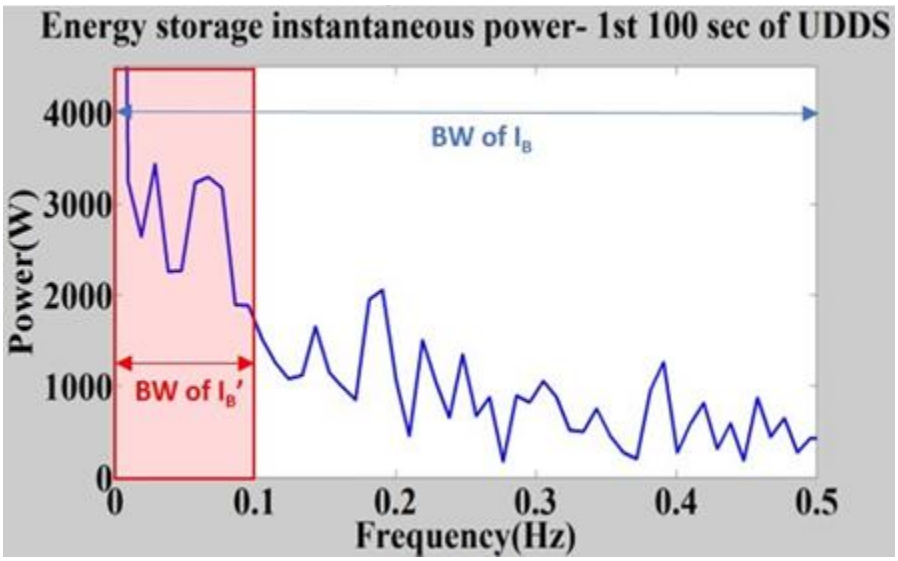

Figure 4.2 UDDS power spectrum. The time domain ESS power signal has been transformed to the frequency domain using the Fast Fourier Transform

Fig. 4.2 shows the result of this study in the frequency domain. The trend shows that the P0, or DC value of the power spectrum, and the very low frequency power spectrum, i.e. for small "nΔf" , are substantially larger than components with higher frequency, larger "nΔf" . In other words, the ESS undergoes large low bandwidth power requests. For example compare the portion below 0.1 Hz with the rest of spectral power. As long as the requested power is within the rated specification of the ESS, under duty ratio control the ESS matches the load and generation over the entire power spectrum. The nominal bus voltage in this case study is 320 VDC.

In the BRZ sports car SHEV, one fourth of the original battery size is available, so the number of cells is reduced to 25 percent and the battery terminal voltage is 80 VDC. A bidirectional DC-to-DC converter integrates the 80 VDC battery to the 320 VDC power bus. In this case, the current on the ESS side of the converter will be four times

greater than the corresponding current in the original design for the same requested power at the wheels of the car (see Fig 4.3). Based on the case study, in city driving it is expected that motor current requests with magnitudes in the range 100 A to 190 A will happen frequently. By taking into consideration the DC-to-DC converter current ratio of four, the battery supplies current amplitudes in the range 400 A to 760 A. These large currents are beyond the nominal discharge rating of the battery. In other words, the current requested from the ESS is beyond the rated pulse current of the APM14 cell. Therefore, in the new design a more sophisticated controller is needed to control this problem and also to manage the engine to maintain operation in efficient regions of the brake-specific fuel consumption map.

4.3 Innovative bandwidth based control strategy

A new control strategy is required in order to distribute the power between engine and the reduced size ESS in a way that the requested load at the electrical motor is fulfilled, maximum and minimum power constraints of the energy sources are observed, and overall power-train efficiency is maximized. For a sports car SHEV, it is necessary to mitigate the low bandwidth power variations as mentioned in the previous section. The engine is the only source of energy which is able to deliver the power in the low frequency bandwidth. By extending the bandwidth delivered by the engine, the ESS power in the low bandwidth part will be reduced. In the plot in Fig 4.2, the blue horizontal arrow specifies the bandwidth of the ESS in the original control strategy. The red rectangle highlights the hypothetical frequency band which in the new control strategy should be removed from ESS responsibility and added to the engine/generator responsibility.

It is hypothesized that developing a controller that features engine duty cycling and proportional control will allow an efficient power-train with extremely light ESS to be realized. If instead of two constant engine operating modes, multiple constant operating modes defined by various driving behaviors are created, the low frequency power requested from the ESS can be diminished. The new operating points are selected for low fuel consumption rates which is assumed to lead to a higher fuel economy compared to the situation where the engine operating point varies proportionally over the entire drive cycle load. However, to have the engine function with some form of a duty cycling scheme in a HEV with an extremely light ESS, proportional control is required to filter the low bandwidth portion of the drive cycle in a way that the ESS operates within its rated capabilities.

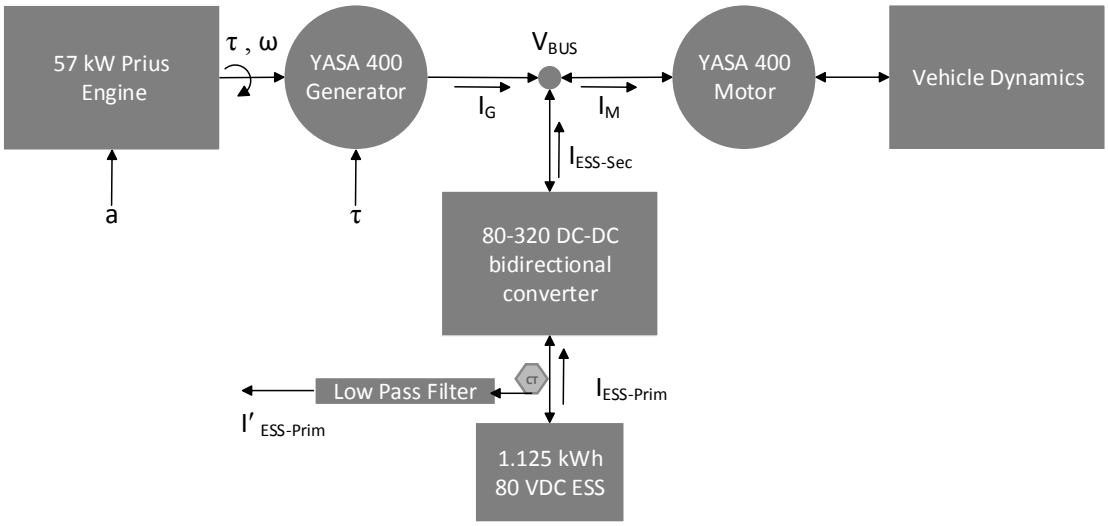

Figure 4.3 Block diagram of the power-train and the variables involved in the bandwidth-limited engine power controller.

The objective is to find the optimum bandwidth below which engine operation is actively controlled to supply the load and above which the ESS passively supplies the drive cycle power requirements. The frequency range which is the subject of this search is within the bandwidth of engine and battery operation. The bandwidth of other sources of energy, for instance an ultracapacitor if it is available, is outside the domain of this search. Therefore, the results of this study will not be affected by adding high bandwidth energy storage devices.

A block diagram of the power train and variables involved in bandwidth based engine control are shown in Fig. 4.3. Power-train variables which are impacted by the controller are defined below:

A block diagram of the power train and variables involved in bandwidth based engine control are shown in Fig. 4.3. Power-train variables which are impacted by the controller are defined below:

V_{BUS}: Bus voltage is an instantaneous voltage shared between motor, generator, and battery at a common node. In the following analysis, the voltage is considered as a constant variable compared to the large variation in currents.

I_M: Motor current is instantaneously varying in proportion to drive cycle power requested at the wheels if bus voltage is considered constant.

$I_{ESS\text{-}prim}$: ESS current is an instantaneous variable which matches the difference between generator output power and motor power request on the ESS side of the converter.

$I'_{ESS-prim}$: Bandwidth-limited (BWL) ESS current is the filtered ESS current which is measured by a sensor facilitated with a low pass filter on the ESS side of the converter.

I_B: Battery current is an instantaneous variable which contributes to matching the difference between generator output power and motor power request.

I'_B: BWL battery current is a filtered battery current which is measured by a sensor facilitated with a low pass filter. The battery is not measured by a separate BWL sensor. I'_B is defined for more clarity. $I'_{ESS-prim}$ and I'_B are technically the same thing because the Ultra-Capacitor contribution to BWL portion of load is negligible.

I_G: Generator current by definition is a BWL current because it is controlled using the bandwidth limited battery current as an output in the proportional control process ($I_G = I'_G$.

τ: Generator torque is a BWL torque which can be adjusted at the generator side of the engine. The generator controller adjusts the torque as a load on the engine drive shaft using a reference input "τ".

ω: Engine shaft speed which is controlled via an accelerator reference input "*a*" in the engine control unit (ECU). Closed-loop feedback speed control is assumed to be used ($\omega = \omega_{Ref}$).

V_{BUS}: Bus voltage is an instantaneous voltage shared between motor, generator, and battery at a common node. In the following analysis, the voltage is considered as a constant variable compared to the large variation in currents.

I_M: Motor current is instantaneously varying in proportion to drive cycle power requested at the wheels if bus voltage is considered constant.

$I_{ESS\text{-}prim}$: ESS current is an instantaneous variable which matches the difference between generator output power and motor power request on the ESS side of the converter.

$I'_{ESS-prim}$: Bandwidth-limited (BWL) ESS current is the filtered ESS current which is measured by a sensor facilitated with a low pass filter on the ESS side of the converter.

I_B: Battery current is an instantaneous variable which contributes to matching the difference between generator output power and motor power request.

I'_B: BWL battery current is a filtered battery current which is measured by a sensor facilitated with a low pass filter. The battery is not measured by a separate BWL sensor. I'_B is defined for more clarity. $I'_{ESS-prim}$ and I'_B are technically the same thing because the Ultra-Capacitor contribution to BWL portion of load is negligible.

I_G: Generator current by definition is a BWL current because it is controlled using the bandwidth limited battery current as an output in the proportional control process ($I_G = I'_G$.

τ: Generator torque is a BWL torque which can be adjusted at the generator side of the engine. The generator controller adjusts the torque as a load on the engine drive shaft using a reference input "τ".

ω: Engine shaft speed which is controlled via an accelerator reference input "*a*" in the engine control unit (ECU). Closed-loop feedback speed control is assumed to be used ($\omega = \omega_{Ref}$).

4.3.1 Duty cycling and battery size

In Section 4.2, using Fig. 4.2, it has been shown that engine duty cycling with a two-state operating point increases efficiency. However, two-state engine operation is realized at the cost of a large ESS. Using multiple operating points allows the ESS size to be reduced. In the following analysis, the battery size needed for a two-state controller and a multiple-state controller are compared. In both cases, the expected value of the requested motor current is $E\{I_M\} = 27A$. In the "two-state engine control" case, the engine duty cycles between $I_{G-Mode2} = 62.5A$, and $I_{G-Mode1} \approx 0$. A duty cycle $D = 0.43$ is required. It is assumed that $V_{BUS} = 320\ VDC$. The ESS needs to produce and absorb the difference between generation and demand; therefore, the ESS current will be a square wave with peak-to-peak amplitude of 62.5A.

In the multiple-state engine control case, it is assumed that mode 2 of the duty ratio control strategy is replaced by two intermediate operating points, which are defined by the expected average power required by the highway driving and the city driving conditions, respectively. In Fig. 4.4, the 57-kW engine efficiency map is drawn again, but this time multiple operating points are considered and tagged to the different driving conditions. New operating points have $I_{hw} = 36A$, which is the average value of the published highway drive cycle for the reference vehicle, and $I_{urban} = 18A$, which is the average value of the published city drive cycle for the same reference vehicle, as nominal current specifications. To meet the same expected value of motor current, $E\{I_M\} = 27A$, the ESS current will be a square wave with peak-to-peak amplitude of 18 A while the engine goes back and forth between I_{hw} and I_{urban} with duty ratio of 50%. The size of the ESS can be reduced in the second case at the cost of lower engine efficiency. On the

other hand, this can be offset by the additional fuel economy achieved from reducing the ESS size. Of course, a vehicle and a control model are required to study the impacts of duty cycling on the overall efficiency of the power train.

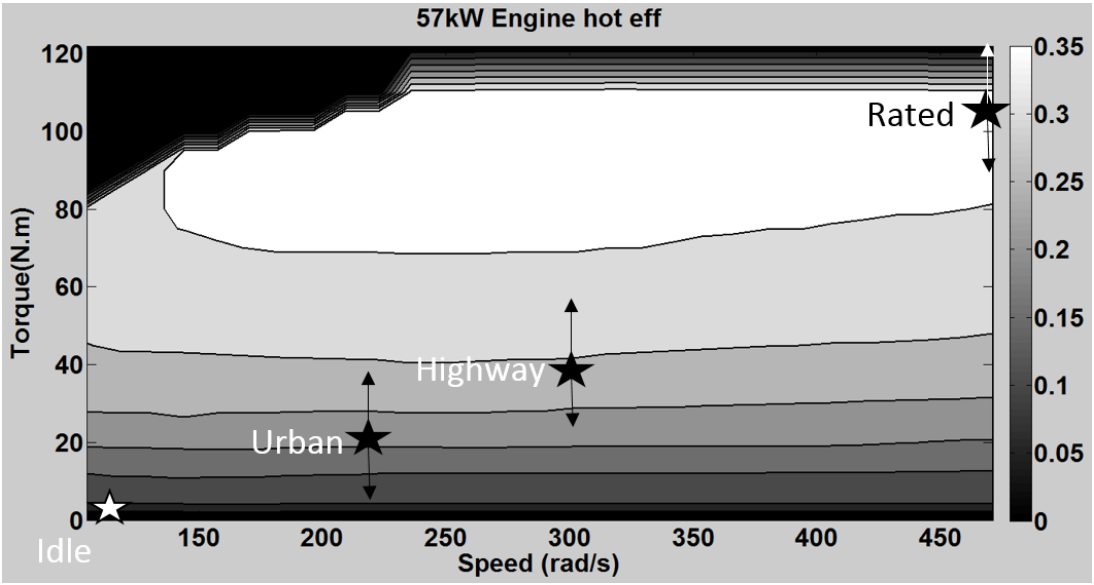

Figure 4.4 Engine efficiency map. Multiple operating points proportional to different driving conditions are labeled.

If threshold-crossings of an internal state indicator, for example battery SOC, is used for changing the states, limit cycling can happen. Limit cycling is an oscillatory situation that occurs in some nonlinear systems. In other words, the controller oscillates back and forth between different states with potentially undesirable impacts on power train component reliability and consumer perceptions. One way of controlling the limit cycling and delaying the transition is to combine the duty cycling function with a limited proportional control feature in each state. In the engine map plot in Fig. 4.4, a range of limited proportional control is shown about nominal discrete operating points with up and

down arrows. The hysteresis band prolongs the period of time when the controller operates in a current state.

Overall engine efficiency is affected both in a positive and a negative way when proportional mode is added while the ESS low bandwidth current variation is always mitigated with this feature. The low bandwidth current mitigation leads to a reduction in ESS size. In addition, partial elimination of SOC modulation within the bandwidth of controller operation is achieved which results in reduced ESS losses, and reduced thermal and electrical cycling.

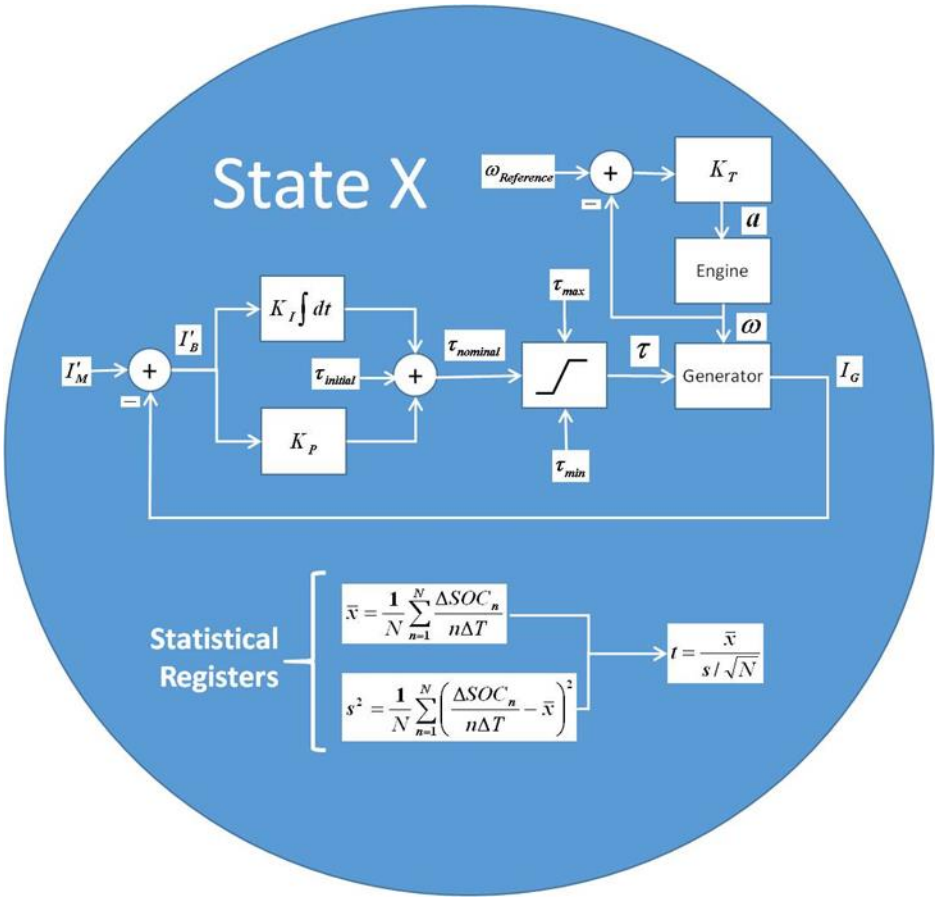

Figure 4.5 Block diagram of the limited bandwidth based proportional-integral controller in arbitrary state of X.

Controller variables are defined in section 5 nomenclature.

4.3.2 Limited bandwidth proportional controller algorithm

Because the conditions causing state changes are affected by proportional controller performance in each state, first the proportional control algorithm is described. In the following analysis, the error equation for proportional control is derived. VBUS is considered constant, which is a reasonable approximation to the actual situation if SOC variation is limited. Total harmonic distortion (THD) of the bus voltage is small on the power bus of a HEV while that of the motor current signal is significant [42]. Therefore, the current variable can be used as a replacement for power in the small signal analysis. For a common node on Fig. 4.3 between motor, generator, and ESS, Kirchhoff's law is written. Most of the involved variables in the following analysis are defined in section 4.3.

$$I_{ESS-Sec} = I_M - I_G \tag{4.5}$$

(4.5) can be re-written in the form of (4.6)

$$I'_{ESS-Sec} = \frac{I'_B}{R} = I'_M - I_G \quad \Rightarrow \quad I'_B = N_c \times (I'_M - I_G) \tag{4.6}$$

$$(4-6)$$

Where $I'_{ESS-Sec}$, I'_B and I'_M are BWL version of true currents, and N_c = 4 is the converter ratio. Again, It is noted that $I'_G = I_G$, because the generator current is the output of a bandwidth limited control process. (4.6) is the error equation required for proportional control. The controller only receives I'_B as an input which is measured by a BWL sensor.

Figure 4.5 illustrates the block diagram of the BWL proportional-integral (PI) controller in arbitrary state X. In state X, a specific hysteresis band defines nominal,

upper and lower torque thresholds. In this study, standard published drive cycles are used as examples for defining the nominal set points and the thresholds of intermediate states. In Fig. 4.4, the stars and the tips of up and down arrows mark the nominal, maximum, and minimum torque, respectively, for urban, and highway condition at constant engine speed. For example if the urban state is selected during the duty cycling process, proportional controller torque is limited to the range 10-40 Nm at 235 rad/s constant shaft speed. PI controller will zero the BWL portion of the battery current, $I_B^{'}{}'$, as long as the requested power is within the proportional range of the current state.

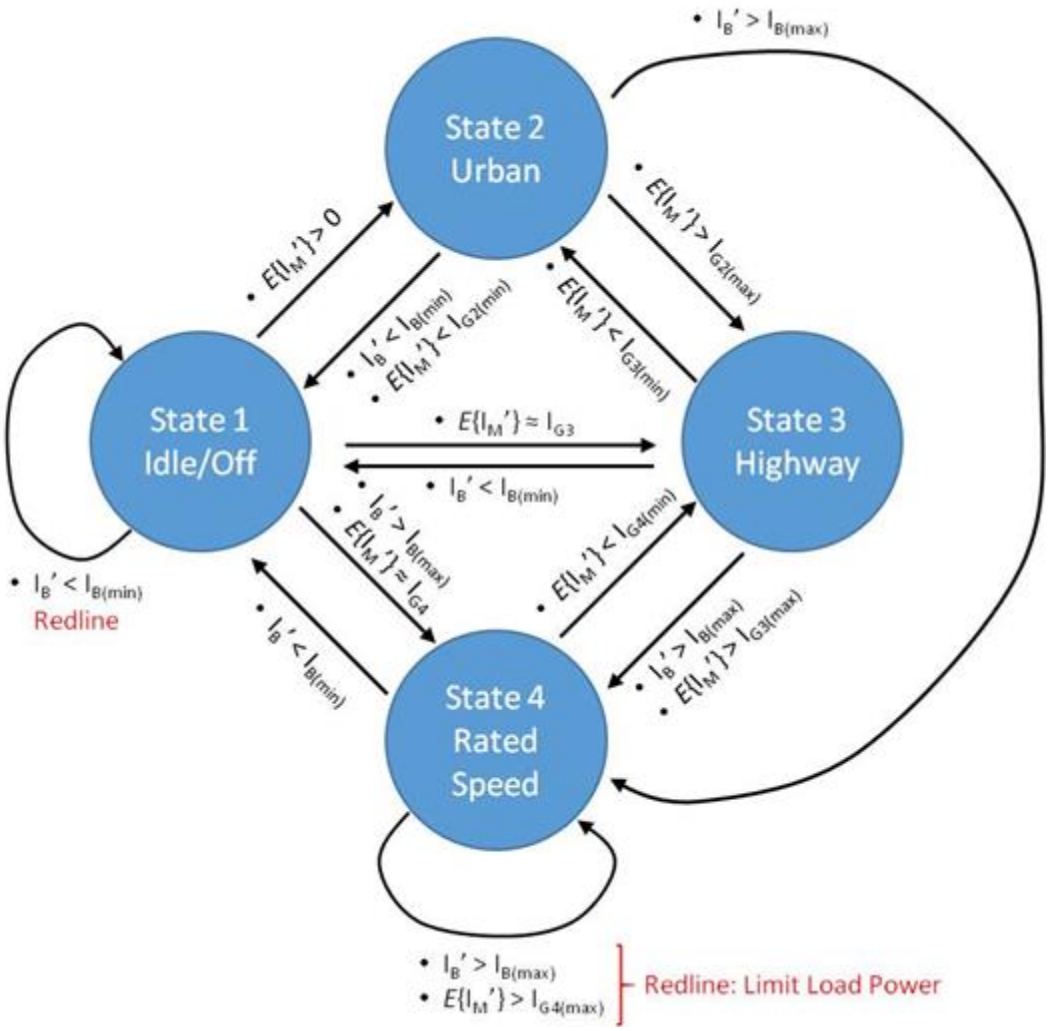

Figure 4.6 Proposed state machine uses decision making for changing the states when the mismatch between expected motor current and expected generator current is statistically significant.

4.3.3 State machine controller algorithm for duty cycling

As long as the controller operates within the proportional range of the current state, there is no need to change the state; however, when the power requested by the motor is outside the range, the controller is not able to match the generation to the bandwidth limited demand. In this case, a state machine is required to decide when

transition to higher or lower states should occur. Fig. 4.6 shows the proposed state machine control algorithm. Four states represent four different driving behaviors. In state X, parameters of the BWL PI controller and the engine such as nominal, upper and lower torque threshold, and shaft speed are defined. Parameters in the specific states 2 and 3 are defined based on standard urban and highway drive cycles, respectively. State 4 is defined by the continuous rated power of the engine which is usually determined by the vehicle's top speed requirement, so torque hysteresis band and driveshaft speed of this state is selected proportional to the top speed requirement. Arrows between states specify the conditions via which states transitions occur. These conditions are classified into two categories. The first category includes ESS rated specifications. If the BWL current of the battery is detected to be either in excess of maximum battery discharge rating (positive by assignment of current polarity in Fig. 4.3) or less than the minimum battery charging rating (negative by assignment of the current polarity in Fig. 4.3, e.g., during regenerative braking), these conditions are activated and a state change occurs. This is a protective feature for the battery at the state machine controller level, but obviously other independent protective functions are also required at the supervisory control level. The second category of conditions checks the mismatch between motor demand and generator supply. The latter is the subject of the following analysis.

4.3.3.1 Estimation of the expected motor current

Two reasons persuade deriving the motor current expected value, $E\{I_M\}$. First, in actual driving conditions, the arbitrary driver never follows the standard published drive cycles. The actual drive cycle must be considered a random process the statistics of which are different from statistics of standard drive cycles. A possible scenario may

occur where $E\{I_M\}$ is in between the nominal currents of two states. In this case, duty cycling between two states is required (eventually) to meet $E\{I_M\}$. To recognize this situation, estimating the average motor current is necessary. Second, even the standard drive cycles are long time-domain sequences which can be assumed to be composed of multiple sub drive cycles with different average values. This fact sometimes makes the moving-average value of motor current over a specific short period of time quite different from the overall $E\{I_M\}$. Therefore, even in standard drive cycles, there is a need for estimating $E\{I_M\}$ in order to make decisions for changing the state so as to avoid intolerable changes in battery SOC and to reduce the impact of proportional control on engine efficiency.

By taking expectation from both sides of (4.6), the expected value of the BWL variable is found:

$$E\{\frac{I_B^{'}}{Nc}\} = E\{I_M^{'} - I_G\} = E\{I_M^{'}\} - E\{I_G\} \tag{4.7}$$

If the drive cycle random process is assumed to be an ergodic random process, meaning the average and variance of a sufficiently long sample of the process represent the statistical property of the process, then the expected value of the BWL variables can be rewritten in average form over all time:

$$\lim_{T\to\infty} \frac{1}{T}\int_0^T \frac{I_B^{'}}{Nc}dt = E\{I_M^{'}\} - \lim_{T\to\infty} \frac{1}{T}\int_0^T I_G dt \tag{4.8}$$

Over a finite period of time, an estimate of the expected value of BWL motor current, $E\{I_M'\}_{est}$, can be calculated from (4.9).

$$E\{I_M'\}_{est} = \frac{1}{T}\int_0^T \frac{I_B'}{Nc}dt + \frac{1}{T}\int_0^T I_G dt \quad (4.9)$$

where $T < \infty$

The second term of (4.9) is the average value of BWL battery current at the output of the converter. This term can be estimated from the battery SOC, because as shown in Fig. 4.2, the BWL portion of the actual current is significantly higher than the high bandwidth portion of the actual current. As a result,

$$E\{I_M'\}_{est} = -\frac{Q_C}{Nc \times T}[SOC(T) - SOC(0)] + \frac{1}{T}\int_0^T I_G dt \quad (4.10)$$

Where Q_C, is the capacity of the battery in amp-seconds. In (4.10), the discharging current is considered positive. (4.10) can be re-arranged to show the mismatch between average demand and average generation.

$$-\frac{Q_C}{Nc \times T}\Delta SOC = E\{I_M'\}_{est} - \frac{1}{T}\int_0^T I_G dt \quad (4.11)$$

(4.11) is another version of the error equation which was first written in (4.6). The first term is proportional to the rate of change of SOC. The SOC can be sampled over a time T and stored in a register. The register values can be evaluated by a statistical test to make a decision to duty cycle.

4.3.3.2 Statistical test for state changes

As long as torque limits in each state produce corresponding current thresholds which bracket $E\{I_M'\}$, the controller zeroes the battery current within its bandwidth of proportional control. In this case, the BWL battery state of charge is sustained, although

smaller out-of-bandwidth variations will occur to balance the instantaneous power in the drive cycle. However, if $E\{I'_M\}$ exceeds the thresholds of the proportional controller, then BWL battery current becomes non-zero and the rate of change of the battery state of charge within the bandwidth of proportional control is accumulated in the statistical register. This information is useful for making decisions about state changes specifically when $E\{I'_M\}$ is close to the limits of proportional control.

Null hypothesis - null hypothesis is (4.12) because when this equation is true there is no need for changing the state, but when it is not true a change should occur.

$$E\{I'_M\} = \frac{1}{T}\int_0^T I_G\,dt \tag{4.12}$$

Test method - a statistical test, known as Student's-*t* test, is used to evaluate the null hypothesis for state changes. Based on (4.11), state-of-charge rate of change is a variable which can be tested to show if the null hypothesis is not true. In this test, the *t* parameter is computed in (4.13) for evaluation.

$$t = \frac{\bar{x}}{s/\sqrt{N}} \tag{4.13}$$

$$\bar{x} = \frac{1}{N}\sum_{n=1}^{N}\frac{\Delta SOC}{n\Delta T} \tag{4.14}$$

$$s^2 = \frac{1}{N}\sum_{n=1}^{N}\left(\frac{\Delta SOC}{n\Delta T} - \bar{x}\right)^2 \tag{4.15}$$

In (4.13)-(4.15), N is the number of samples of ΔSOC accumulated in the register, $\bar{x}$ and s are respectively the sample mean and the sample variance of the state-of-charge

rate of change over N samples, and ΔT is the sampling interval. t is the variable which depends on number, mean, and variance of samples. Table 4.1 shows the null hypothesis is rejected if either *t* is greater or less than a selected threshold. The *t* parameter threshold, $t_{\propto,N}$, is selected from standard Student's-*t* look-up table. $t_{\propto,N}$ is selected depending on the number of samples and the desired probability of correctness for making decisions (i.e., rate of unnecessary state changes).

Table 4.1 Testing null hypothesis for state changes

Reject Null Hypothesis because:	**When *t* Test Condition is:**	**Resulting Action is:**
$E\{I'_M\} > I_{G(max)}$	$t < -t_{\propto,N}$	Change state to the next higher state
$E\{I'_M\} < I_{G(min)}$	$t > t_{\propto,N}$	Change state to the next lower state

4.4 SHEV model for validating bandwidth-based control algorithm

In order to validate the feasibility of realizing a series HEV with extremely light ESS, the BWL control strategy should be modeled and evaluated. However, before implementing the controller, an appropriate vehicle model must be developed.

4.4.1 Series hybrid electric vehicle model

One way is to use the available SHEV model in Autonomie which already has been customized for the reference vehicle of Fig. 3.1. However, integrating a BWL based controller with the current model is too complicated because key variables such as generator torque and engine speed cannot be easily manipulated. Fig. 4.3 shows a block diagram of a series power train model developed for this study. Vehicle dynamic and motor models are both borrowed from the Autonomie model of the reference vehicle of

Fig. 3.1. However, independent behavioral models of the generator and the engine using respectively the YASA-400 efficiency map and the 57-kW Prius engine efficiency map are created and integrated to the rest of the power train in a way that key variables can be controlled. The ESS is modeled with SimPowerSystems of the Simulink library [44]. A simplified bidirectional DC-DC converter is also modeled in order to interface the 80-VDC ESS to the 320-VDC bus.

4.4.2 Implementing the limited bandwidth proportional controller algorithm

Proportional controller variables such as ESS current, and generator current are accessible in the model. A block diagram in Fig. 4.5 is used to explain the implementation of the proportional controller in Simulink. BWL ESS current is created with the second-order low pass filter, the Laplace domain transfer function of which Tf_{Filter} is written in (4.16).

$$Tf_{Filter} = \frac{I_B'}{I_B} = \frac{1}{\frac{s^2}{\omega_0^2} + \frac{2}{\omega_0}s + 1} \quad (4.16)$$

$$-16)$$

Where $\omega_0 = 2\pi f_0$ and f_0 is the frequency of cut-off in rad/s and Hz respectively. Comparing (4.16) to a standard from of second order low pass filter, the above filter has quality factor of 0.5 and DC gain of 1. The latter means no change occurs in magnitude of the BWL portion of battery current after passing through the filter. Referring to Fig. 4.5, $K_P = 10$ and $K_I = 0$ are set as proportional and integral coefficients in the PI controller to compensate the plant transfer function, meaning for this example only proportional control is used. These coefficients guarantee that I_G is ten times larger than $Nc \times I_B'$while in closed-loop control where the error equation of (4.6) is minimized by the

available open-loop gain. The only variable which the controller observes is the BWL battery current I_B', as the out-of-bandwidth battery current is determined passively by Kirchhoff's law at the common node of the power bus and load conditions. The state hysteresis thresholds are produced for generator current, the electrical dual of generator torque, by the state machine and applied through a saturation block into the output of the proportional controller.

4.4.3 Implementing supervisory control and state machine algorithm

A simple supervisory controller and state machine are developed in State Flow of Simulink. Overall, four blocks operate in parallel: (1) regenerative braking protection, (2) charging mode, (3) Student's-*t* calculation, and (4) state machine. The first two are sub-sections of supervisory control. Regenerative braking protection makes sure that the charging current to the battery is not beyond the battery capability. Most of the time, the controller operates in charge sustaining mode, but for the special scenario, a charging mode is available to bring the SOC back to its operational hysteresis range if it goes below a minimum threshold. The Student's-*t* calculation block is a pre-processing function that samples SOC every ΔT seconds and stores it in a registry with N samples for *t* parameter calculation. Obviously the oldest sample in the register is overwritten by the most recent sample when it becomes full. *t* parameter is computed from (4.13)-(4.15) every sampling time, ΔT, and delivered to the state machine block. The fourth block is the state machine that is shown in Fig. 4.6. In each state, corresponding engine speed and generator current thresholds are set for the engine and generator block in the vehicle model. As mentioned in section 4.3, two types of transitions are available for state

changes. In the state machine block, transitions are allowed to be executed every sampling time, n.

4.4.4 Controller tuning

To have acceptable performance, the controller should be tuned. f_0 and $t_{\propto,N}$ are tuning variables that are manipulated to optimize the controller performance. Smaller f_0 leads to a smaller engine contribution and increases the capacity, and thus size, of the battery as well as increasing overall power-train efficiency. Smaller $t_{\propto,N}$, for a given number of samples N in the registry, increases the risk of false decision making for engine duty cycling. These two variables are selected through a multi-objective genetic algorithm optimization process to maximize both the combined city and highway fuel economy and the controller performance. The optimal controller tuning variables so found are $f_0 = 0.042\ Hz$ and $t_{\propto,N} = 0.7669$.

Table 4.2 ESS and controller parameters used for using in controller performance validation test

I_batt_Max_10 sec pulse. (A)	**I_batt_Min_10 sec pulse. (A)**	**I_batt_Max_Cont. (A)**	**I_batt_Min_Cont. (A)**	**Engine_Ctrl_BW (Hz)**	**Power Interface voltage Ratio, N_c**	**Battery Capacity, Resistance, and Nom Voltage**	**Capacitor Capacity, ESR, and Nom Voltage**
400	-190	180	-70	0.042	4	A123, 14 Ah, 37.5 mΩ,b80 VDC	Maxwell, 46.4 F, 27.5 mΩ, 80 VDC

4.5 Validating controller performance

Performance of the BW based controller is assessed for the extremely light ESS SHEV with both city and highway driving behaviors. The reference vehicle with the

power-train architecture given in Fig 4.3 is used for this study. Parameters for the ESS and the controller are shown in Table 4.2. Although the controller is designed to operate under actual driving conditions, the example scenarios are based on standard drive cycles, HWFET for highway, and UDDS for urban, to excite the power-train. Although for a regular passenger vehicle, f_0 and $t_{\propto,N}$ can be tuned to limit the battery discharge current under very harsh acceleration, for the sports-car class SHEV to satisfy the performance requirement under harsh acceleration, a 46.4 F UC is added which is able to deliver 50% of the power associated with the most aggressive acceleration in the US06 drive cycle (see Chapter 3 section 3.3.1).

4.5.1 Performance test under highway driving condition

Fig. 4.7 to 4.12 show the key variables of the state machine controller regarding the first 300 seconds of HWFET. As noted in section 4.3 and also shown in Fig. 4.5, the current state determines the engine operating region. In Fig.4.7, a numeral representing one of four states is shown on the vertical axis. As expected, just over 50% of the time, the state machine dwells in state 3 which has the average power of highway driving as the nominal power. Fig. 4.8 and 4.9 display two other state machine key variables: Student's-*t* and I'_B, respectively. The state varies when each of these variables reach their negative or positive thresholds. In the case of the Student's-*t* variable, when a negative threshold (-0.7669) is reached, the state-of-charge rate of change is judged to be statistically significant, which means the battery has been discharging because demand is higher than the available power generation in the current state. At this moment transition to a higher state happens. These types of transitions happen three times in the first 50 seconds (see Fig. 4.7 and 4.8). When the positive threshold (+0.7669) is hit, the minimum generation

of the current state is higher than the requested demand, and state-of-charge rate of change is again statistically significant, so the state machine goes to a lower state. I'_B. Minimum and maximum thresholds are set slightly below the continuous charge/discharge capability of the battery shown in Table 4.2. Two lines on Fig. 4.12 specify the battery minimum and maximum current setting. A few seconds before 150 sec, I'_B hits the limits and consequently the state machine takes the engine from state 3 to state 1 to protect the battery from over current. Fig 4.7 to Fig 4.10 show, while motor current is varying, how the state machine manages the engine performance efficiently by taking it to efficient states (regions in the BSFC map) based on the Student's-*t* value. As a result of this power management a combination for torque and speed is selected in a way that the engine operates in a hysteresis band as shown on Fig. 4.4. Fig. 4.11 and 4.12 shows the combination of torque-speed in a specific state. Fig. 4.11 shows the control of the battery SOC.

Fig 4.13 and Fig 4.14 depict a selected window of this study between 500-600 second. These plots show the performance of the BWL proportional controller which operates in parallel with the state machine controller to minimize the BWL battery current on the ESS. In Fig 4.13, from 500 to 540 seconds, the proportional controller is able to command the generator current to track motor current very closely. As a result of this sophisticated controller's performance the bandwidth limited ESS current, which is the error signal of control loop, is being continuously controlled about zero. Before 540 s, the state machine stays in state 3; however, after 540 s, the state machine begins duty cycling because the torque range of state 3 is not appropriate for following the motor load.

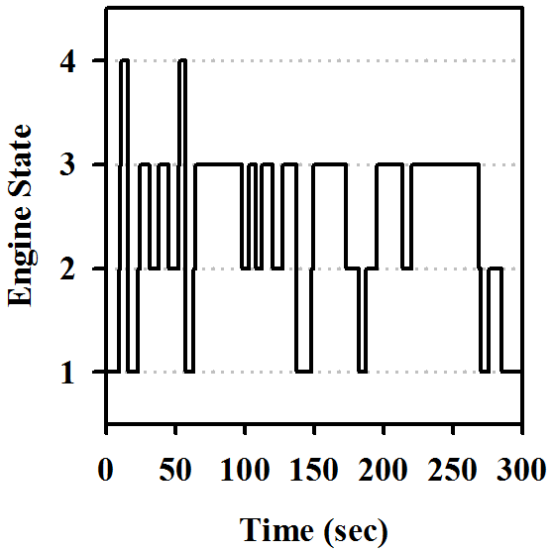

Figure 4.7 State in state machine controller

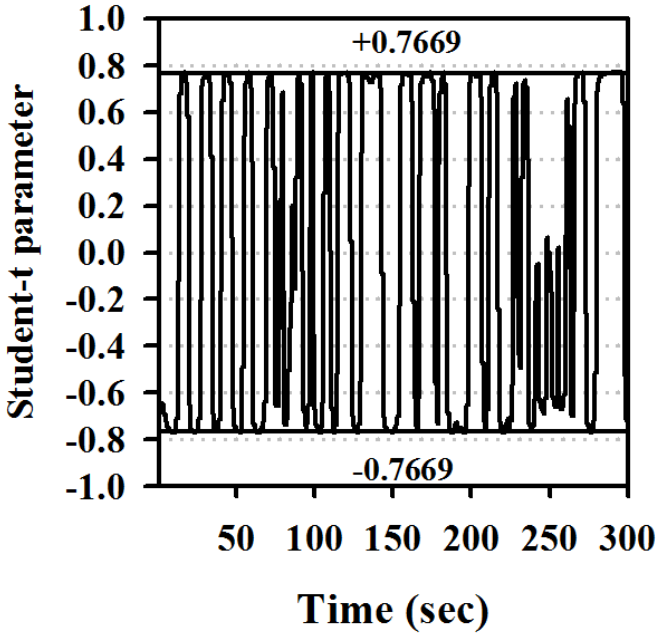

Figure 4.8 Student-t parameter

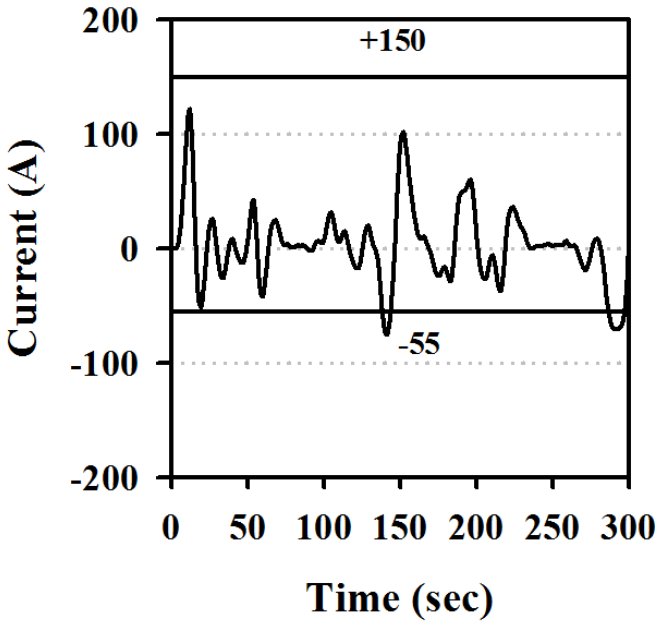

Figure 4.9 BWL battery current

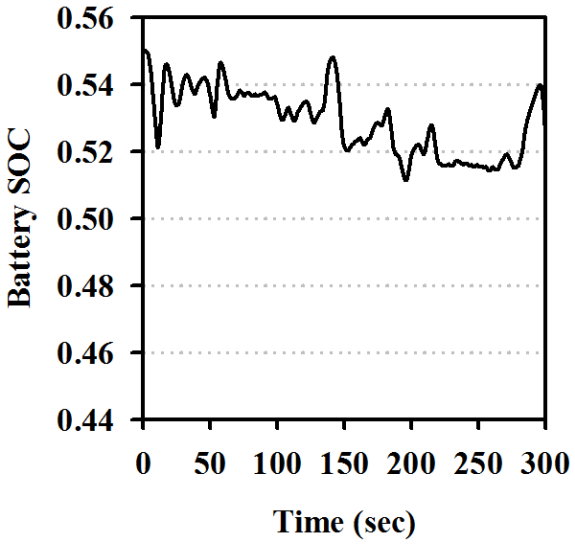

Figure 4.10 Battery state of charge

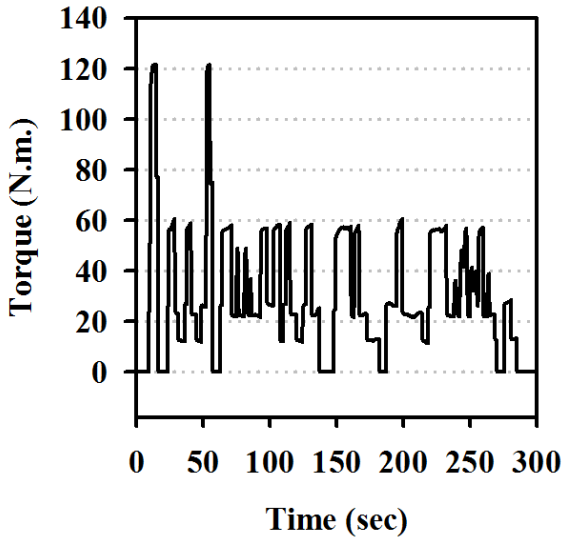

Figure 4.11 Engine torque

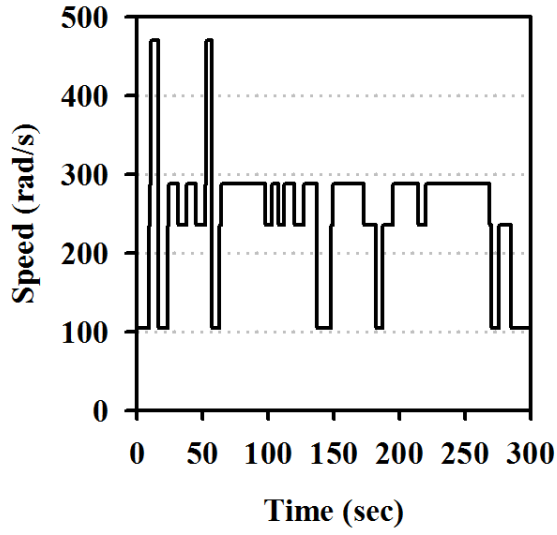

Figure 4.12 Engine speed

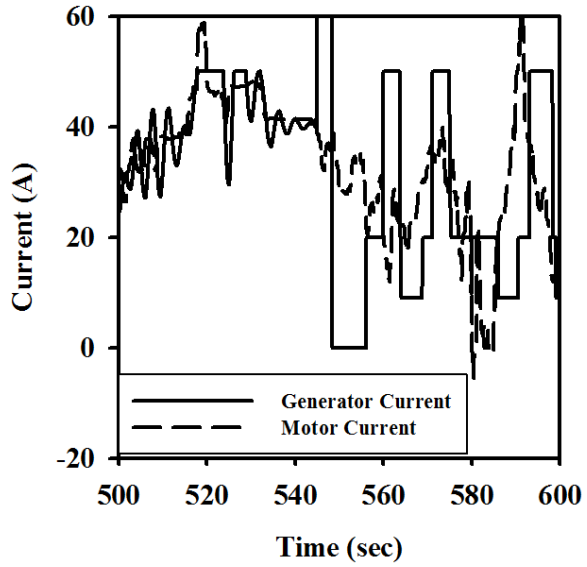

Figure 4.13 Generator/motor current

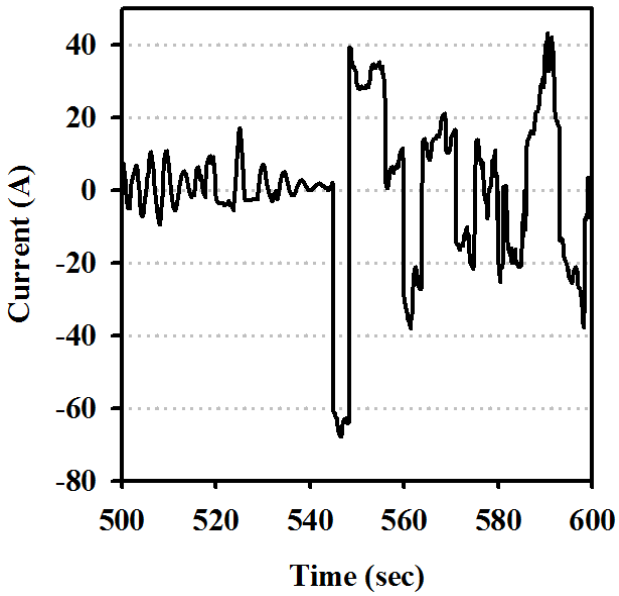

Figure 4.14 ESS current

4.5.2 Performance test under city driving condition

There are few differences for controller performance under city test compared to highway test. The city driving behavior has frequent acceleration/deceleration moments which makes the variance of motor current significantly larger than that of highway driving. In addition, in many occasions, the vehicle is in stop mode. Therefore, it is not expected that the controller dwells in state 2 most of the time. This fact is shown in Fig. 15. The state machine is settled in state 1 for almost 50% of the time. The rest of the time the controller dwells in state 2 or duty cycles between state 2 and 3. The contribution from state 2 is sufficient to limit the BWL battery current within the rated zone. As mentioned, in section 4.4.4, Student's-t and f_0 are tuned to maximize both the controller performance and the combined FE.

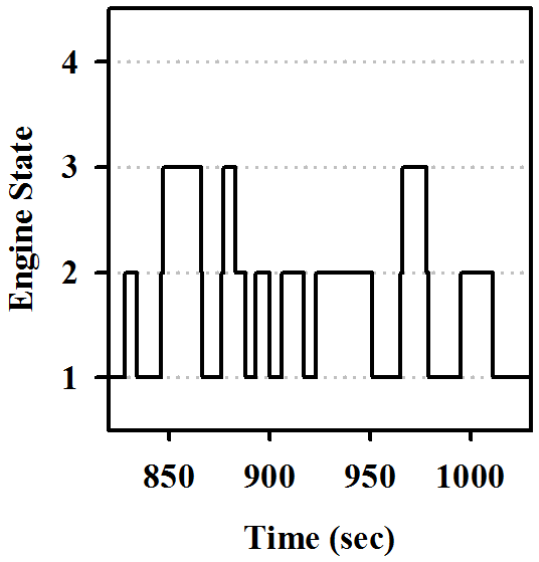

Figure 4.15 State in state machine controller

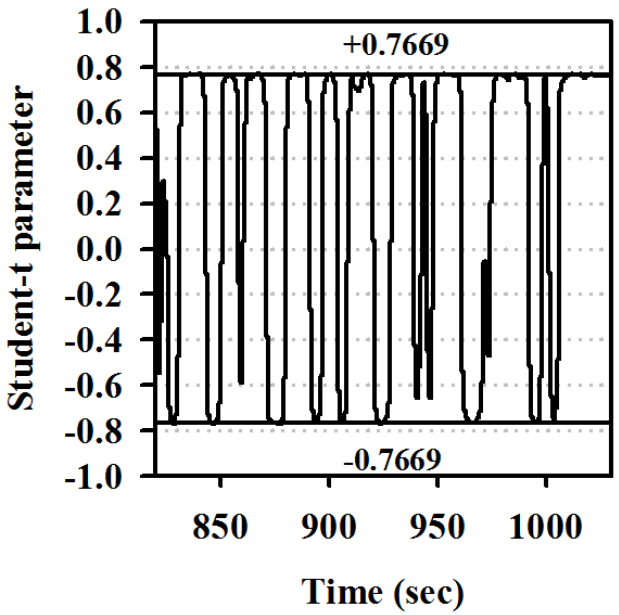

Figure 4.16 Student-t parameter

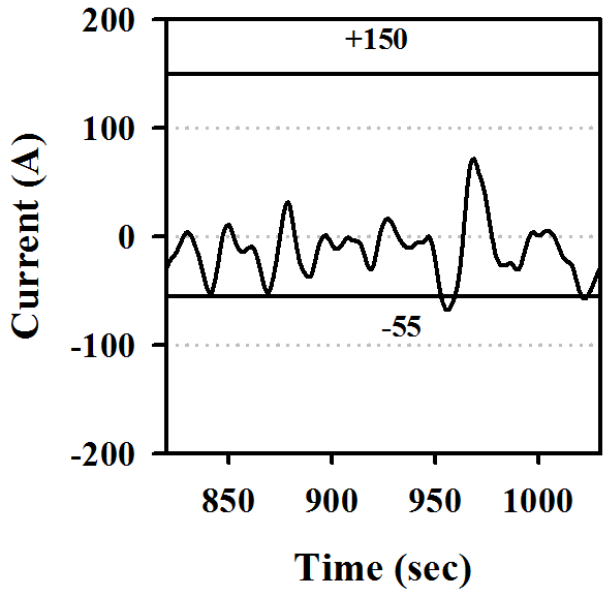

Figure 4.17 BWL battery current

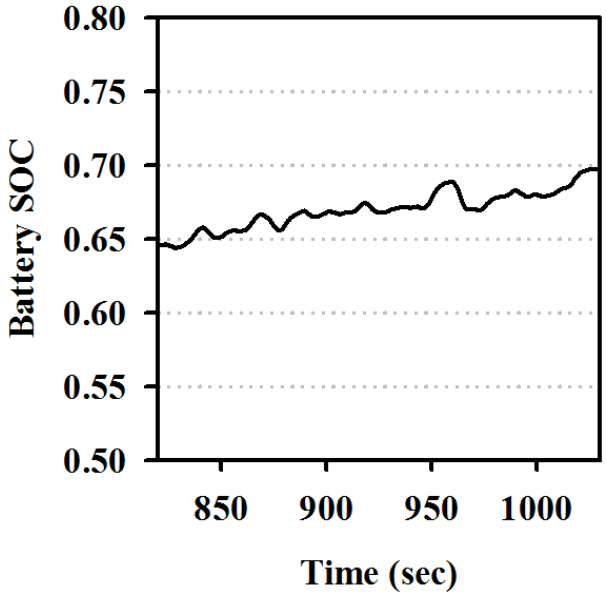

Figure 4.18 Battery state of charge

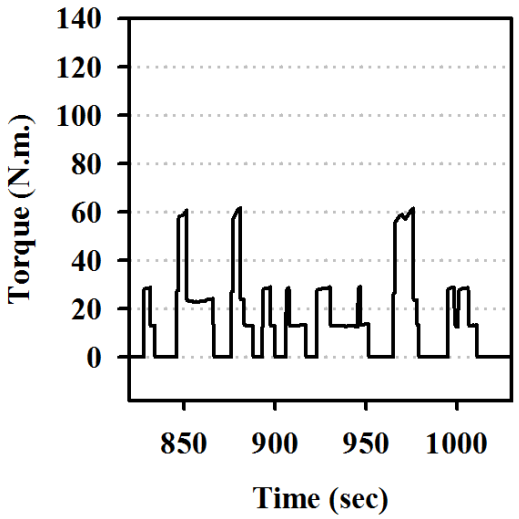

Figure 4.19 Engine torque

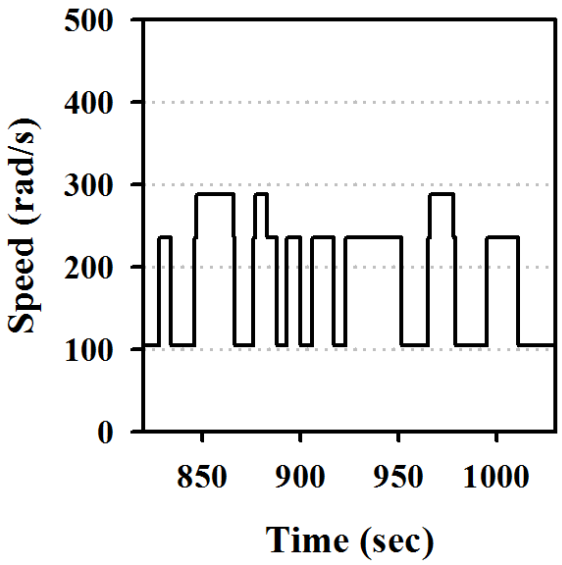

Figure 4.20 Engine speed

Therefore, there is a tradeoff between having a larger dwell time in state 2 to optimize controller performance which leads to smaller BWL battery current and having smaller state 2 dwell time which results in better FE. It is noted again that state 2 has the highest fuel consumption among states and less time in state 2 prevents the low FE. As a result of the sophisticated management of the state machine controller (Fig. 4.16 and Fig.4.17), the state of charge is controlled (Fig. 4.18) and engine torque and speed are managed within the efficient regions (Fig. 4.19 and 4.20). The performance of the BWL proportional controller under the city driving condition is similar to the corresponding performance in the highway driving condition. One difference though is that the proportional controller mainly operates at the torque limits.

A comparison between the performance of the vehicle model in figure 4.3 and its conventional version shows that combined city/highway fuel economy is increased by 13

percent (note: the reference vehicle cited here is not the Subaru BRZ, but instead is a notional "mid-size" vehicle with nominal dynamic modelling parameters since those of the Subaru BRZ are not precisely known).

4.5.3 Performance under 10 second acceleration condition

Power required for acceleration is calculated by (4.17).

$$P_a = \frac{\delta M}{2t_a}\left(V_f^2 + V_b^2\right) + \frac{2}{3} Mgf_r V_f + \frac{1}{5}\rho_a C_D A_f V_f^3 \quad (4.17)$$

For the Subaru BRZ, the following parameters are estimated. M is the total vehicle mass in kg (1256 kg), t_a is the expected acceleration time in s (10 s), V_b is the vehicle speed in m/s (13.36 m/s), corresponding to the motor-based speed, V_f is the final speed of the vehicle during acceleration in m/s (26.82 m/s), g is gravitational acceleration in m/s^2, 9.80 m/s^2, f_r is the tire rolling resistance coefficient (0.01 for concrete or asphalt road), ρ_a is the air density in kg/m^3, 1.202 kg/m^3, A_f is the front area of the vehicle in m^2 (2.125 m^2), and C_D is the aerodynamic drag coefficient (0.325).

$P_a = 64.2$kW is calculated for the acceleration period of 10 s. When the acceleration power is requested, the state machine takes the engine to state 4 where the engine peak power, 57 kW, is produced. 48.24 kW of this power is available for acceleration after considering generator and motor losses. The error in proportional controller will not be zero, because the generator power is limited to the peak power. The error will be supplied by the battery. The battery is able to supply up to 22.15 kW for 10 s, which is more than the difference between acceleration demand and engine generation.

4.5.4 Performance under grade condition

Power requirement to overcome the grade is calculated by (4.18).

$$P_{grade} = \left(Mgf_r cos\alpha + \frac{1}{2}\rho_a C_D A_f V^2 + Mgsin\alpha\right) \times V \quad (4.18) \qquad (4-18)$$

Where α is the angle of the grade in radians. It is a reasonable assumption that a passenger vehicle should sustain 55 mph for 20 minutes with a 4.5% slope. 19.88 kW is the required power to fulfill the mentioned gradeability specification which is met efficiently by the engine in state 3. Hence the BRZ could be expected to do better, but other factors like thermal management which are not considered here will set the true limit.

4.6 Chapter Summary

In this chapter the challenge of hybridizing a sporty Subaru BRZ was described. In this problem, the ESS space allocation is severely limited. Regular control strategies are not able to manage the engine operation efficiently while keeping the ESS variables, such as currents and SOC, in a nominal zone. A bandwidth-based power flow algorithm was developed which allows a sports-car class SHEV with 80-VDC, 1.125-kWh energy storage system to be realized. The result shows that a statistical test method on the rate-of-change of the state of charge enables a state-machine controller to manage engine duty cycling between efficient regions. The results also show that the bandwidth-based proportional controller protects the ESS against over current.

CHAPTER V

MULTI-OBJECTIVE OPTIMIZATION ON THE ENERGY STORAGE SYSTEM COST AND FUEL ECONOMY OF A SERIES HEV USING BANDWIDTH-BASED CONTROL STRATEGY

5.1 Introduction

Two main optimization strategies are applied in the EV literature. One of these seeks to optimize the size/cost of the components of the power train. The other seeks to maximize the FE by optimizing the performance of the control strategy. In the former category the cost is defined as an objective function while performance requirements such as FE are set as constraints [45]. To size the ESS or other powertrain components in series/parallel HEV's and fuel cell HEV's, single and multi-objective genetic algorithms [46] [47] [48] [49] are more common although other algorithms such as the GIAO software optimization routine [50] and gclsove of ADVISOR [51] are also used. In the second category in which optimal control strategies for better performance are sought, references are made to the use of regular dynamic programming [52], stochastic dynamic programming or equivalent consumption minimization [53], genetic-fuzzy [54], particle swarm [55] and [56], Pontryagin's minimum principle [57], or neural network algorithms [58] for developing optimal control. These optimal control strategies distribute the power between energy sources based on time domain techniques, so distributing the load between sources, particularly engine and battery, based on their

bandwidth characteristics is not explicitly considered which may limit the optimization results.

In this chapter, a Pareto Frontier, including Energy Storage System (ESS) costs and FE, for a Series HEV (SHEV) with limited All-Electric-Mode (AEM), is introduced using an advanced bandwidth-based control strategy teamed up with a duty ratio control strategy. The bandwidth-based control strategy allows the engine management advantage of the SHEV to be extended to a much smaller ESS compared to the sizes of ESS available in products on the market. To produce the Pareto Frontier, an Autonomie-based vehicle model is customized and used in parallel-mode Multi-Objective Genetic Algorithm (MOGA) optimization. This chapter is organized as follows. Section 5.2 describes the performance requirement of a mid-size HEV. Section 5.3 defines the design space of ESS size when AEM is not required. Section 5.4 defines optimization problems and constraints, and introduces the Pareto Frontier. Section 5.5 summarizes the chapter.

5.1 Mid-size vehicle performance requirements

A mid-size vehicle such as the reference vehicle of this study (Fig. 5.2) must meet customer expectations such as acceleration and gradeability. Vehicle specifications and other necessary parameters of Table 5.1 are used for computing acceleration and gradability. The vehicle dynamic specifications of a typical mid-size vehicle found in the Autonomie library are used; for other parameters required to compute the acceleration and gradeability, the specifications of the reference vehicle used in this research are applied [59] which are a good estimate of what consumers want [60]. The acceleration and gradeability power requirements are calculated as follows [26].

5.1.1 Acceleration

The acceleration performance requirement of a mid-size vehicle is usually defined by the power that is required to speed up the vehicle from zero speed to the vehicle's top speed in a specified amount of time. The acceleration power equation is presented in (5.1).

$$P_a = \frac{M}{2t_a}\left(V_f^2 + V_b^2\right) + \frac{2}{3}\, Mgf_r V_f + \frac{1}{5}\,\rho_a C_D A_f V_f^3 \qquad (5.1) \qquad (5-1)$$

Where M is the total vehicle mass in kg, t_a is the anticipated acceleration time in s, V_f is the final speed of vehicle after acceleration in m/s, V_b is the vehicle speed in m/s, corresponding to the YASA-400 motor-based speed, g is the acceleration of gravity in m/s^2, f_r is the tire rolling resistance coefficient, ρ_a is the air density in kg/m^3, A_f is the effective frontal area of the vehicle in m^2, and C_D is the aerodynamic drag coefficient. Table 5.1 tabulates the values used to calculate that P_a = 68.4 kW is required to achieve an 11.5 s zero-to-top speed acceleration time.

5.1.2 Gradeability

The gradeability performance requirement of a mid-size vehicle is usually defined by the power required to sustain the vehicle at the specified speed for a specific amount of time on a road with a certain slope.

$$P_{grade} = \left(Mgf_r cos\alpha + \frac{1}{2}\rho_a C_D A_f V^2 + Mgsin\alpha\right) \times V \qquad (5.2) \qquad (5-2)$$

Where M is the total vehicle mass in kg, V is the expected speed of vehicle during hill climbing in m/s, corresponding to the YASA-400 motor-based speed, g is the

acceleration of gravity in m/s^2, ρ_a is the air density in kg/m^3, A_f is the effective frontal area of the vehicle in m^2, $\propto$ is the angle of the grade in radians, and C_D is the aerodynamic drag coefficient. Once again referring to Table 5.1 P_{grade} = 25 kW to climb a 5% grade for 20 minutes at 55 MPH .

Although, for different types of applications vehicle requirements will vary, the variance of the acceleration and gradeabiliy for a regular mid-size passenger vehicle is not very large.

Table 5.1 Vehicle performance specifications and vehicle dynamic parameters

M	1600 kg
V_f	26.82 m/s
V_b	11.02 m/s
g	9.8 m/s2
f_r	0.008
ρ_a	1.202 kg/m3
A_f	2.25 m2
C_D	0.3

5.2 Design space for the size of ESS and the FE in SHEV with minimal AEM

In contrast with acceleration and gradeability requirements, which do not have too much variance, the efficiency of the power train, FE, varies for passenger vehicles. The FE may range from around 40 Mile per Gallon (MPG), calculated as a combination of highway and city driving, for a conventional vehicle (see section 5.3.1), up to the equivalent FE of about 89 MPGe, combined, for a BEV [61].

It is a hypothesis that a series HEV with minimal ESS may be of interest as an intermediate alternative which bridges between conventional vehicles and HEV's with large ESS such as PHEV's, extended range EV's (with both ICE's and fuel cells), and

finally BEV's, all with the series architecture. To answer the question of how small the ESS could be to realize a viable SHEV, a simulation analysis is carried out to determine both ends of the range of sizes of the ESS. Two case studies are presented in the following which show the performance of a conventional vehicle with zero ESS as one extreme and a SHEV with minimally sized but passive ESS (meaning no power converter interface between ESS and power bus) as the other extreme. The former is the major shareholder of the market by far, and the latter is hypothesized to be a surrogate for the large-ESS HEV's available in the marketplace today. These two designs are used at either end of a Pareto Frontier created from a multi-objective optimization with both ESS cost and FE objective functions. For the analysis that follows in section 5.3.1 and 5.3.2, Autonomie software will be used because it is reported that: "On the light duty side, several conventional vehicles (e.g., Chevy Equinox, Ford Explorer) have been validated within 1% fuel economy. Hybrid electric vehicles (e.g., Honda Insight, Toyota Prius, Lexus RX400) have been validated within 5% for both fuel economy and battery State-of-Charge for several driving cycles." [62].

5.2.1 Case study 1: performance of a conventional reference vehicle

A conventional reference vehicle model is developed in the Autonomie simulation environment (Fig.5.1). In Autonomie, each component is defined by a behavioral model in the Simulink environment and Autonomie basically integrates these models to run an overall model of the vehicle over selected drive cycles. An existing mid-size conventional vehicle model is modified for this study. For engine modeling, a validated Prius model available in the software's library is scaled up to 85 kW to meet the acceleration requirement in (5.1). Table 5.1 specifies the vehicle dynamic parameters.

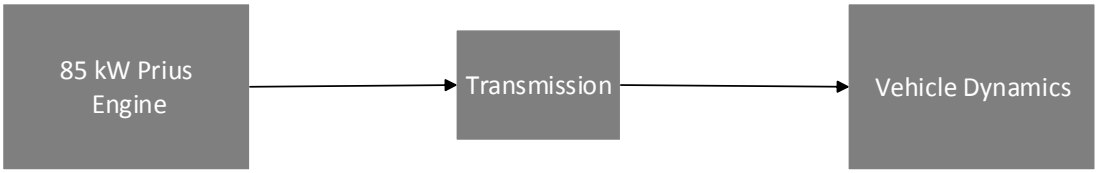

Figure 5.1 The architecture of the conventional reference vehicle

The vehicle meets the calculated acceleration and gradeability power requirements in (5.1) and (5.2). The city, highway and combined FE are computed and shown in Table 5.2. The combined MPG is 37 percent higher than those of available mid-size vehicles such as Toyota Camry [63] in the market. This is simply because the engine is sized for the requirements of (5.1) and (5.2) which are also the bases for the sizing of the energy sources in the reference SHEV in case study 2. The FEs computed in this case study are used as the worst case scenario design point that must be met by the hybrid design.

Table 5.2 Major components specifications and results of simulation for conventional reference vehicle

Mass	1560 kg
Engine	85 kW (scaled up 57 kw Prius engine)
Transmission	100 kg
ESS	-
Electric Machines	-
City FE	34.3 MPG
Highway FE	47.7 MPG
Combined FE	40.3 MPG
Available power for acceleration	> 68.4 kW
Available power for gradeability	> 25 kW

5.2.2 Case study 2: performance of a SHEV reference vehicle with minimal ESS

Figure 5.2 illustrates the architecture of the SHEV reference vehicle which was used in the parametric study of Chapter 3 (see Fig. 3.1). Two changes from that vehicle to this one are the use of a Prius 57 kW gasoline engine as the main source of energy and the use of a version of the YASA-400 generator scaled down to 57 kW. The duty ratio control strategy of Chapter 3 is used for this case study; however, the algorithm of regenerative braking has been revised. Similar to the bandwidth-based control in Chapter 4, the bandwidth limited battery current is compared to and limited by the negative rated battery current during charging mode. The power rating and other specifications of the main components of the power train are shown in Table 5.3.

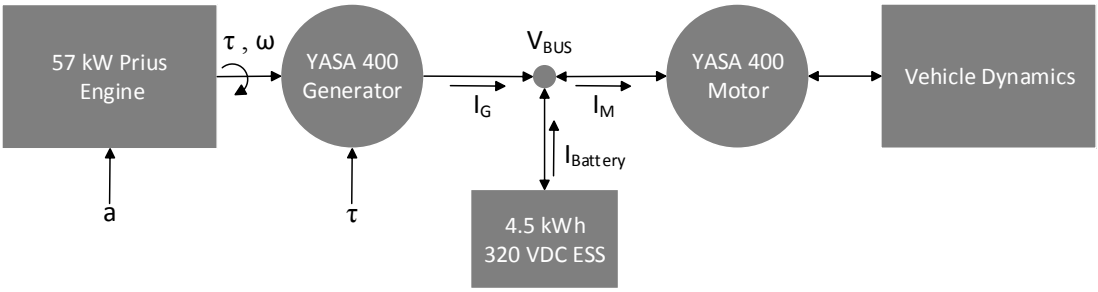

Figure 5.2 The series-hybrid architecture of the reference vehicle

The result of the case study shows that the vehicle meets the calculated acceleration and gradeability power requirements in (5.1) and (5.2). The city, highway and combined FE are listed in Table 5.3. The combined FE is 67 % greater than the FE of the properly sized conventional reference vehicle in case study 1.

Table 5.3 The results of simulation for the SHEV reference vehicle

Mass	1600 kg
Engine	57 kw Prius engine
Transmission	-
ESS	4.5 kWh Li-Ion battery, 100 kg total, 50 kg cells weight, 100 cells
Electric Machines	Two YASA-400, each 25 kg
City FE	75.0 MPG
Highway FE	57.6 MPG
Combined FE	67.2 MPG

5.2.3 ESS minimization limitations

The 4.5 kWh-ESS in 5.3.2 was a solution found through a parametric study over different types and sizes of passive ESS for maximizing combined FE, which is not the same as a formal optimization process and no claim is made as such. The term passive means that no power interface is used to decouple the battery pack voltage from the bus voltage. In this case the bus voltage must be made up by connecting multiple battery modules in series. To go further in the process of optimally minimizing the size of the ESS, similar to the sports-car concept vehicle in Chapter 4, one solution is to use a power interface which allows fewer cells in series to be used. However, in order to cover all possibilities from zero ESS to the ESS in case study 2, in addition to adding a power converter, an advanced power management strategy is required. Bandwidth-based and engine duty ratio control strategies for SHEV's with minimal ESS have been described in Chapter 3 and Chapter 4, respectively. Both control strategies are applied in this chapter to cover a wide range of ESS sizes required by the optimization process in the next section.

5.3 Optimization objective functions and constraints

The focus of the previous section was defining the design space for the ESS size. In this section, optimization objective functions, design constraints, and side constraints are defined in general form in (5.3). It is noted that because this is a simulation-based optimization, the main design constraints such as current, voltage, torque, and speed are already considered in the control strategies algorithms. The analysis in this section is presented for the reference vehicle model in Fig. 5.2 and Fig. 4.3; the ESS size is the variable of the optimization process.

$$\begin{aligned} \min \quad & \boldsymbol{f}(\boldsymbol{X}) = [f_1(\boldsymbol{X}), f_2(\boldsymbol{X}), \dots, f_N(\boldsymbol{X})] \\ s.t. \quad & g_j(\boldsymbol{X}) \le 0 \qquad j = 1, \dots, N_g \\ & X_i^l \le X_i \le X_i^u \qquad i = 1, \dots, NDV \end{aligned} \tag{5.3}$$

5.3.1 Objective functions

Based on the design concept of this research, AEM is not a requirement and can be traded to achieve the lighter ESS which eventually leads to a cheaper vehicle and more consumer adoption. The ESS cost equation is specified as a function of the number of ESS cells in (5.4).

$$Cost_{ESS}\,(n_s) = (n_s \times CW + PC(n_s) \times PCW) \times EP \tag{5.4}$$

Where n_s is the number of cells, CW is the cell weight considering packaging factor (kg), $PC(n_s)$is the power converter continuous power which is a function of the number of cells (kW), PCW is the mass of power converter per 1 kW continuous power

(kg/kW), and EP is the \$/kg for the ESS of a HEV. (5.4) can be rewritten as following to represent a first objective function in (5.5):

$$f_1(\boldsymbol{X}) = (\boldsymbol{X} \times CW + PC(\boldsymbol{X}) \times PCW) \times EP \quad (5.5) \quad (5-$$

$where: \boldsymbol{X} = X_1 = \ n_s$

The second objective function in this study is the combined city and highway FE. For each control strategy, a separate equation is derived. For the engine duty ratio control strategy, the FE is a function of n_s:

$$FE(n_s) = 0.55 \times FE_{city}(n_s) + 0.45 \times FE_{highway}(n_s) \quad (5.6) \quad (5-6)$$

(5.6) can be rewritten as follows to represent the second objective function in (5.7). The negative of FE is minimized:

$$f_2(\boldsymbol{X}) = -1 \times [0.55 \times FE_{city}(\boldsymbol{X}) + 0.45 \times FE_{highway}(\boldsymbol{X})] \quad (5.7) \quad (5-7)$$

$where: \boldsymbol{X} = X_1 = \ n_s$

However, if the bandwidth based control strategy is used, the fuel economy varies by changing three variables: number of cells, n_s, Student's-*t* threshold, $t_\propto$, and filter cut-off frequency, f_0; therefore in (5.7):

$\boldsymbol{X} = [X_1, X_2, X_3]; where: X_1 = n_s, X_2 = t_\propto, and, X_3 = f_0$

For computing FE, the conditions in standard SAE J1711 for vehicle weight are applied [64], so the vehicle curb weight plus cargo weight is considered in the calculation.

5.3.2 ESS side and design constraints

In Chapter 3, it is shown that sizing the engine for average power rather than peak power increases the overall efficiency. The engine size, in Fig 5.2 or Fig 4.3, is selected based on this concept. Therefore, for the acceleration scenario which is the peak demand for short durations, both engine and ESS are required to contribute. This determines the minimum constraint for the ESS size. (5.8) specifies the available power from the engine for acceleration:

$$P_{a-Eng} = P_{Eng-max} \times \eta_{Gen} \times \eta_{Mot} \tag{5.8}$$

$P_{Eng-max}$ is the engine peak power, 57 kW; η_{Gen}, is the YASA-400 generator efficiency at 57 kW, 0.93; η_{Mot}, is the YASA-400 motor efficiency at 68.4 kW, 0.91. From (5.8) the engine acceleration power $P_{a-Eng} = 48.24\ kW$ is calculated. The power required from the ESS for acceleration is calculated in (5.9).

$$P_{a-ESS} = \frac{P_a - P_{a-Eng}}{\eta_{Mot}} = \frac{(68.4 - 48.24)kW}{0.91} = 22.15\ kW \tag{5.9}$$ $(5-9)$

The minimum number of cells constraining optimization is found from (5.10).

$$n_{s-min} = \frac{P_{a-ESS}}{P_{ESS-10s}} = \frac{22.15\ kW}{1.058\ kW} = 20.94 \approx 21 \tag{5.10}$$ $(5-10$

Where: $P_{ESS-10s}$ is the maximum discharge pulse power for 10 s extracted from the ESS specifications. Therefore, the number of cells in series is bracketed by (5.11), which is the side constraint of the optimization problem. Table 5.4 shows the specifications of the ESS, which was recognized as the best candidate in the parametric study.

$$n_{s-min} < n_s < n_{s-max} \tag{5.11}$$

Where $n_{s-max} = 100$ is the number of cells in series for the 4.5 kWh ESS found by the parametric study in case study 2. (5.11) can be rewritten as following to represent a side constraint in (5.12):

$$21 \leq X_1 \leq 100 \tag{5.12}$$

ESS energy variation at the end of a drive schedule must be kept within the bounds of acceptable state of charge variation; therefore:

$$SOC_{min} < \Delta SOC < SOC_{max} \tag{5.13}$$

Table 5.4 The specifications of AMP14 cells found through a parametric study on size for the reference vehicle in case study 2 in Chapter 3.

Manufacturer/model	A123/AMP14
Capacity	14 Ah
Cell weight (CW)	0.51 kg
Nominal Voltage	3.2 V
Discharge Pulse Power (10 sec)	1.058 kW
Discharge Power (continuous)	0.48 kW
Discharge Pulse Current (10 sec)	400 A
Discharge Power (continuous)	180 A
Cost* (EP)	83.33 $/kg
Specific mass of power converter PCW	0.21 kg/kW

Notes: data is extracted from [28], for a Chevrolet Volt 16 kWh/150 kg battery

(5.13) can be rewritten as follows to represent a design constraint on (5.3); 30% and 80% are set for upper and lower limits:

$$0.3 < g_j(\boldsymbol{X}) = \Delta SOC(\boldsymbol{X}) \leq 0.8 \tag{5.14}$$

(5.12) and (5.14) are respectively side and design constraints for the defined problem in (5.3).

5.3.3 Pareto Frontier-Duty Ratio Control Strategy

The result in this section is obtained using the duty ratio control strategy. Fig. 5.3 shows the Pareto Frontier in criterion space which includes optimal ESS costs versus optimal FE. The optimum values of (5.5) are displayed on the vertical axis, and the optimum values of (5.7) are displayed on the horizontal axis. The sign of FE shown on the plot is negative because the negative of FEs have been minimized. A problem arises with duty ratio control which limits its use with smaller ESS's. The following analysis describes the problem. When the number of cells is reduced, the ESS nominal voltage decreases; therefore, a power interface such as a bidirectional DC-DC converter is required to build the same voltage at the bus. Different voltage ratios are required for different numbers of cells, so the range of N_c, the converter voltage ratio, is determined by (5.15) for corresponding ESS sizes in (12).

$$1 < N_c \leq 4.17 \tag{5.15}$$

The expression (5.16) can be written for primary ESS current:

$$I_{ESS-Prim} = N_c \times I_{ESS-Sec} \tag{5.16}$$

Where $I_{ESS-Sec}$ is the current at the secondary side of the converter connected to the power bus.

In duty ratio control, when the engine is off and the vehicle is in AEM mode, the $I_{ESS-Sec}$ is equal to the requested motor current. It can be shown that for the case study 2 in section 5.3.2, frequently, a motor current up to 190 A is requested, so based on (5.16), $I_{ESS-Prim} = N_c \times 190\ A$. From Table 5.4, the pulsed current capability of the ESS is limited to 400 A; therefore, $N_c = \frac{400\ A}{190\ A} = 2.11$ is the maximum ratio of the converter.

The associated number of cells for this boundary is 48. Therefore, for duty ratio control (5.12) is revised as following:

$$48 \leq X_1 \leq 100 \tag{5.17}$$

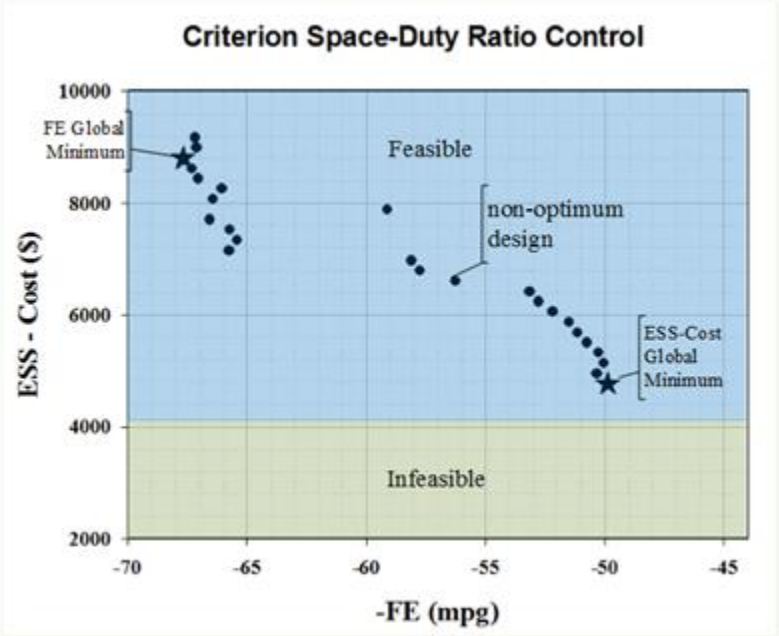

Figure 5.3 Pareto Frontiert in criterion space using duty ratio control strategy. Green area is infeasible domain.

$21 \leq X_1 < 48$ is unfeasible for duty ratio control alone; the corresponding unfeasible domain in criterion space is shown on the plot in Fig. 5.3. In addition to the out-of-boundary current problem, larger N_c results in increased ESS losses, and thermal and electrical cycling of the battery cells. It is noted that ESS loss increases proportional with N_c^2. Consequently, with duty ratio control as N_c increases the ESS efficiency drops and lifetime may be reduced.

5.3.4 Pareto Frontier Bandwidth Based Control Strategy

In this section the Pareto Frontier is achieved using a bandwidth based control strategy. Engine duty cycling as one of the features of the bandwidth based strategy that is responsible for switching between states to manage the engine in the efficient regions of the engine efficiency map. However, the number of cycles should be controlled because frequent engine cycling might cause customer anxiety and may pose long term reliability issues with the power train components themselves. To control the occurrence of duty cycling, a third objective function is defined in (5.18) which maximizes the dwell times of the nominal states. The nominal state dwell time is the percent of time that the controller dwells in the state, which is proportional to the average or expected motor power defined for that state by a corresponding driving behavior. Therefore, for city and highway drive cycles, “Urban” state 2, and “Highway” state 3 are nominal states respectively (See Fig. 4.6).

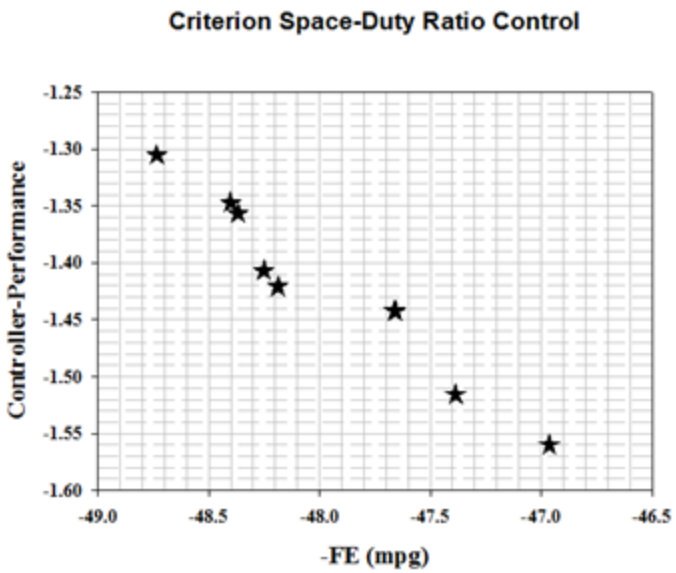

Figure 5.4 Pareto Frontier in criterion space using bandwidth based control strategy for optimizing both FE and controller performance.

$$f_3(\boldsymbol{X}) = -1 \times \left(\frac{DT_{city}(\boldsymbol{X})}{DT_{city-w}} + \frac{DT_{Hw}(\boldsymbol{X})}{DT_{Hw-w}}\right) \quad (5.18)$$

Where $DT_{city}(\boldsymbol{X})$ and $DT_{Hw}(\boldsymbol{X})$ are respectively city and highway nominal dwell times, and $DT_{city-w} = 30\%$ and $DT_{Hw-w} = 50\%$ are respectively the minimum threshold for dwell time in city and highway states. The negative sign behind the equation is to change the maximization problem to a minimization problem in order that it can be incorporated into the general form of (5.3). Similar to (5.7), $\boldsymbol{X} = [X_1, X_2, X_3]; where: X_1 = n_s, X_2 = t_\propto, and, X_3 = f_0$.

Table 5.5 Optimum design variables and their associated optimum points on criterion space

$f_2(\boldsymbol{X})$ (MPG)	$f_3(\boldsymbol{X})$	$t_\propto$	f_0(Hz)
-46.96	-1.56	0.7687	0.0309
-48.73	-1.31	0.7690	0.0282
-48.37	-1.36	0.7690	0.0293
-47.66	-1.44	0.7689	0.0307
-47.39	-1.52	0.7687	0.0288
-48.19	-1.42	0.7689	0.0307
-48.40	-1.35	0.7690	0.0293
-47.66	-1.44	0.7689	0.0306
-48.25	-1.41	0.7689	0.0307
-48.73	-1.31	0.7690	0.0282
-46.96	-1.56	0.7687	0.0309

Dwell time is also affected by the hysteresis band shown in Fig 4.3 (see the up and down arrows). For example, if the hysteresis band regarding urban state 2, moves upward compared to what is shown on the plot, smaller dwell time and higher FE is expected. For best performance the hysteresis bands should also be tuned based on a requirement. By setting $X_1 = n_s$ constant, $f_1(\boldsymbol{X})$ becomes constant. In this case, a Pareto Frontier of $f_2(\boldsymbol{X})$ and $f_3(\boldsymbol{X})$ can be computed by finding the corresponding optimum design space variables, $X_2 = t_\propto, and, X_3 = f_0$. An example for $X_1 = 33$ is drawn in Fig. 5.4. Table 5.5 shows the optimum values for the Student's-*t* threshold, $t_\propto$, and the cut-off frequency, f_0 corresponding to each point on the Pareto Front in criterion space. All points are optimum. Depending on the weight that is dedicated to each of objective function, f_2 and f_3, one final design can be selected. For example, to be consistent in the following analysis, the best FE point, or minimum f_2, is selected as a final optimum design at this stage. A similar analysis can be carried out for a selected X_1 within the defined range in (5.12). A parametric study in this range is carried out and the final

Pareto Front optimal set using the bandwidth-based control strategy, which shows the ESS costs versus FEs, is drawn in Fig. 5.5. The bandwidth based control strategy increases the FE by enlarging the ESS. It stops improving the FE when N_c approaches unity because the ESS mass becomes significant which adversely affects the FE.

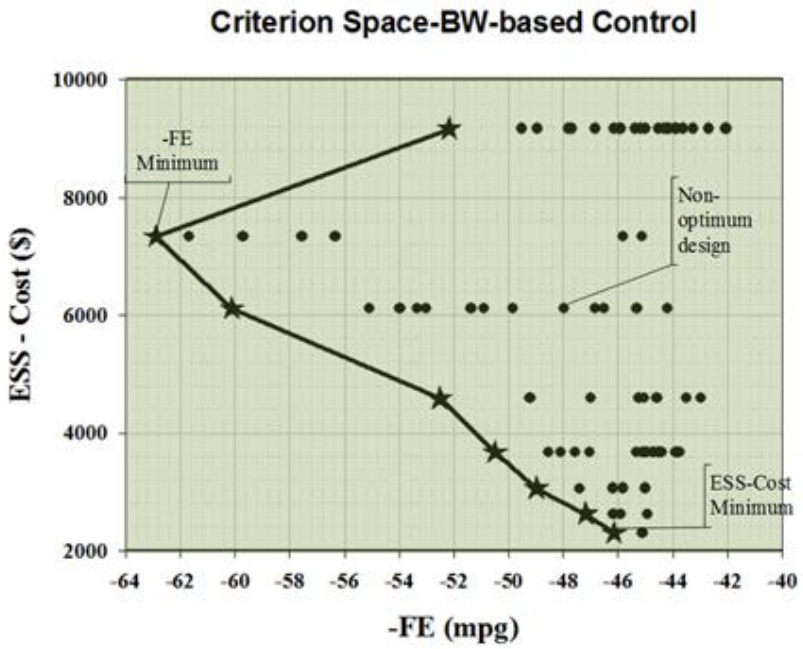

Figure 5.5 Pareto Front optimal set in criterion space using bandwidth-based control strategy.

5.3.5 Combined Pareto Front set

Bandwidth-based control allows a smaller ESS than duty ratio control alone. However, this control is more useful for smaller ESS's; for larger ESS's pure duty cycling performs better. To cover the defined ESS range in (5.12) efficiently, both controllers can be used in their own efficient regions. Fig. 5.6 shows the combination of

two Pareto Front optimal sets in one plot where bandwidth-based is applied for the range specified in (5.19) and duty cycling is applied for the rest of the design space.

$$21 < X_1 < 80 \tag{5.19}$$

5.3.6 Computational challenges

The optimization and parallel computing tool boxes of MATLAB are used for solving the optimization problem in this study. This is a nonlinear simulation-based framework relying on mechanical and electrical subsystems.

MOGA, which is an advanced zeroth order method based on a random search that operates by evaluating the objective functions, is applied. This algorithm is also known for its effective performance in finding optimum points in design problems. Computing results in fig. 5.6 with a four processor machine requires almost 192 hours. The result displayed in Fig. 5.6 was achieved in 30 hours by using eight 12-processor nodes of a cluster computer.

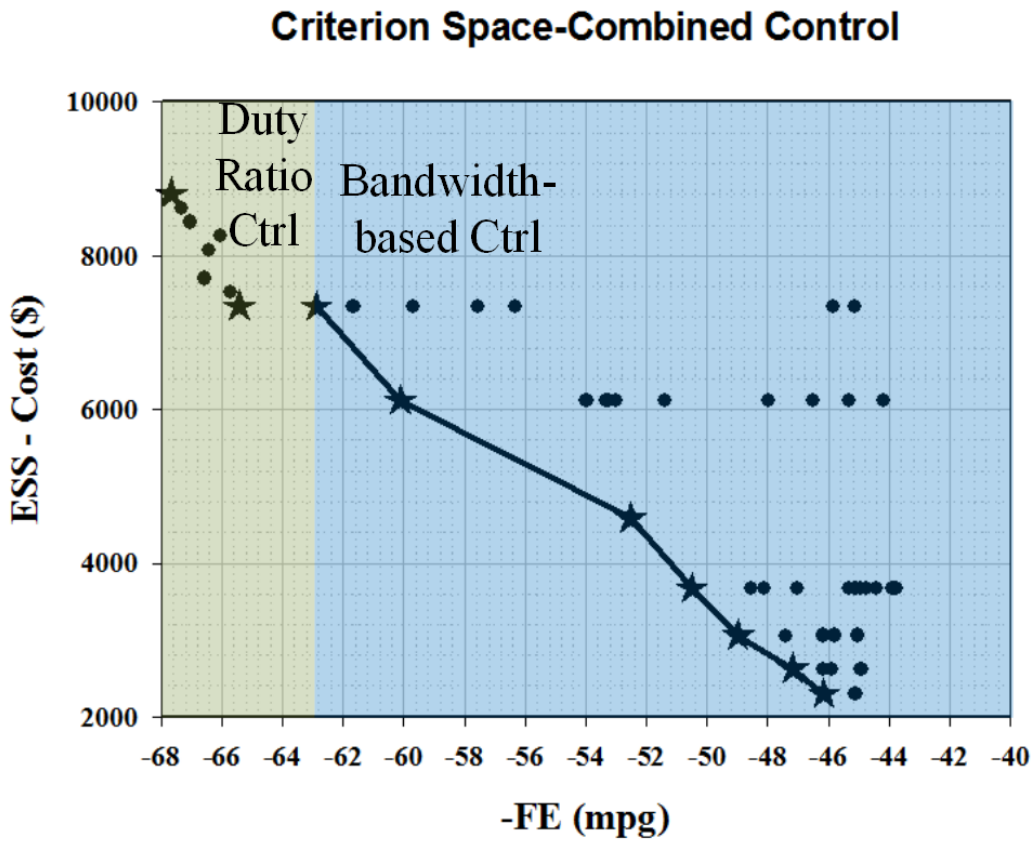

Figure 5.6 Pareto Front optimal set in criterion space using combination of bandwidth-based and duty ratio control strategy in their efficient zones.

5.3.7 Model limitations

Although as mentioned in section 5.3, Autonomie presents conventional and hybrid vehicle models with decent accuracy, other model limitations are introduced by customizing the model. For the electric machine, a YASA-400, the efficiency map provided by the manufacturer is used, so the accuracy of the model is affected by the accuracy of manufacturer data. In this system level optimization study, the associated time constants of engine acceleration and deceleration power are ignored. For the conventional-vehicle reference model, a 57 kW Prius engine is scaled up to 85 kW which

might affect the result to some extent. However, the result can be justified by comparing to similar conventional vehicles available in the market. The power converter losses are not included in the model, so it is expected that after considering this dissipation the Pareto Frontier will move somewhat to the right.

5.4 Chapter Summary

In this chapter, an advanced bandwidth-based power flow control method is used to extend the SHEV engine management benefit to smaller ESS. The bandwidth-based control strategy introduced in Chapter 4 was joined with an engine duty ratio control strategy that together cover the full range of feasible ESS designs for realizing a SHEV with limited AEM. At the end, the Pareto Frontier, including optimal ESS costs and FE's, is computed using a simulation-based parallel multi-objective optimization based on the genetic algorithm.

CHAPTER VI

CONCLUSIONS AND FUTURE WORK

In this dissertation, a bandwidth-based methodology for designing the energy storage system (ESS) has been proposed for a series hybrid electric vehicle (SHEV). The motivation for selecting a frequency domain approach is the fact that with the benefit of engine management a small ESS can play the role of a filter rather than be a major energy source. In three phases, a design approach is developed for the twin goals of maximizing the fuel economy (FE) and minimizing the ESS cost. In phase one, a parametric study is conducted over different sizes and types of passive non hybrid and hybrid ESS's for maximizing FE. A vehicle model in Autonomie is used to simulate the performance of the power train and a customized engine duty ratio control strategy is applied for distributing the load between engine and ESS. A specific high power battery is recognized as a winning candidate in this phase of the research. A series HEV emulator has been built to empirically validate the performance of the selected design and the reported results show close agreement between simulation and experiment. However, a 4.5 kWh battery is still required. Control strategy limitations and the passive interconnection of the ESS to the bus are found to be the obstacles to further ESS minimization. These issues were addressed in phase two.

In phase two, a bandwidth-based control strategy is proposed which manages the power flow between ICE and ESS to allow additional minimization of the ESS. The

controller has two features: efficient ICE duty-cycling management and bandwidth-limited proportional control. Two features limit the ESS current spectrum, the major obstacle for ESS minimization, within the ICE operational bandwidth, BW. A BW was found via a multi-objective optimization to optimize both FE and controller performance. A feasibility study was presented that tested the controller performance for a sports-car concept SHEV with severely limited ESS space allocation. The controller permits a SHEV power-train with the ESS capacity as low as 1.125 kWh to be realized.

In phase three, the bandwidth-based control strategy was teamed with engine duty ratio control to cover the entire design space for the size of the ESS in a SHEV reference vehicle. The bandwidth-based controller allows the engine management benefits of the SHEV architecture to be extended to smaller-sized ESS. The minimum size is constrained by vehicle acceleration requirements and the maximum size was bounded by that found in phase one. A Pareto Frontier, including optimized FE's and ESS costs, is computed. The Pareto Frontier is a valuable design information which defines optimum designs in response to different customer requirements.

For future work, it is recommended that the bandwidth-based control strategy be tested on the emulator for validating the feasibility study of the Subaru BRZ concept SHEV. In addition to that, a library of statistically distributed drive cycles should be developed and used to test the bandwidth-based controller for sensitivity of performance over a broad range of random driving styles. Finally, the design of the specific engine used in a Series HEV should be rethought for the purpose of maximizing the efficiencies at favorable operating points, as opposed to relying on engines intended for the continuously changing power demands of a conventional automobile.

REFERENCES

[1] Energy Information Administration, "Annual Energy Outlook 2007 With Projections to 2030," Department of Energy, 2007.

[2] U.S. Energy Information Administration, "Annual Energy Outlook 2011 with Projections to 2035," Department of Energy, 2011.

[3] International Energy Agency, "Key World Energy Statistics 2009," 2009.

[4] C. C. Chan, "The state of the art of electric and hybrid vehicles," Proceedings of the IEEE, vol. 90, pp. 247-275, 2002.

[5] C. C. Chan, "The State of the Art of Electric, Hybrid, and Fuel Cell Vehicles," Proceedings of the IEEE, vol. 95, pp. 704-718, 2007.

[6] S. M. Lukic, et al., "Energy Storage Systems for Automotive Applications," IEEE Transactions on Industrial Electronics, vol. 55, pp. 2258-2267, 2008.

[7] S. Vazquez, et al., "Energy Storage Systems for Transport and Grid Applications," IEEE Transactions on Industrial Electronics, vol. 57, pp. 3881-3895, 2010.

[8] J. Li, "Performance-Driven Behavioral Battery Modeling for Large Format Batteries," Mississippi State university PhD. dissertation, 2012.

[9] U.S. Energy Information Administration, "Annual Energy Review 2009," US Dept Energy, 2010.

[10] Davis SC, Diegel SW, Boundy RG, Transportation Energy Data Book, Washington, DC: Oak Ridge Natl Lab, US Dept Energy, 2010.

[11] Michalek, Jeremy J., Mikhail Chester, Paulina Jaramillo, Constantine Samaras, Ching-Shin Norman Shiau, and Lester B. Lave, "Valuation of plug-in vehicle life-cycle air emissions and oil displacement benefits," Proceedings of the National Academy of Sciences, vol. 108, no. 40 (2011), pp. 16554-16558, 2011.

[12] S. Eaves and J. Eaves, , "A cost comparison of fuel-cell and battery electric vehicles," Journal of Power Sources, vol. 130, pp. 208-212, 2004.

[13] Jeff Cobb, hybridcars auto alternative for the 21th century[Online]. "Available: http://www.hybridcars.com/november-2014-dashboard/" [Online].

[14] Karden, Eckhard, Servé Ploumen, Birger Fricke, Ted Miller, and Kent Snyder., "Energy storage devices for future hybrid electric vehicles," Journal of Power Sources, vol. 1, no. 2007, pp. 2-11, 2007.

[15] Desai, Chirag, and Sheldon S. Williamson, "Optimal design of a parallel Hybrid Electric Vehicle using multi-objective genetic algorithms," In Vehicle Power and Propulsion Conference, 2009, VPPC'09, IEEE, pp. 871-876, 2009.

[16] Paladini, Vanessa, Teresa Donateo, Arturo De Risi, and Domenico Laforgia, "Super-capacitors fuel-cell hybrid electric vehicle optimization and control strategy development," Energy Conversion and Management, vol. 48, no. 11, pp.3001-3008, 2007.

[17] Huang, Bufu, Zhancheng Wang, and Yangsheng Xu, "Multi-objective genetic algorithm for hybrid electric vehicle parameter optimization," Intelligent Robots and Systems, IEEE/RSJ International Conference on, pp. 5177-5182. , 2006.

[18] Cericola D, Ruch P, Kotz R, Novak P, Wokaun A., "Simulation of supercapacitor/ Li-ion battery hybrid for pulsed applications.," J Power Sources, vol. 195, pp. 2731-6, 2010.

[19] J. P. Zheng, T.R. Jow, M. S. Ding , "Hybrid power sources for pulsed current applications," IEEE Trans Aerospace Elect Syst, vol. 37, no. 1, pp. 288-92, 2001.

[20] R. A. Dougal, L. Shengyi, R. E. White, "Power and life extension of battery-ultracapacitor hybrids," IEEE Trans Compon Packag Technol, vol. 25, no. 1, p. 120–31, 2002.

[21] S. M. Lukic, J. Cao, R. C. Bansal, F. Rodriguez, A. Emadi, "Energy Storage Systems for Automotive Applications," IEEE Trans. on Industrial Electronics, vol. 55, no. 6, pp. 2258-2267, June 2008..

[22] M. Pagano, L. Piegari, "Hybrid electrochemical power sources for onboard applications.," IEEE Trans Energy Convers, vol. 22, no. 2, p. 450–6, 2007.

[23] M. T. Penella, M. Gasulla, "Runtime extension of low power wireless sensor nodes using hybrid storage units," IEEE Trans Instrum Measure, vol. 59, no. 4, p. 857–65, 2010.

[24] H. Liu, Z. Wang, J. Cheng, D. Maly, "Improvement on the cold cranking capacity of commercial vehicle by using supercapacitor and lead-acid battery hybrid," IEEE Trans Vehicular Technol, vol. 58, no. 3, p. 1097–105, 2009.

[25] Y. Gao, M. Ehsani, "Parametric design of the traction motor and energy storage for series hybrid off road and military vehicles.," IEEE Trans Power Electron, vol. 21, no. 3, p. 749–55, 2006.

[26] M. Ehsani, Y. Gao, and A. Emadi, Modern Electric, Hybrid Electric, and Fuel Cell Vehicles. Fundamental, Theory, and Design, second edition, CRC Press Taylor & Francis Group, Chap. 7 and Chap. 13, 2010.

[27] L. Wang, E. G. Collins, and H. Li, "Optimal Design and Real-Time Control for Energy Management in Electric Vehicles," IEEE Trans Vehicular Technology, vol. 60, no. 4, pp. 1419-1429, 2011.

[28] A. Khaligh, Z. Li, "Battery, Ultracapacitor, Fuel Cell, and Hybrid EnergyStorage Systems for Electric, Hybrid Electric,Fuel Cell, and Plug-In Hybrid Electric Vehicles: State of the Art," Vehicular Technology, IEEE Transactions, vol. 59, no. 6, pp. 2806 - 2814, July 2010.

[29] J. Cao, and A. Emadi, "A New Battery/UltraCapacitor Hybrid Energy Storage System for Electric, Hybrid, and Plug-In Hybrid Electric Vehicles," IEEE Transactions Power Electronics, vol. 27, no. 1, pp. 122-132, 2012.

[30] J. Cao, A. Emadi, "A New Battery/Ultra-Capacitor Hybrid Energy Storage System for Electric, Hybrid and Plug-in Hybrid Electric Vehicles," in Vehicle Power and Propulsion Conference, 2009.

[31] O. C. Onar, A. Khaligh, "A Novel Integrated Magnetic Structure Based DC/DC Converter for Hybrid Battery/Ultracapacitor Energy Storage Systems," Smart Grid, IEEE Transactions, vol. 3, no. 1, pp. 296 - 307, 2012.

[32] A. L. Allègre, A. Bouscayrol, R. Trigui, "Influence of control strategies on battery/supercapacitor hybrid Energy Storage Systems for traction applications," in Vehicle Power and Propulsion Conference, Dearborn, pp. 213-220, 2009.

[33] J. S. Lai, D. J. Nelson , "Energy Management Power Converters in Hybrid Electric and Fuel Cell Vehicles," in Proceedings of the IEEE, vol. 95, no. 5, pp. 766-777, 2007.

[34] A. Kuperman, I. Aharon, A. Kara, and S. Malki, "A frequency domain approach to analyzing passive battery–ultracapacitor hybrids supplying periodic pulsed current loads," Energy Conversion and Management, vol. 52, no. 12, p. 3433–3438, 2011.

[35] M. A. Brubaker, D. El Hage, T. A. Hosking, H. C. Kirbie, and E. D. Sawyer, "Increasing the Life of Electrolytic Capacitor Banks Using Integrated High Performance Film Capacitors," in CIPS, Nuremberg, 2010.

[36] A. Tani, M. B. Camara, and B. Dakyo, "Energy Management Based on Frequency Approach for Hybrid Electric Vehicle Applications: Fuel-Cell/Lithium-Battery and Ultracapacitors," IEEE Trans Vehicular Technology, vol. 61, no. 8, pp. 3375-3386, 2012.

[37] Zandi, Majid, Alireza Payman, J-P. Martin, Serge Pierfederici, Bernard Davat, and Farid Meibody-Tabar., "Energy management of a fuel cell/supercapacitor/battery power source for electric vehicular applications," Vehicular Technology, IEEE Transactions on, vol. 60, no. 2, pp. 433-443, 2011.

[38] Schaltz, Erik, Alireza Khaligh, and Peter Omand Rasmussen, "Influence of battery/ultracapacitor energy-storage sizing on battery lifetime in a fuel cell hybrid electric vehicle," Vehicular Technology, IEEE Transactions on, vol. 58, no. 8, pp. 3882-3891, 2009.

[39] Adzakpa, K. P., K. Agbossou, Y. Dubè, M. Dostie, M. Fournier, and A. Poulin, "PEM fuel cells modeling and analysis through current and voltage transient behaviors," Energy Conversion, IEEE Transactions on, vol. 23, no. 2, pp. 581-591, 2008.

[40] Liu, Wei-Shih, Jiann-Fuh Chen, Tsorng-Juu Liang, and Ray-Lee Lin., "Multicascoded sources for a high-efficiency fuel-cell hybrid power system in high-voltage application," Power Electronics, IEEE Transactions on, vol. 26, no. 3, pp. 931-942, 2011.

[41] Wu, Xiaolan, Binggang Cao, Xueyan Li, Jun Xu, and Xiaolong Ren, "Component sizing optimization of plug-in hybrid electric vehicles," Applied Energy , vol. 88, no. 3, pp. 799-804, 2011.

[42] Shahverdi, Masood, Michael Mazzola, Nicolas Sockeel, and Jim Gafford, "High bandwidth energy storage devices for HEV/EV energy storage system," in Transportation Electrification Conference and Expo (ITEC), 2014 IEEE, Dearborn, 2014.

[43] Sissine, Fred, "CRS Report for Congress: The Partnership for a New Generation of Vehicles (PNGV)". National Library for the Environment, 2006.

[44] "Review of the Research Program of the Partnership for a New Generation of Vehicles: Seventh Report," National Research Council, pp. 1-133, 2001.

[45] ""FreedomCAR: Getting New Technology into the Marketplace".," U.S. House of Representatives Charters: Committee on Science, Subcommittee on Energy, 2002.

[46] E. Karden, S. Ploumen, B. Fricke, T. Miller, K. Snyder,, "Energy storage devices for future hybrid electric vehicles," Journal of Power Sources, vol. 168, no. 1, pp. 2-11, 2007.

[47] "http://electricdrive.org/index.php?ht=d/sp/i/20952/pid/20952," [Online].

[48] Autonomie, Argonne National Laboratory. [Online]., "Available: http://www.autonomie.net/," [Online].

[49] YASA MOTORS. [Online], "Available: http://www.yasamotors.com/products/yasa-400/," [Online].

[50] Sevcon. [Online], "Available: http://www.sevcon.com/ac-controllers/gen-4-size-8.aspx," [Online].

[51] J. M. Miller, T. Bohn, T. J. Dougherty, U. Deshpande, "Why hybridization of energy storage is essential for future hybrid, plug-in and battery electric vehicles," in Energy Conversion Congress and Exposition, San Jose, 2009.

[52] A. F. Burke , "Batteries and Ultracapacitors for Electric, Hybrid, and Fuel Cell Vehicles," Proceedings of the IEEE, vol. 95, no. 4, pp. 806 - 820, 2007.

[53] J Li, MS Mazzola, J Gafford, B Jia, M Xin, "Bandwidth based electrical-analogue battery modeling for battery modules," Journal of Power Sources, vol. 218, p. 331–340, 2012.

[54] Chau, K.T., and Wong, Y.S. , "Overview of power management in hybrid electric vehicles," Energy Conversion and Management, vol. 43, no. 15, pp. 1953–1968, 2002.

[55] Wirasingha, S. G., and Emadi, A. , "Classification and Review of Control Strategies for Plug-In Hybrid Electric Vehicles," IEEE Trans Vehicular Technology, vol. 60, no. 1, pp. 111-122, 2011.

[56] Bradley, T. H., and Frank, A. , "Design, demonstrations and sustainability impact assessments for plug-in hybrid electric vehicles," Renewable and Sustainable Energy, vol. 13, no.1, pp. 115–128, 2009.

[57] Mapelli, F., Mauri, M., and Tarsitano, D., "Energy control strategies comparison for a city car Plug-In HEV," in Industrial Electronics, 2009. IECON '09. 35th Annual Conference of IEEE, Porto , 2009.

[58] Yoo, H., Sul, S. K., Park, Y., and Jeong, J., "System Integration and Power-Flow Management for a Series Hybrid Electric Vehicle Using Supercapacitors and Batteries," IEEE Trans Industry Applications, vol. 44, no.1, pp. 108-114, 2008.

[59] Camara, M. B., Gualous, H., Gustin,F., "DC/DC Converter Design for Supercapacitor and Battery Power Management in Hybrid Vehicle Applications—Polynomial Control Strategy," IEEE Trans Industrial Electronics, vol. 57, no.2, pp. 587-597, 2010.

[60] Yan, W. Utkin, V., and Rizzoni, G., "Power Flow Control for a Series Hybrid Electric Vehicle," in ISIE 2005, Dubrovnik, Croatia, 2005.

[61] He, X., Parten, M., and Maxwell, T. , "Energy Management Strategies for a Hybrid Electric Vehicle," Vehicle Power and Propulsion, IEEE Conference, pp. 536-540, 2005.

[62] Li, S. G. , Sharkh, S. M. , Walsh, F. C. and Zhang, C. N., "Energy and Battery Management of a Plug-In Series Hybrid Electric Vehicle Using Fuzzy Logic," IEEE Trans Vehicular Technology, vol. 60, no. 8, pp. 3571-3585, 2011.

[63] Lin, C. C., Peng, H., Grizzle, J. W., and Kang, J. M., "Power Management Strategy for a Parallel Hybrid Electric Truck," IEEE Transactions On Control Systems Technology, vol. 11, no. 6, pp. 839-849, 2003.

[64] Liu, J., and Peng, H., "Modeling and Control of a Power-Split Hybrid Vehicle," IEEE Trans Control Systems Technology Vol. 16, no. 6, pp. 1242-1251, 2008.

[65] Poursamad, Amir, and Morteza Montazeri., "Design of genetic-fuzzy control strategy for parallel hybrid electric vehicles.," Control Engineering Practice vol. 16, no.7, pp. 861-873, 2008.

[66] Wu, Xiaolan, Binggang Cao, Jianping Wen, and Yansheng Bian, "Particle swarm optimization for plug-in hybrid electric vehicle control strategy parameter," in Vehicle Power and Propulsion Conference, pp. 1-5, 2008.

[67] Wu, J., C-H. Zhang, and N-X. Cui, "PSO algorithm-based parameter optimization for HEV powertrain and its control strategy," International Journal of Automotive Technology, vol. 9, no.1, pp. 53-59, 2008.

[68] Kim, Namwook, Sukwon Cha, and Huei Peng, "Optimal control of hybrid electric vehicles based on Pontryagin's minimum principle," Control Systems Technology, IEEE Transactions, vol. 19, no.5, pp. 1279-1287, 2011.

[69] Moreno, Jorge, Micah E. Ortúzar, and L. W. Dixon, "Energy-management system for a hybrid electric vehicle, using ultracapacitors and neural networks," Industrial Electronics, IEEE Transactions, vol. 53, no. 2, pp. 614-623, 2006.

[70] Wang, Lei, Emmanuel G. Collins Jr, and Hui Li, "Optimal design and real-time control for energy management in electric vehicles," , IEEE Trans Vehicular Technology, vol. 60, no.4, pp. 1419-1429, 2011.

[71] Tani, Abdallah, Mamadou Baïlo Camara, and Brayima Dakyo, "Energy management based on frequency approach for hybrid electric vehicle applications: Fuel-cell/lithium-battery and ultracapacitors," IEEE Trans Vehicular Technology, vol 61, no. 8, pp. 3375-3386, 2012.

[72] Li, Jianwei, Michael S. Mazzola, James Gafford, Bin Jia, and Ming Xin, "Bandwidth based electrical-analogue battery modeling for battery modules," Journal of Power Sources, vol. 218, no. 2012, pp. 331-340, 2012.

[73] Wu,Xiaolan, Binggang Cao, Xueyan Li, Jun Xu, and Xiaolong Ren, "Component sizing optimization of plug-in hybrid electric vehicles.," Applied Energy, vol. 88, no. no. 3, pp. 799-804, 2011.

[74] Hasanzadeh, A., B. Asaei, and A. Emadi., "Optimum design of series hybrid electric buses by genetic algorithm," Industrial Electronics, 2005. ISIE 2005. Proceedings of the IEEE International Symposium, vol. 4, pp. 1465-1470, 2005.

[75] Desai, Chirag, and Sheldon S. Williamson, "Optimal design of a parallel Hybrid Electric Vehicle using multi-objective genetic algorithms," Vehicle Power and Propulsion Conference, 2009. VPPC'09. IEEE, pp. 871-876, 2009.

[76] Paladini, Vanessa, Teresa Donateo, Arturo De Risi, and Domenico Laforgia, "Super-capacitors fuel-cell hybrid electric vehicle optimization and control strategy development," Energy Conversion and Management, vol. 48, no. 11, pp. 3001-3008, 2007.

[77] Huang, Bufu, Zhancheng Wang, and Yangsheng Xu., "Multi-objective genetic algorithm for hybrid electric vehicle parameter optimization," Intelligent Robots and Systems, 2006 IEEE/RSJ International Conference on, pp. 5177-5182, 2006.

[78] Romaus, Christoph, J. Bocker, Katrin Witting, Albert Seifried, and Oleksiy Znamenshchykov, "Optimal energy management for a hybrid energy storage system combining batteries and double layer capacitors," Energy Conversion Congress and Exposition, ECCE, IEEE, pp. 1640-1647, 2009.

[79] Schupbach, Roberto M., Juan C. Balda, Matthew Zolot, and Bill Kramer, "Design methodology of a combined battery-ultracapacitor energy storage unit for vehicle power management," Power Electronics Specialist Conference, PESC'03., vol. 1, pp. 88-93, 2003 IEEE 34th Annual.

[80] Office of Public Affairs, "MSU building 'Car of the Future'," Center For Advanced Vehicular System, 03 09 2014. [Online]. Available: http://www.msstate.edu/web/media/detail.php?id=6790. [Accessed 03 11 2014].

[81] Moore TC, Lovins AB., "Vehicle design strategies to meet and exceed PNGV goals.," Future transportation technology conference. SAE paper Technical Paper, p. no. 951906., 1995.

[82] "Green Car Congress," 21 06 2012. [Online]. Available: http://www.greencarcongress.com/2012/06/models-20120621.html. [Accessed 23 10 2014].

[83] "Autonomie," 09 2010. [Online]. Available: http://www.autonomie.net/projects/model_valid_21.html. [Accessed 23 10 2014].

[84] Toyota, "Toyota," [Online]. Available: http://www.toyota.com/camry/features.html#!/capacities/2532/2546/2548/2540. [Accessed 06 01 2015].

[85] Hybrid-EV Committee, "SAE," 08 06 2010. [Online]. Available: http://standards.sae.org/j1711_201006/. [Accessed 31 10 2014].

APPENDIX A

CALIBRATION AND SETTING ASSOCIATED TO CHASSIS DYNAMOMETER TEST

A.1 Calibration and setting associated to chassis dynamometer

Rolling resistance causes a significant vehicle loss; the associated force is calculated from the following equation:

$$F_r = Mg(f_{r0} + f_{r1} \times V) \tag{A.1}$$

Where M is vehicle mass, g is 9.8 m.s^{-2}, V is vehicle linear speed in m.s^{-1}, and f_{r0} and f_{r1} are the rolling resistance coefficients.

Aerodynamic drag also causes a significant vehicle loss; the corresponding force is expressed by the following equation:

$$F_w = \frac{1}{2}\rho_a A_f C_D V^2 \tag{A.2}$$

Where ρ_a is the air density in kg/m^3, A_f is the effective frontal area of the vehicle in m^2, and C_D is the aerodynamic drag coefficient. So the combined force of both losses is expressed by following equation in Newtons. No grade force is applied in this test.

$$F_{loss} = F_r + F_w \tag{A.3}$$

Autonomie acceptsf_{r0}, f_{r1}, A_f, and C_D as inputs for calculating the vehicle loss.The chassis dynamometer software also uses the same equation but in pound force as follows.

$$F_{loss} = F_0 + F_1 \times V + F_2 \times V^2 \tag{A.4}$$

Where $F_0 = Mgf_{r0}$ in lbsf, $F_1 = Mgf_{r1}$ in lbsf/mph, and F_2 is lbsf/mph^2

In addition to F_{loss} in (4) which is generated to model the vehicle loss behavior, additional losses are present due to drag of the tires on rolling steel and the transmission's loss already included in the road-load model. So these losses are seen twice by the vehicle. These losses can be measured by finding additional coefficients for equation (4) like shown in (5) below:

$$F_{cal} = V_0 + V_1 \times V + V_2 \times V^2 \tag{A.5}$$

In the following table values for F_0, F_1, F_2 in the dynamometer software and typical values previously measured for V_0, V_1, and V_2 are presented.

Table A.1 Parameters of chassis dynamometer software

F_0	F_1	F_2	V_0	V_1	V_2
111 lbsf	-1.2 lbsf/mph	0.0314 lbsf/mph^2	47 lbsf	0.57 lbsf/mph	0.0140 lbsf/mph^2

In the experimental work section the vehicle sees the modeled vehicle losses and the calibration losses. So, adjusted Autonomie's input parameters can be calculated as follows:

Table A.2 Parameters of Autonomie software

f_{r0}	f_{r1}	A_f	C_D
0.0448	-3.74e^{-4} lbsf/mph	0.0314 m^2	0.4338

By applying these parameters the total energy of mechanical power at the output of the motor has a 7% difference between simulation and experiment. According to the manual, one reason might be the friction calibration issue of the dynamometer. To take into consideration the entire the loss before the motor mechanical power, the parameters

are tuned and presented below which leads to very close motor average power in both simulation and experiment.

Table A.3 Tuned parameters of Autonomie software

f_{r0}	f_{r1}	A_f	C_D
0.0540	-4.03e^{-4} lbsf/mph	0.0314 m^2	0.4338